RESEARCH REPORT
RESULTS OF TESTS ON A
FRACTURING/CEMENTING TRAILER FRAME

by

Benjamin J. Wallace
and
Thomas M. Murray
CoPrincipal Investigators

Submitted to

Engineering Department
Halliburton Services
Duncan, Oklahoma

Report No. FSEL/HALLIBURTON 85-01

December 1985

FEARS STRUCTURAL ENGINEERING LABORATORY
School of Civil Engineering and Environmental Science
University of Oklahoma
Norman, Oklahoma 73019

TABLE OF CONTENTS

LIST OF FIGURES

LIST OF TABLES

CHAPTER I

INTRODUCTION

1.1 Objective

This report documents the results of a series of tests conducted at the Fears Structural Engineering Laboratory of the University of Oklahoma on a pair of built-up curved beams. These beams are used as rails by Halliburton Services Inc. in the manufacture of cementing and fracturing equipment trailers. Recently several of these beams have cracked and fractured in the curved portion approximately seven feet behind the trailer kingpin. The purpose of this research project was to identify the causes of these cracks in order to suggest appropriate improvements in the design of the beams.

1.2 Scope

A single trailer frame consisting of two curved beams and the associated crossmembers was tested in this study. This frame was supported at each end by stands resting on

the reaction floor at Fears Lab. A whiffletree was used to distributed the total force to each of the two beams at two points as shown in Figure 1.1.

Experimentation on the curved beams included a brittle lacquer analysis, static tests, dynamic tests and fatigue tests. The brittle lacquer analysis was conducted to locate the most highly stressed regions in the curved portion of one beam. Data was collected during the static and dynamic tests to determine load-deflection and load-strain relationships for the beams. The fatigue test was conducted to determine the fatigue life of the beams under the idealized load used.

In addition to the experimentation conducted on the curved beams, various sections of the frame were measured, the resulting section properties calculated, and a stiffness analysis performed using these properties. This analysis was used to obtain a theoretical load-deflection relationship to compare with the experimentally determined value.

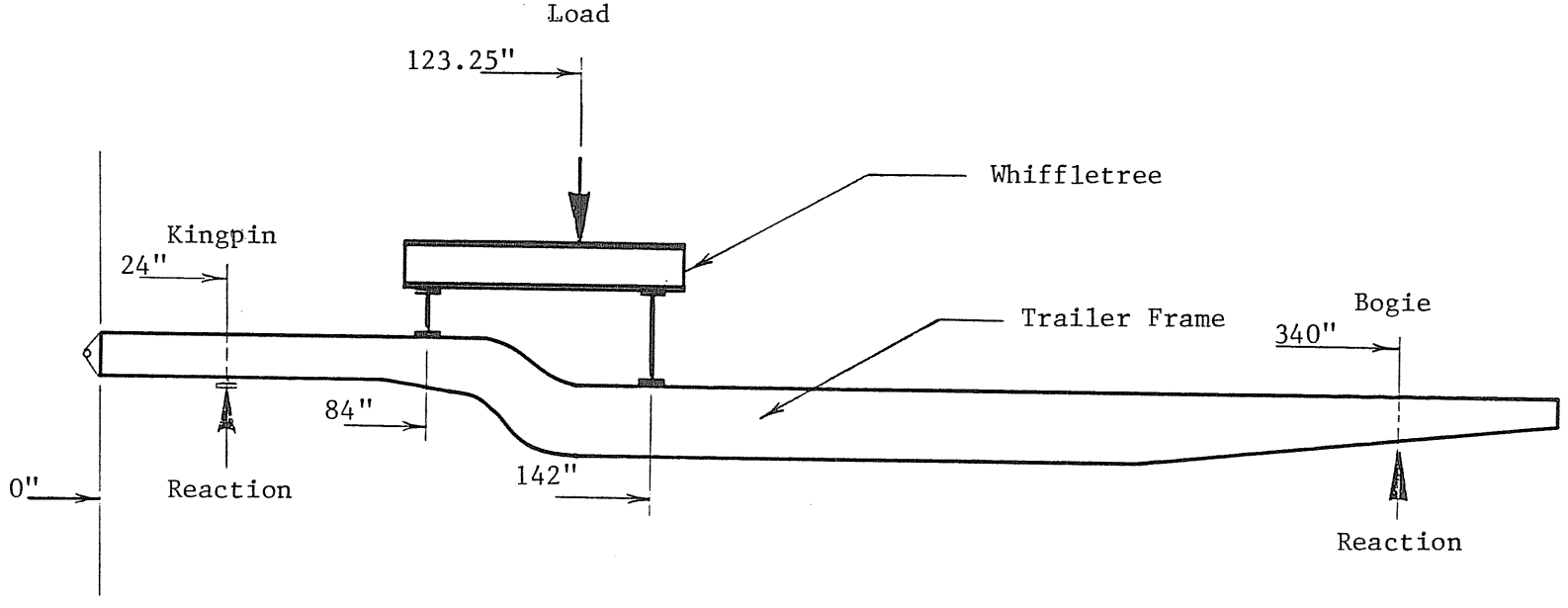

Figure 1.1 Test Specimen and Whiffletree

CHAPTER II

TEST DETAILS

2.1 Test Specimen

The test specimen was a trailer frame manufactured by Halliburton Services Inc. for use as the basic structure under their fracturing and cementing units. This frame consisted of the two curved beams under study which were the side rails, and connecting crossmembers. Overall dimensions of the beams are shown in Fig. 2.1. Measurements of the driver's side beam web and flanges were made at the sections shown in Fig. 2.2. The parameters measured are shown in Fig. A.1 and listed in Table A.1 of Appendix A. Properties of the cross sections were calculated and are listed in Table A.2 of Appendix A.

The specimen was manufactured from Nicop-80, which is a high strength, low alloy steel meeting the requirements of ASTM A710-79 Type A. This material has yield and tensile strengths of 75 and 85 ksi in the thicknesses used.

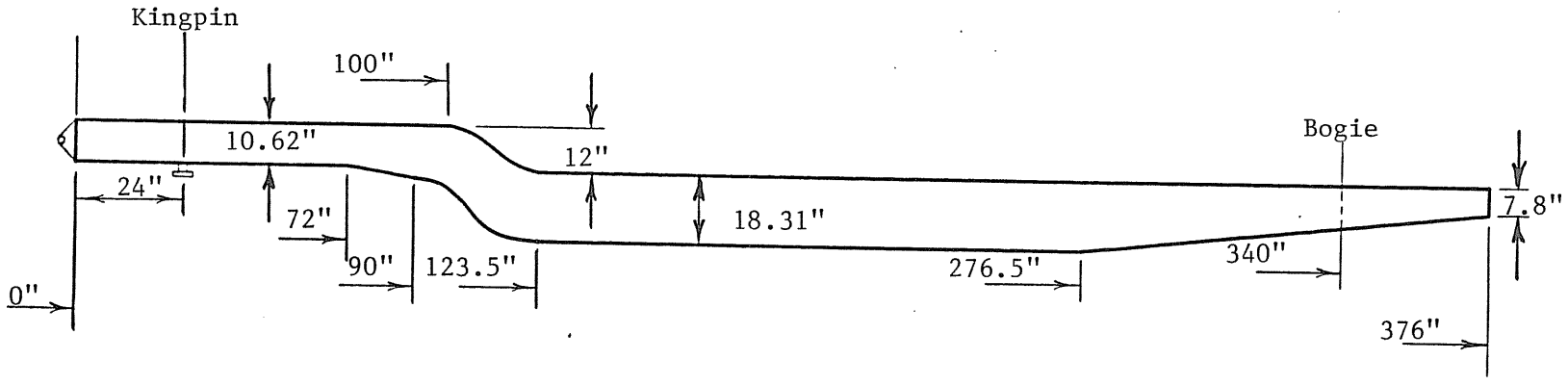

Figure 2.1 Specimen Dimensions

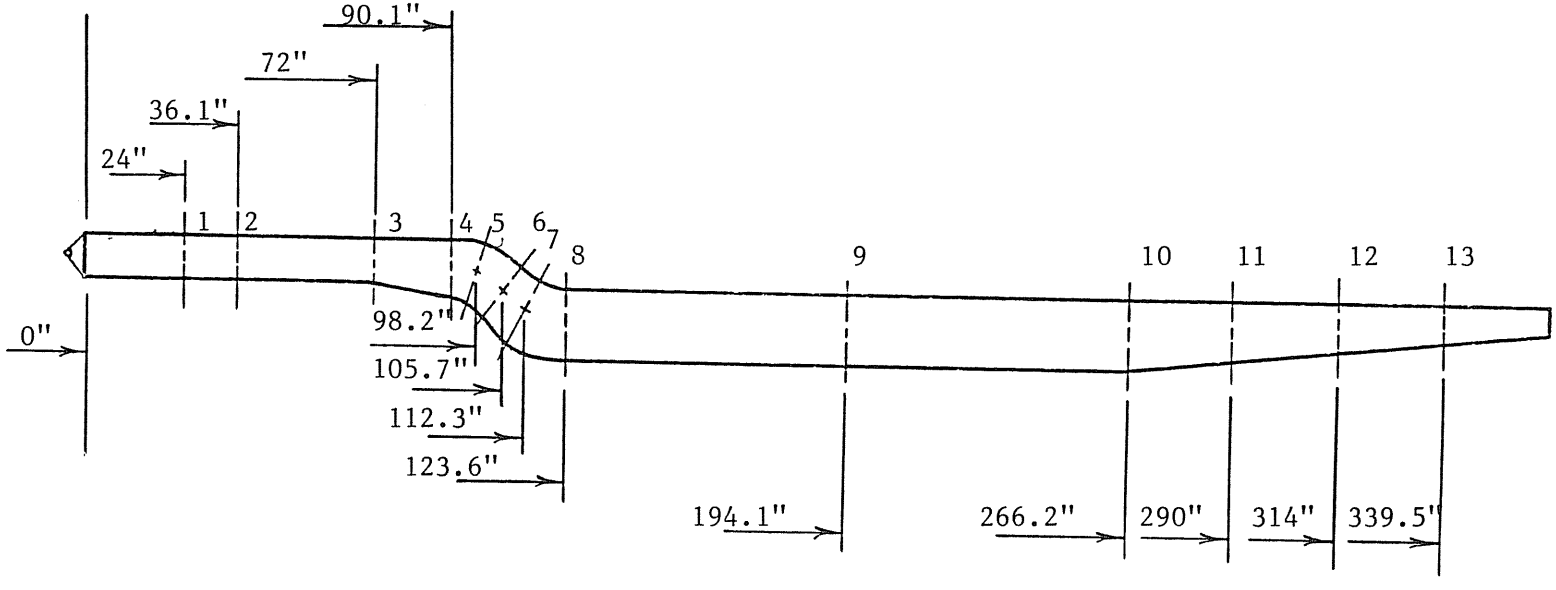

Figure 2.2 Locations of Measured Sections

2.2 Test Setup

The front of the specimen was supported by a fifth wheel mounted on a stand which rested on the static reaction floor of Fears Lab. The fifth wheel included a hinge which allowed the trailer frame to rock, resulting in zero moment at the kingpin location. The rear of each beam was supported at the trailer bogie centerline by an elastomeric bearing pad and a steel stand which rested on the reaction floor as shown in Figure 1.1. The elastomeric pad in each of these rear supports allowed the trailer frame to rock with no moment at the supports.

A whiffletree was used to distribute the applied load to two points on each of the two curved beams. The whiffletree, shown in Fig. 2.3, consisted of one longitudinal and two cross beams. The longitudinal beam distributed the actuator load to the cross beams in proportions calculated to produce a moment diagram in the curved beams which was similar to that produced by normal service loading. Moment diagrams supplied by Halliburton for rails of a fracturing unit and the passenger's side rail of a cementing unit were considered to be normal service loading. The whiffletree cross beams distributed their portion of the total load equally between the two curved beams.

Load was applied with a 55 kip capacity MTS actuator connected to the whiffletree. The other end of the actuator

was connected to a reaction frame which spanned the specimen and was bolted to the reaction floor. The actuator was controlled with an MTS 406 controller and 436 control unit which included a cycle counter and function generator. Hydraulic power was provided by an MTS 10 gpm pumping unit.

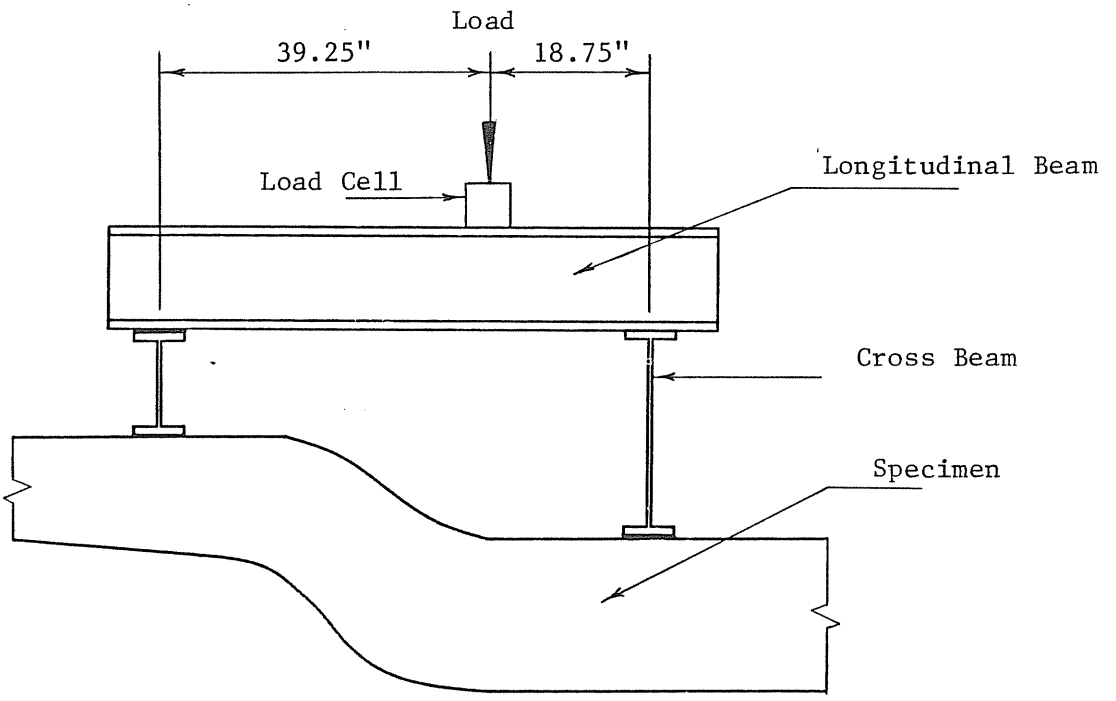

Figure 2.3 Whiffletree Details

2.3 Instrumentation

Different quantities were measured during the various tests conducted on the specimen. Total load applied was measured in all tests. Vertical deflections of each curved beam were measured during all static tests and the dynamic strain test. Deflections of the beam flange toes with respect to the beam web (flange rolling) in the curved portion of each beam and strains in the web and lower flange at the curved portion of one beam were measured in the later static and dynamic tests. Strains in a specimen crossmember were measured in the later static test.

Measurements collected during the static tests were taken with a Hewlett-Packard 3497A Data Acquisition and Control Unit driven by an H-P 85 microcomputer. Measurements collected during the dynamic test were taken with a Trans-Era analog to digital converted attached to a Tektronix 4052 microcomputer. All data was plotted on a Tektronix 4662 X-Y plotter driven by the Tektronix 4052 microcomputer.

Total load applied by the actuator was measured by an electronic load cell mounted on the whiffletree as shown in Fig. 2.3. The MTS control console provided excitation, signal conditioning, and a display for this transducer.

Wire potentiometers were used to measure the vertical displacement of each curved beam just behind the curved

portion as shown in Fig. 2.4. These transducers were held to the reaction floor with weights and the wire was attached to the lower flange near the beam web with small magnets. These transducers were excited with a 5 volt power supply and the resulting signal was read directly with the H-P and Tektronix data acquisition systems during the static and dynamic tests.

Direct Current Displacement Transducers (probes) were used to measure the "rolling" of the flanges in the curved portion of the passenger's side beam. These transducers consist of spring-loaded plungers which move a ferrite core in a transformer. The transformer and related electronics are mounted in bodies which were attached to the beam web with magnetic indicator stands. These transducers were positioned to hold their plungers against the lower beam flange as shown in Fig. 2.4. Probes #1 and #2 were used to measure the rolling of the beam bottom flange (inside of the beam web) in tests conducted on both the unreinforced and reinforced frames. Probes #3 and #4 were located to measure the rolling of the reinforcing flange which protruded from the outside of the beam web in the test of the reinforced frame and are also shown in Fig. 2.4.

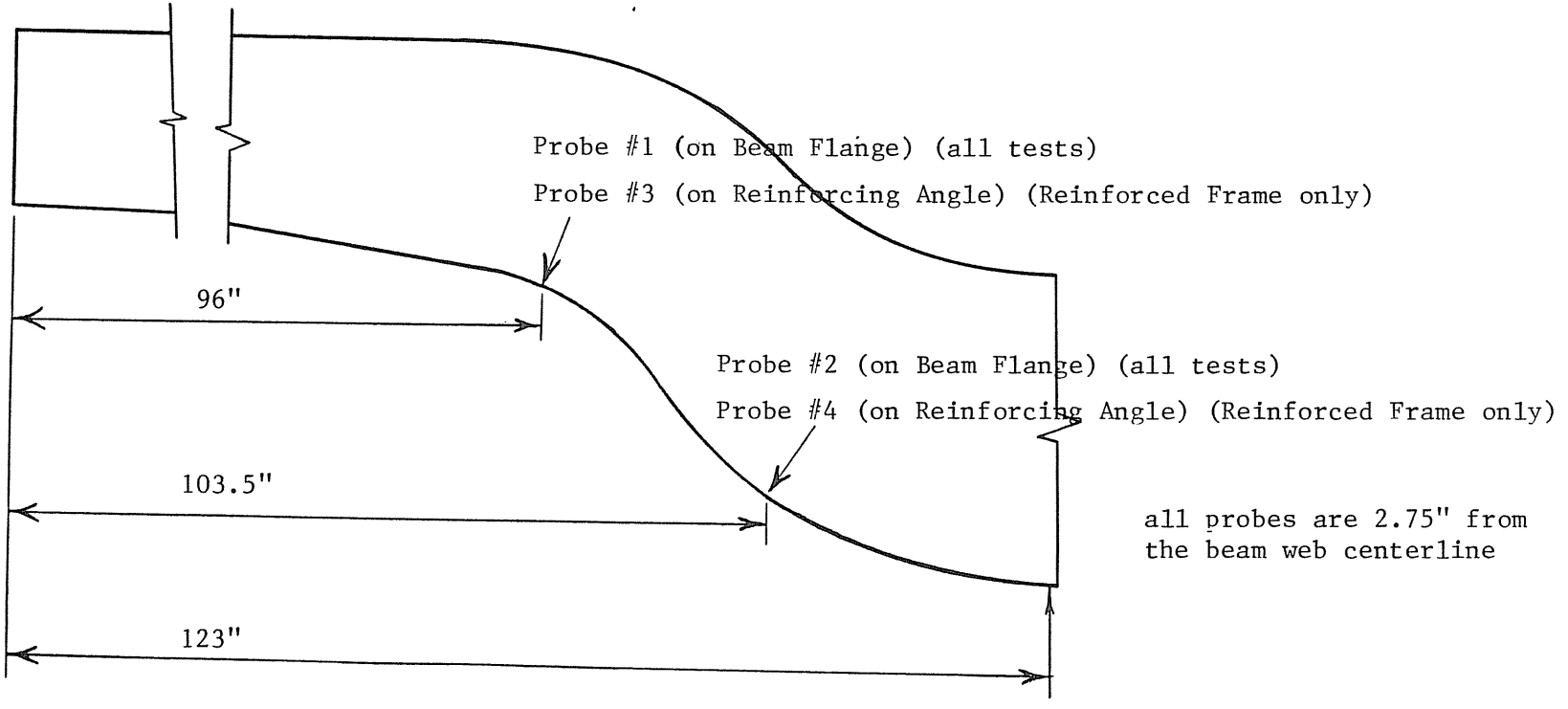

Figure 2.4 Locations of Deflection Transducers

Electrical resistance strain gages were applied to the web and lower flange in the curved region of the passenger's side beam. First, an area of paint was removed from the steel surface with an abrasive flap wheel. Next the area was wet sanded with a conditioner fluid and then wiped with a neutralizer solution. After this surface preparation, the gages were glued to the specimen with cyanoacrylic adhesive.

Three 0-45-90^{o} rosette gages were applies to each side of the beam web. Locations and orientations of these gages are shown in Figs. 2.5 and 2.6. Three uniaxial strain gages were installed on the top surface of the lower flange at a distance of 93 3/4 inches from the front of the frame. These gages were oriented with their active axes parallel to the beam flange and installed at the locations indicated in Fig. 2.7 (a). Four uniaxial strain gages were installed on the bottom surface of the lower flange at a distance of 93 1/2 inches from the front of the frame and at the locations shown in Fig. 2.7 (b).

For the static test on the reinforced frame, three uniaxial strain gages were installed on the cross-member in the curved portion of the frame to indicate the moment caused by the twisting moment in the curved beams. These strain gages were installed with their active axes parallel to the cross-member at a section 4 inches from the web of the passenger's side beam as shown in Fig. 2.8.

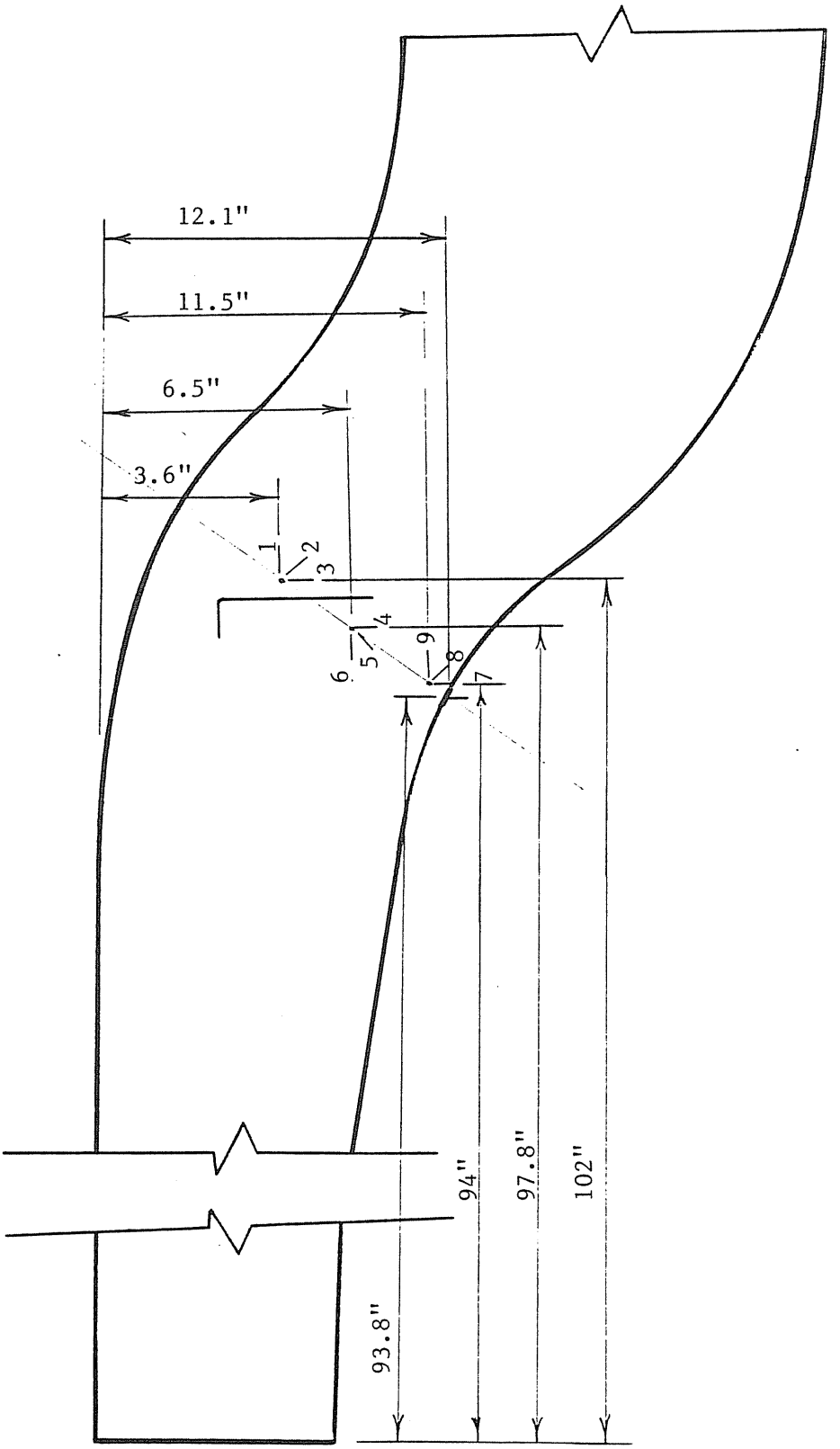

Figure 2.5 Locations of Strain Gages on Inside of Beam Web

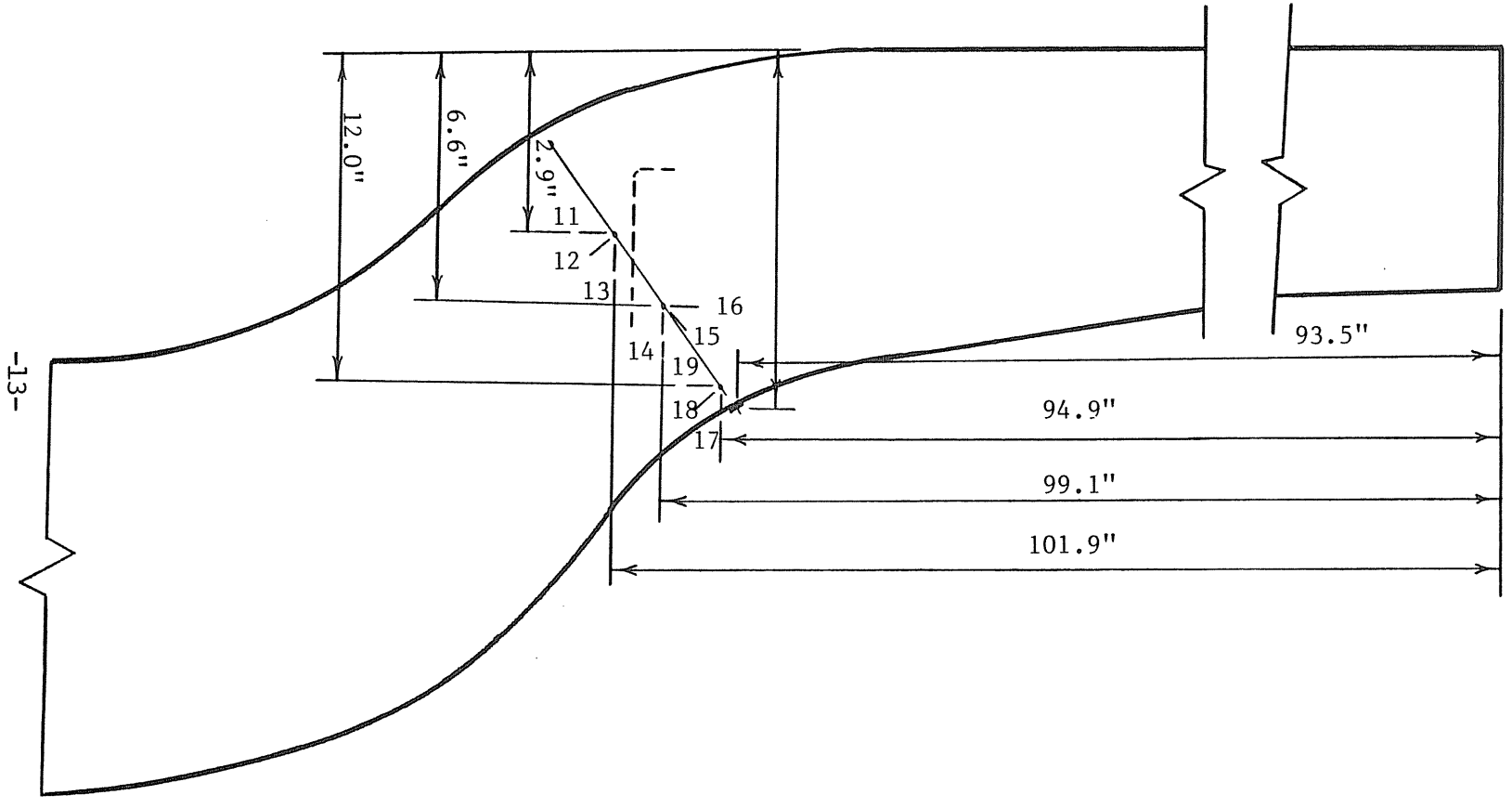

Figure 2.6 Locations of Strain Gages on Outside of Beam Web

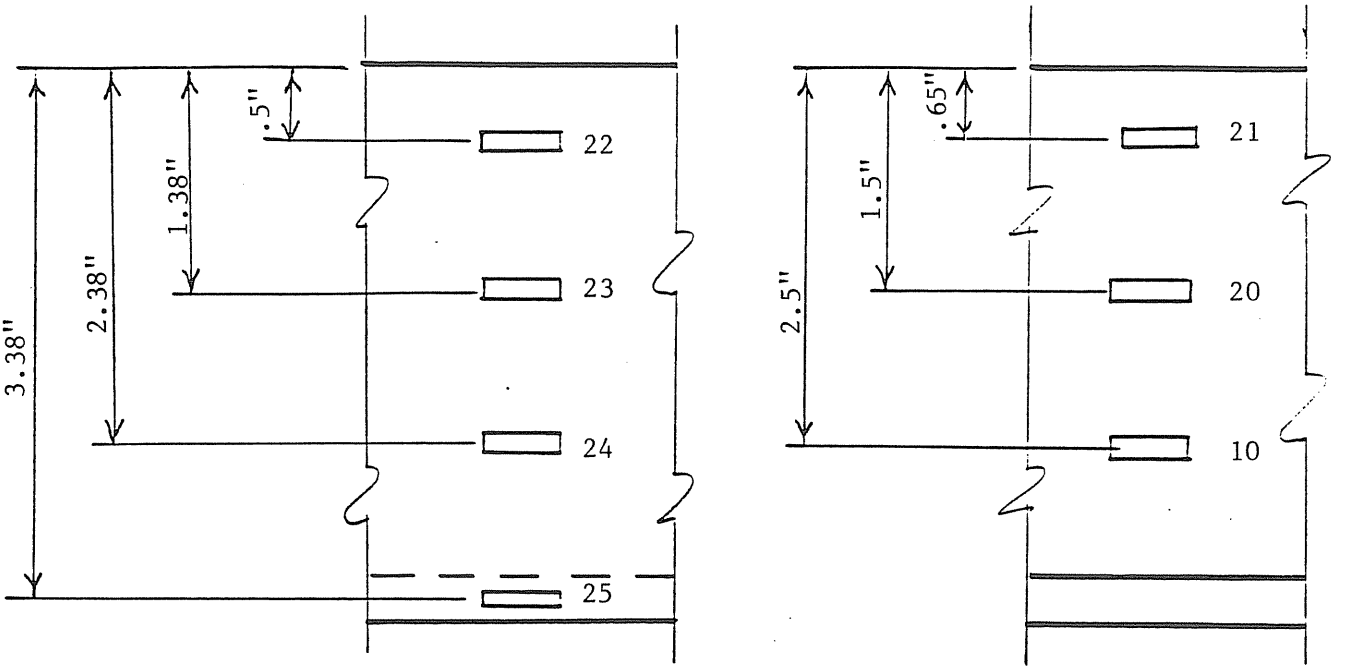

(a) Bottom side of Flange (b) Top side of Flange

Figure 2.7 Locations of Strain Gages on Beam Lower Flange

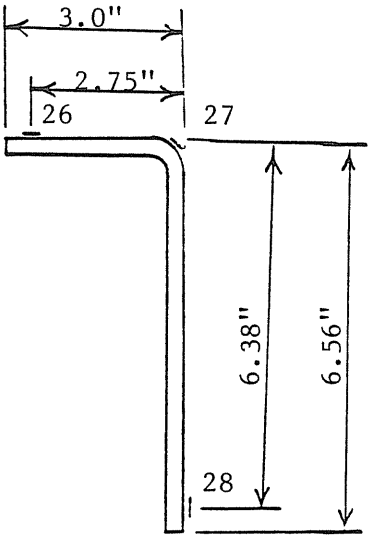

Figure 2.8 Locations of Strain Gages on Frame Cross-Member

2.4 Testing Procedures

Four types of testing procedures were conducted on the specimen in this program. A brittle lacquer analysis was conducted to indicate the most highly strained regions in the curved portion of the beams so that strain gages could be placed in these locations. Static tests were then used to measure and record strains and deflections at these locations under various loads. This data was collected for comparison with analytical studies and predictions of fatigue life based on maximum stresses. Fatigue testing was conducted to determine the number of loading cycles the frame could withstand before cracks could be noticed. This testing was conducted on the frame until cracks were noticed, and again after repairs and modifications were made to the frame. A dynamic test was conducted to measure strains and deflections as they occurred during the fatigue testing.

Brittle Lacquer Analysis

The first experimentation on the curved beams was a brittle lacquer analysis. This analysis was conducted on the lower flange and adjacent web in the curved area of the driver's side beam as shown in Fig. 2.9. This area was first sanded to remove any paint and mill scale. Next, the beam area and five calibration bars were coated with a

reflective paint so that cracks in the lacquer could be more easily observed. Six coats of brittle lacquer were then applied to the beam and calibration bars. After allowing the lacquer to dry overnight, the calibration bars were placed in a fixture and bent to a known deflection to determine the strain at which the lacquer first cracked. Load was then applied to the frame in 5 kip increments and the outline of the region of cracked lacquer was recorded at each load increment. These outlines were used to determine the most highly stressed regions of the specimen.

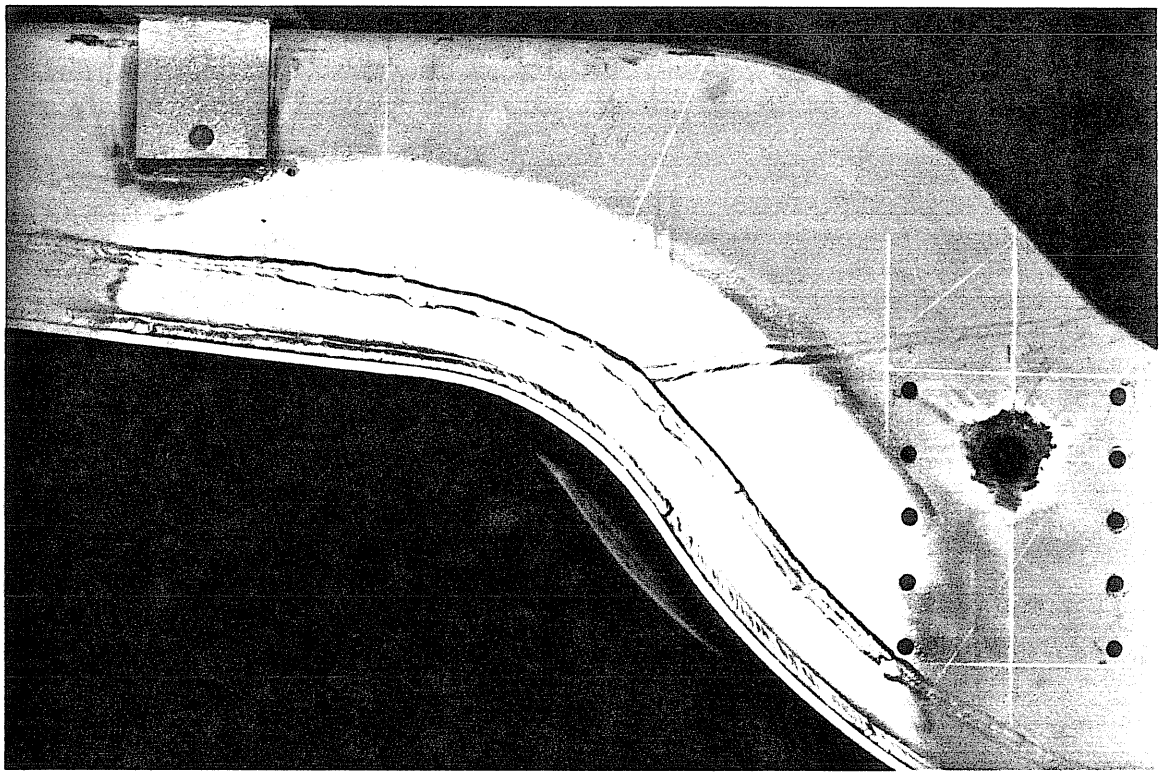

Figure 2.9 Region Analyzed with Brittle Lacquer Coating

Static Test Procedure

Static tests were used to measure deflections and strains while the load was held constant so that the 3496A could scan all the data channels at the same load and displacement. These readings were taken at various intensities of load so that load-strain and load-deflection relationships could be determined. In preparation for these tests, all available instrumentation was connected to the HP 3496A data acquisition and control unit.

The test were initiated by starting the MTS system and reading all data channels while the load was zero. The load was then applied in 4 kip increments and the data channels read after each increment of load. This procedure was continued until the maximum load of 46.1 kips was reached. The specimen was then unloaded using similar increments and data was collected during each unloading increment. This process was performed on the frame after it was first repaired and again after the addition of the reinforcement flanges.

Fatigue Test Procedure

Fatigue testing was accomplished by programming the MTS 406 controller and 436 control unit to operate the actuator in displacement cycles which would result in the desired loads. The minimum and maximum loads reached during each

cycle, 21.3 and 46.1 kips, were applied at a frequency of 1.2 Hz. These loads were chosen because they result in moments in the trailer gooseneck which are similar to those caused by one and two times the static service load, respectively.

The cyclic fatigue load was applied to the curved beams to simulate the beam flexure as the trailer is transported over a rough road. The original plan was to subject the beams to one million cycles, however the beams cracked at a much smaller number of cycles. After the initial cracking, the beams were repaired and testing was continued until cracks were observed again. This was repeated for a total of four series of cyclic tests, each terminated when one or both of the beams had cracked.

Dynamic Test Procedure

Dynamic testing was conducted to measure the load, displacements, and strains of the specimen under the fatigue testing loads. This was accomplished by connecting all desired signals to the A/D converter on the Tektronix 4052 microcomputer so that data could be taken during actual fatigue loading cycles. Signals acquired included load and stroke from the MTS controller, vertical displacements from the wire potentiometers, flange rolling displacement from the probes, and selected strain gage outputs which were conditioned by a set of strain gage amplifiers.

Software was written for the Tektronix 4052 to read initial channel information and then wait until the load exceeded a selected value before continuously scanning. Using this software, the test was initiated by starting the MTS hydraulic pump, adjusting the controller to zero load and stroke, and then taking an initial reading from all data channels. After the initial data was taken, the MTS controller was adjusted to the mean load and the program of cyclic displacement was started. By setting the value at which scanning started to just larger than the mean load, data was taken only during the first programmed cycles, omitting the time when the mean load was manually applied to the specimen. At the conclusion of each test, all acquired data was plotted on the Tektronix 4662 plotter.

CHAPTER III

TEST RESULTS

This section presents results of all tests performed during this study. Results presented include those from the brittle lacquer analysis, static tests, fatigue test, and dynamic test.

3.1 Brittle Lacquer Analysis Results

The brittle lacquer analysis was conducted to find the most highly strained regions of the curved beams and to indicate the magnitude of strains present. The sensitivity of the brittle lacquer used in this test was measured with the calibration bars described in section 2.3. By bending the five calibration bars and noting the limit of the cracked region in the coating of each bar, the lacquer sensitivity was determined to be approximately 1100 x 10^{-6} inches/inch.

During the test, load was applied to the whiffletree in 5 kip increments. Between each increment of loading and the

next, the coating on the specimen was inspected for cracks which would indicate areas where the strain exceeded 1100 x 10^{-6} inches/inch. The first cracks in the lacquer were observed at a load of 25 kips. These cracks occurred on the outside bottom edge of the lower flange cover plate for a distance of approximately 14 inches along the portion of the flange which is concave downward. After these initial cracks were observed, additional loading increments were applied to obtain crack patterns for total loads of 30, 35, and 40 kips. At each of these increments, an outline of the cracked region of the coating was drawn on the specimen. These iso-strain lines can be seen in Fig. 3.1.

3.2 Static Test Results

The static tests were conducted to determine load-deflection and load-strain relationships for various locations on the curved beams. Locations and directions of the measured quantities are shown in Figures 2.4 thru 2.8.

The first of these tests was performed just after the specimen had been repaired for the first time and modified by the removal of the lower portion of one crossmember. Results of this test are presented in the first portion of Appendix B and are titled "HALLIBURTON FRAME". These quantities include load, vertical deflection of each curved beam, deflection (rolling) of the lower flange with respect

to the beam web, and strain at various gages.

A stiffness analysis was performed on the trailer beams using the section properties given in Appendix A and a plane-frame program written at Fears Lab. The resulting relationship between total load and deflection is plotted along with the experimentally obtained results in Fig. B.33 of Appendix B.

The second of these tests was conducted when the specimen had accumulated a total of 227,270. cycles of fatigue loading. This was immediately after the specimen had been repaired for the third time and reinforced by the additional angles at the lower flanges in the curved region. The results of this test are presented in the second half of Appendix B and are titled "REINFORCED FRAME". Displacements measured during this test included those measured in the first static test and also rolling of the reinforcing angle attached to the passenger's side beam (Probes #3 and #4). Only strains from gage numbers 3-6 and 22-28 were measured during this test as the other strain gages were destroyed when the curved beams were repaired and reinforced.

3.3 Fatigue Test Results

Fatigue loading was applied to the specimen in four series, with each series being stopped when cracks were noticed in the curved beams. After each of the first three

series of fatigue tests, the cracks were repaired by Halliburton personnel so that the fatigue testing could be continued. The counter in the MTS 436 control unit was set to zero at the beginning of the test program and was not reset during this project. This procedure resulted in a count which represents the total number of cycles applied to the specimen since the start of the first test series.

The first crack was noticed in the inside surface of the web of the driver's side beam at approximately 50,000 cycles. This crack initiated at the toe of the bottom flange of the crossmember in the curved region of the beam as shown in Fig. 3.2. This cracking was probably accelerated by an undercut into the web from the adjacent weld. Another contributing factor was the large out-of-plane strains present at this location due to the restraining effects of the crossmember on the beam flange rolling.

Testing was continued to determine how fast the crack would grow. The crack was noticed to have penetrated the beam web at 98,000 cycles. At this time two Halliburton employees, Bill Dennison and Steve Parker, brought a welder to repair the frame. While Bill and Steve were at Fears lab the frame was cycled approximately 2000 cycles to demonstrate the opening of the crack and the rolling of the beam flanges, bringing the total cycle count to 100,000 at the time of the first repair.

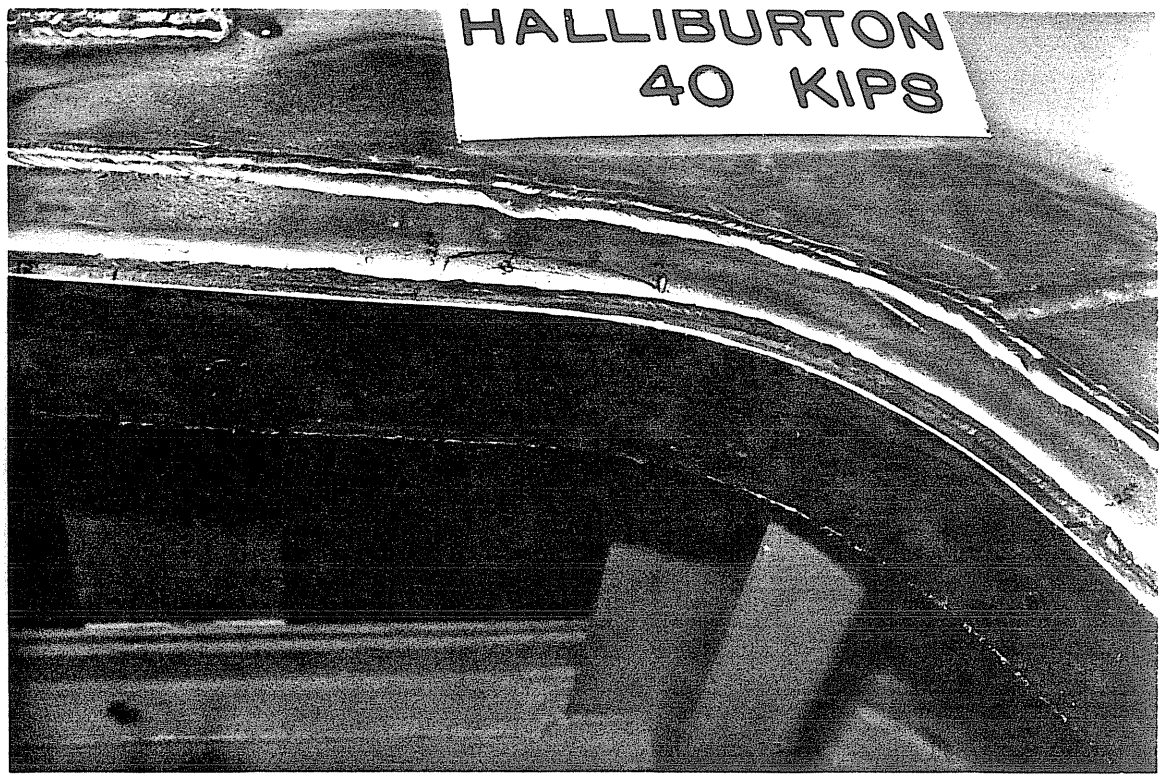

Figure 3.1 Istostrain Lines in the Brittle Lacquer Coating

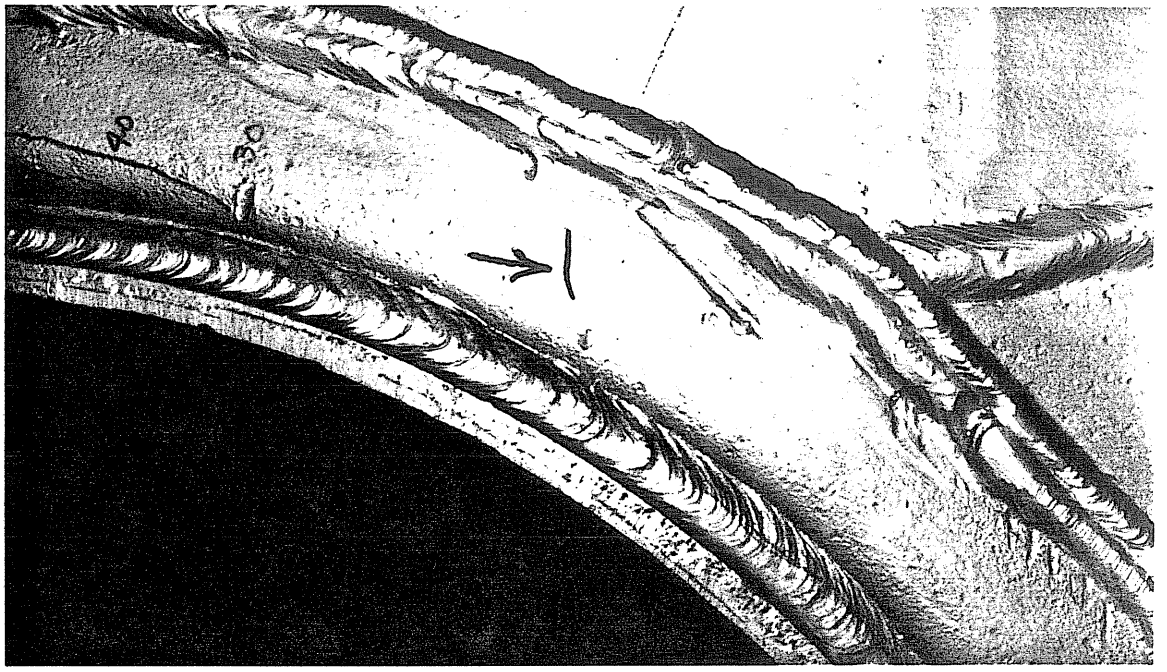

Figure 3.2 Location of First Crack

The frame was modified by cutting away the bottom 3.5 inches of the crossmember to reduce the stress concentrations in the beam web due to the restraint of the beam flange rolling. The crack in the driver's side beam was then repaired by welding along the crack on the inside of the web as shown in Fig. 3.3, grinding through the crack from the outside of the web down into the weld, and then filling the root left from grinding with weld.

Three items were noticed by the Halliburton personnel during the repair operation. One was that the lower flanges of the curved beams were being held apart by the lower portion of the crossmember which was removed. This restraint required that the portion of the crossmember be driven from between the beams with a hammer after it had been cut loose. The second item noticed was that heat generated during the crossmember modification caused the crack in the beam to open up and become more easily visible. The resulting crack can be seen at the left of the discolored area in Fig. 3.4. The third item reported was a discrepancy between the dimensions of the driver's and passenger's side beams which resulted in a shallower section in the curved portion of the driver's side beam.

After the repair was completed, fatigue testing was continued at a total count of 100,000 cycles. At 124,000 cycles, a small crack was noticed in the passenger's side

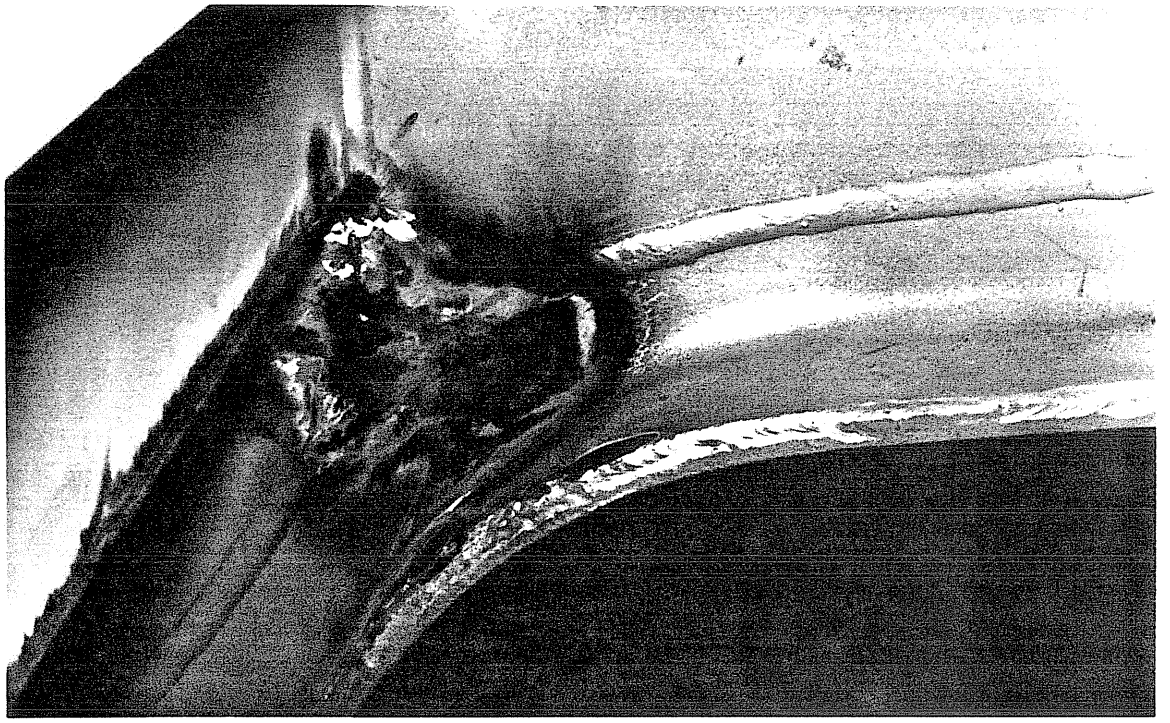

Figure 3.3 Repair Weld on Inside Surface of Beam Web

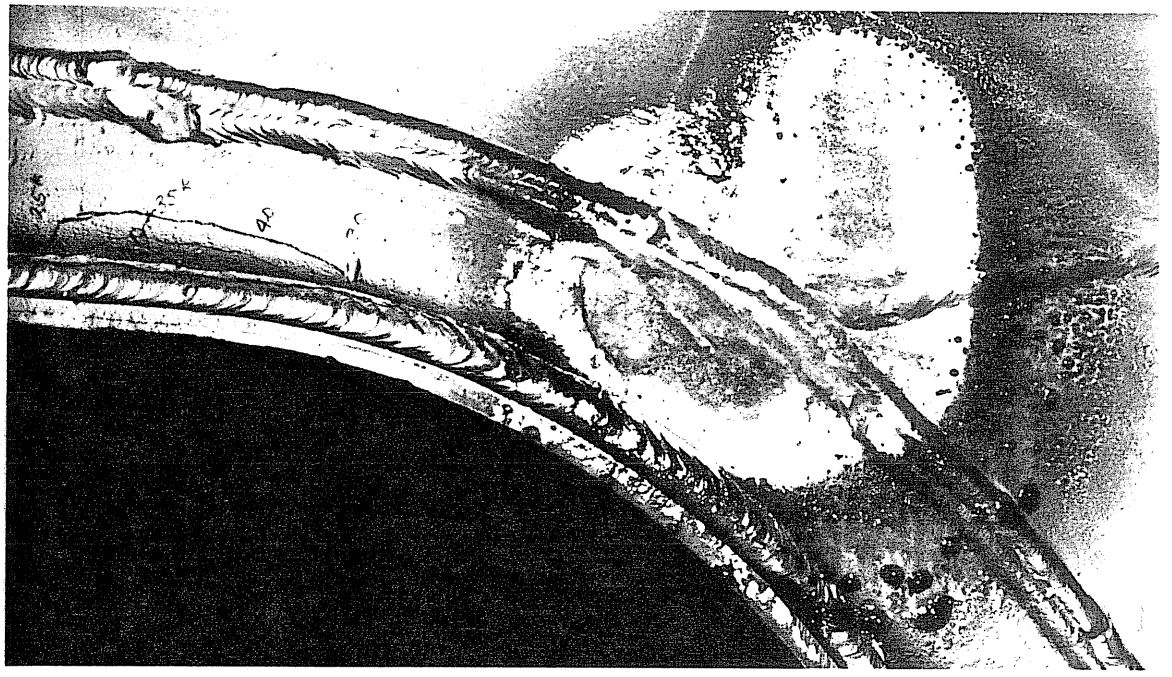

Figure 3.4 First Crack after Removal of Crossmember

beam at the same location as the one repaired in the driver's side beam. It is likely that this crack had initiated before the crossmember was modified at 100,000 cycles, as this location was subjected to large strains before the modification. Other factors which encouraged the formation of this crack were the heat affected zone from the welding to the crossmember and the heat applied to the region during the modification. This crack was approximately 0.5" long when first noticed and could be seen only on the inside surface of the beam web. At 174,000 cycles, the crack in the passenger's side beam had grown to a length of 1.4" on the inside face of the beam, but could not be seen on the outside surface of the beam. This crack lengthened to 1.6" when the total count was 192,000 cycles, but still not be seen on the outside of the web. An inspection with dye penetrant at 200,000 cycles revealed that the crack had penetrated the web and grown to a length of 1" on the outside of the web.

The curved beam on the driver's side was observed to be cracked just below the previous repair at a total count of 192,000. At this time the crack was 1.4" long on the outside surface of the beam web, having completely penetrated the web. The inspection with dye penetrant performed at 200,000 cycles indicated that the crack had grown to 2". This crack is outlined in red in the heat discolored area of

the beam in Fig. 3.5.

Halliburton personnel repaired these crack in a manner similar to the previous one, by grinding out the crack and filling the resulting groves with weld. This was accomplished at a total count of 200,000 cycles.

The fatigue test was then continued with the same loading. This time the first crack was noticed in the driver's side beam at a count of 220,260 cycles. This crack occurred just above the previous repair and was 1.5" long on the inside of the web. At this time it was not visible on the outside.

At a total count of 226,700 cycles a crack was noticed in the passenger's side beam. This crack occurred just below the previously repaired one. Fatigue testing was interrupted at this time due to the rapid recurrence of cracks in the repaired zones.

At this time, Bill Dennison and two technicians from Halliburton traveled to Fears Lab to repair and reinforce the frame. The cracks in both beams were repaired as previously, by grinding out the crack and filling the resulting grove with weld.

The curved region of each beam was then reinforced by the addition of a bent angle opposite to the lower flange as shown in Fig. 3.6. These angles were welded to the beam webs along the toe of their vertical leg only, to avoid

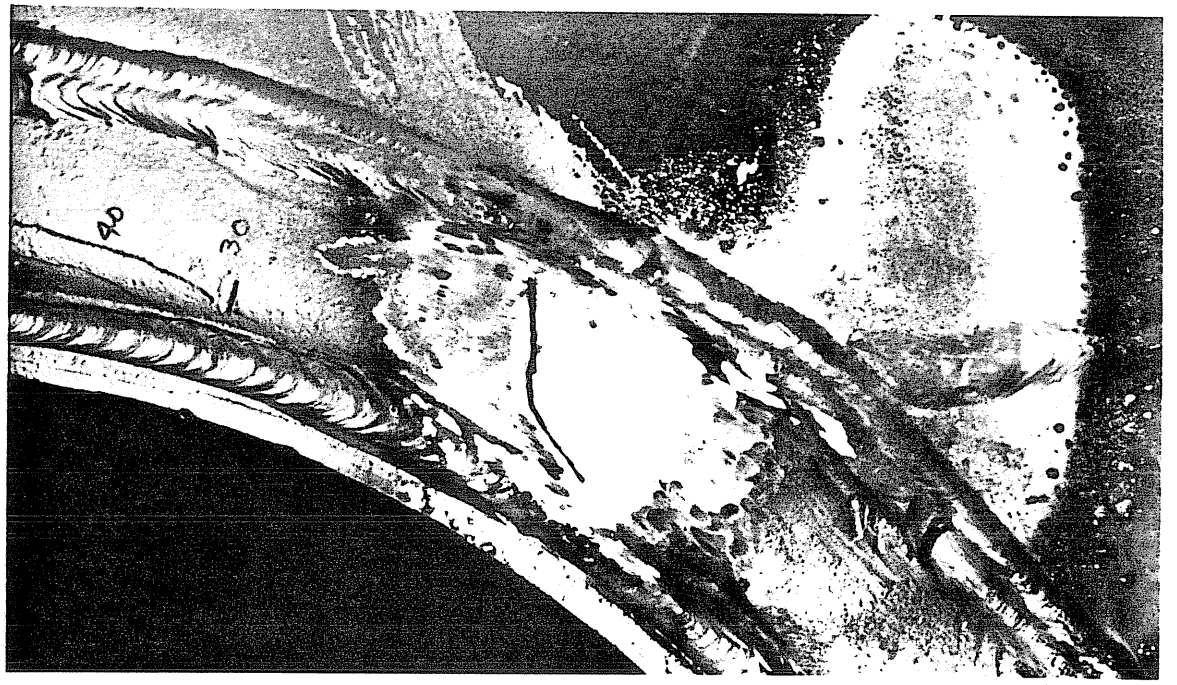

Figure 3.5 Location of Second Crack

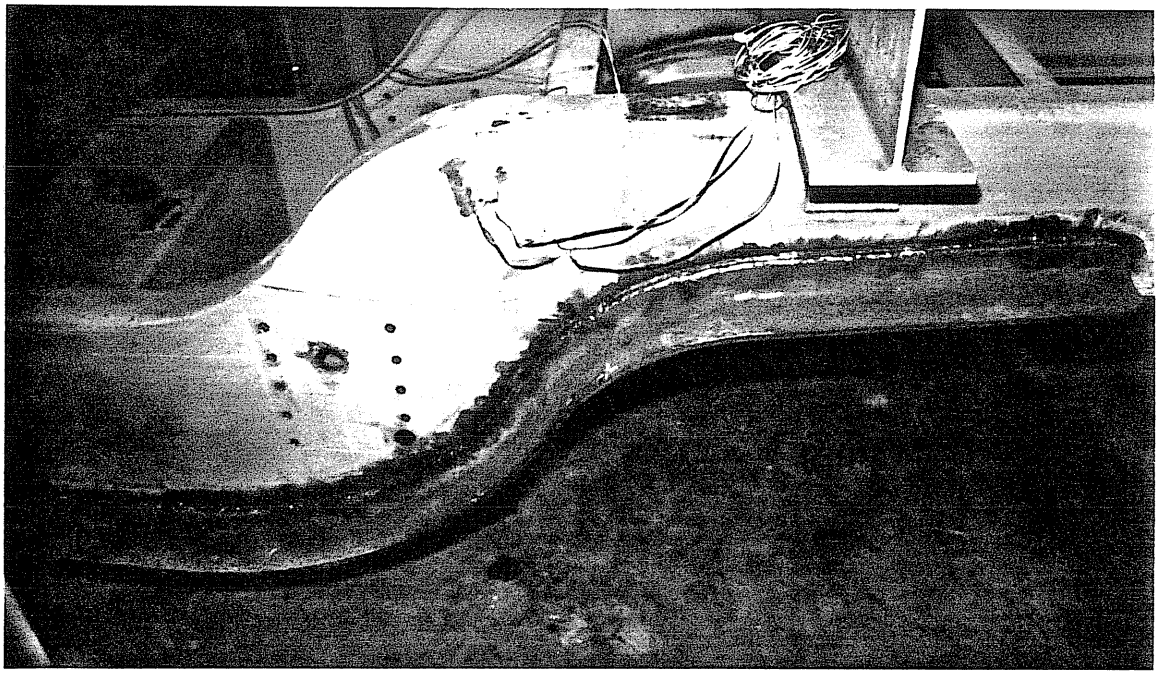

Figure 3.6 Reinforcing Angles added to Specimen

welding to the cover plate of the existing flange. This method of reinforcement was used to reduce stresses in the web by two mechanisms. The first mechanism is the reduction of in-plane stresses in the web due to the increased section modulus and moment of inertia of the beam. The second mechanism is the reduction of out-of-plane stresses in the web due to flange rolling caused by the unsymmetric lower flange. By creating a flange which is more symmetric with respect to the web, the rolling tendencies of the two projecting legs will cancel, reducing the out-of-plane forces applied to the web.

After the repair, reinforcement, and static and dynamic tests, fatigue testing was resumed. The total count at this time was 227,400 cycles.

A crack at the top of passenger's side crossmember was noted at a total count of 254,800 cycles. This crack was approximately 0.5" long when first noticed and did not grow appreciably during the remainder of testing.

At a count of 290,800 cycles, a crack was noted in the passenger's side beam. This crack occurred in the repaired region and was 2" long. Fatigue testing was terminated at this point due to the consistent reoccurrence of cracks in the repaired regions.

3.4 Dynamic Test Results

The dynamic test was conducted to document some of the strains and displacements which were occurring during the fatigue test. This test was conducted just after the specimen was repaired for the second time, at a total count of 202,400 cycles.

The original plan was to load the specimen at a frequency of 1.2 Hz, which was used in the fatigue tests. This was reduced to 0.25 Hz because phase errors between channel readings resulted in false indications of hysteresis in the results collected at the higher loading frequency. Data collected from this test includes load, deflection of the driver's side beam, and strains from gages #17 thru 19, 22, and 25. Plots of this data are presented in Appendix C.

CHAPTER IV

SUMMARY

In this test program, the behavior of curved beams used as frame rails in cementing and fracturing trailers has been measured. These measurements included the relationships between load and various deflections and strains. This section summarizes these results and discusses some of their implications for the fatigue life of the frames.

The relationship between applied load and beam deflection at the wire potentiometers was predicted using a plane-frame stiffness analysis program. This prediction is shown as the solid line in Fig. B.33 of Appendix B. In this figure it can be seen that the predicted stiffness of the frame was significantly greater than actual. The most important reason for this over estimation of the frame stiffness is that the analysis failed to account for the tendency of the flanges in the curved region of the beam to "roll", reducing the stress in the flange at locations away from the web. This reduced flange effectiveness resulted in a

smaller effective moment of inertia for curved region of the beams which caused the reduced stiffness of the frame.

The distribution of stresses in the lower flange of the curved portion of the beams can be seen in both the brittle lacquer analysis and static test results. The brittle lacquer analysis indicated that the lower flange next to the beam web reached approximately 1100 microstrain at a load of 25 kips. The test was continued to a load of 40 kips, but the region of the flange which had a strain exceeding 1100 microstrain only extended about halfway across the flange, indicating that the toe of the flange was much less than fully effective.

Similar results were obtained from the static test. Strain gage #25, which is on the bottom of the lower flange near the the web, indicated a strain of 1300 microstrain at a load of 25 kips (see Fig. B.29, Appendix B). At the same load strain gage #22, which is near the toe of the lower flange, indicated a strain of only 400 microstrain (see Fig. B.26).

Cracks initiated in the beam web at the cross member weld during the fatigue tests rather than in the lower flange which conventional analysis would predict to be more highly stressed. This suggests that the beam web is subjected to stress from mechanisms other than those considered in conventional analysis. These additional mechanisms

may be divided into two categories, those causing additional normal stresses and those resulting in bending stresses.

There are two mechanism which add to the normally considered normal stresses in the web at the curved portion of the beam. The first of these mechanisms is the reduced effective cross section properties due to the non-uniform stress in the beam flanges. These additional stress could be included in a beam analysis technique by reducing the cross section properties to reflect the ineffectiveness of the flanges.

The second of the mechanisms which generates normal stresses in the web is the action of the web to resist the component of the force in a length of flange which is perpendicular to a tangent to the flange. This mechanism occurs in any curved beam regardless of the symmetry of the flanges about the web.

Bending stresses in the web are generated as a result of the previously mentioned mechanism which generates web normal stresses due to the curvature of the flanges. The component to be resisted occurs at the resultant of the flange force. This lies outside of the plane of the web in the beams tested due to the asymmetry of the flanges about the web. These bending stresses cause the "rolling" of the flanges in the curved portion of the beams observed during the testing. These bending stresses are distributed along

the length of the beam according to the curvature of the flange. In the curved portion of the beams, a major portion of the resulting bending moment transferred from the web to the cross member, resulting in large stresses at the weld between the web and cross member. The web bending stresses resulting from the curved assymetric flanges would not be considered in a typical beam analysis, but should be predicted by a three-dimensional finite element analysis. The concentration of web bending stresses at the cross member weld could be predicted using a finite element analysis, but would require closely spaced nodes near the weld for accurate results.

Comparisons of strain gage readings for different tests can be made from the data presented in Tables 4.1 and 4.2. These tables include peak values of stresses calculated from strain gage readings taken during the static and dynamic tests on the unreinforced and reinforced frames. Spaces in these tables without data correspond to strain gages which were destroyed during a previous repair.

Table 4.1 contains the maximum values of stress calculated from the uniaxial strain gages installed on the beam lower flange in the locations shown previously in Fig. 2.7. From this data it can be seen that the maximum stress is largest near the beam web at gage #25 and is smaller at each strain gage located farther from the beam web (at strain

TABLE 4.1
MAXIMUM UNIAXIAL STRESSES

Strain Gage Number	Uniaxial Stress (ksi)		
	Static Test (Unreinforced)	Dynamic Test (Unreinforced)	Static Test (Reinforced)
25	71.7	63.9	52.2
10	22.2		
24	52.8		34.8
20	-3.0		
23	33.6		17.1
21	-6.3		
22	23.1	12.3	8.1

TABLE 4.2
MAXIMUM VON MISES STRESSES

Rosette Strain Gage Number	Von Mises Stress (ksi)		
	Static Test (Unreinforced)	Dynamic Test (Unreinforced)	Static Test (Reinforced)
1 - 2 - 3	57.1		
11 - 12 - 13	20.0		
4 - 5 - 6	23.2		29.3
14 - 15 - 16	24.4		
7 - 8 - 9	48.2		
17 - 18 - 19	72.5	79.9	

gages #24, #23, and #22). Another noticeable trend is that stress at the gages on the top of the flange (#10, #20, and #21) are much smaller than stresses at the corresponding gages on the bottom of the flange. This gives an indication of the stresses caused by localized bending of the curved flange, as these stresses add to the tensile stresses in the flange caused by overall bending of the beam on the bottom of the flange and subtract on the top of the flange.

Table 4.2 contains the maximum values of equivalent uniaxial stress calculated for each rosette using the Von Mises yield criterion. The location of the elements of these rosettes were shown previously in Figs. 2.5 and 2.6. The largest equivalent strain in this table occurs at the rosette which consists of gages #17, #18, and #19. This corresponds closely with the location where cracks initiated in the specimen.

In summary, the curved portion of the beams in the test specimen were subjected to higher stresses than predicted using normal beam analysis. The most important reasons for these increased stresses are the curvature of the beams, which creates flange forces which must be resisted by web stresses, and the asymmetry of the flanges which moves the component of the flange force out of the plane of the web, causing bending stresses in the web. These bending stresses caused the flange rolling which further increased stresses

in the beam web by reducing the effective cross section properties. A concentrated support to resist rolling was provided to the web by the cross member, resulting in a stress concentration. All cracks initiated in this area.

APPENDIX A

SPECIMEN DIMENSIONS, PROPERTIES, AND ANALYSIS RESULTS

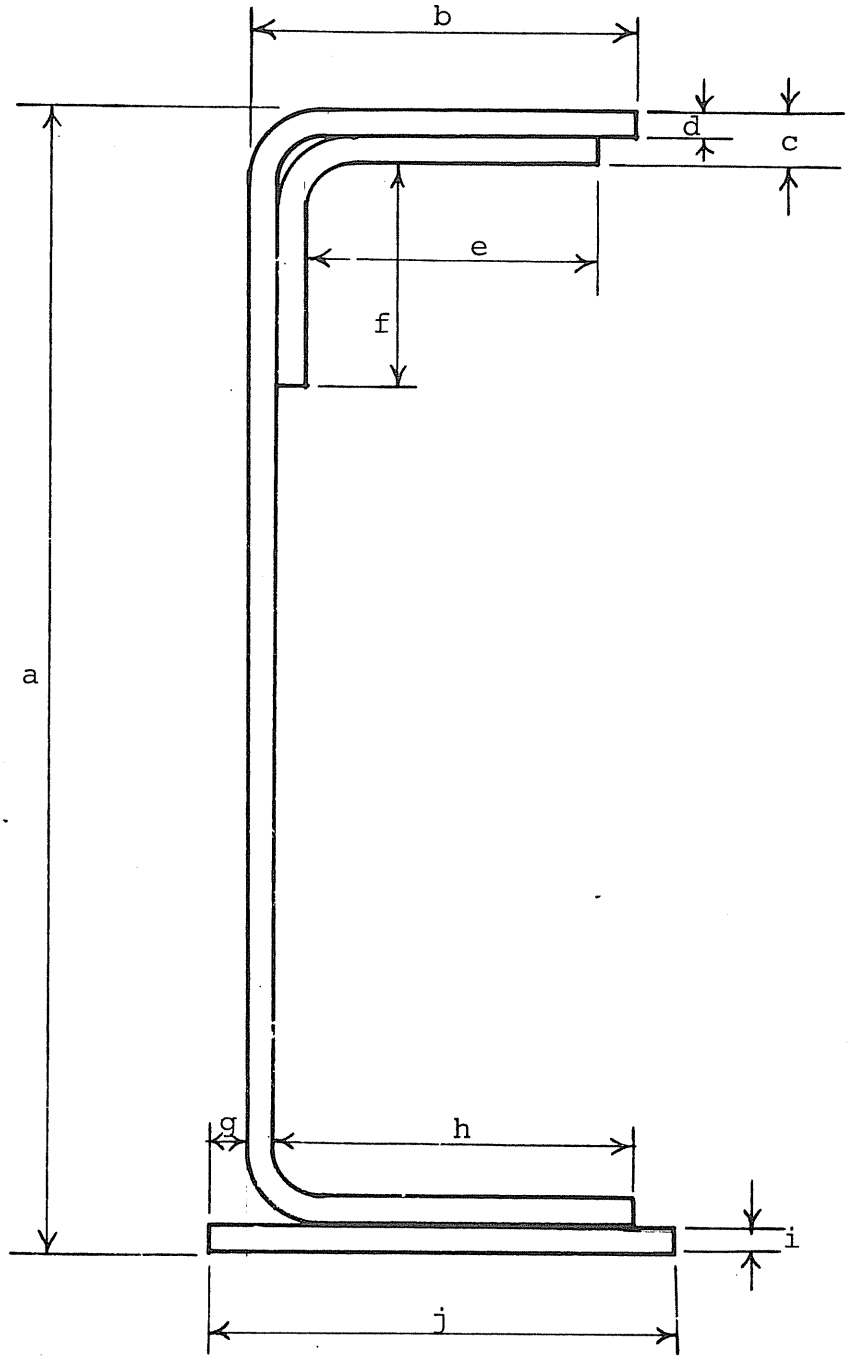

Figure A.1 Dimensions Measured at each Cross Section

Table A.1
Cross Section Dimensions

Cross Sect.	Dimensions (inches) a	b	c	d	e	f	g	h	i	j
1	10.75	3.5	0.603	0.329	1.875	1.875	0.25	3.125	0.385	3.954
2	10.75	3.5	0.588	0.334	2.0	2.0	0.25	3.063	0.385	4.022
3	10.5	3.5	0.601	0.34	2.0	0.75	0.25	3.063	0.376	4.03
4	13.063	3.5	0.61	0.336	2.0	2.0	0.25	3.25	0.375	3.938
5	14.438	3.375	0.596	0.329	2.0	0.75	0.296	3.313	0.363	3.9375
6	16.875	3.375	0.596	0.334	2.125	2.0	0.25	3.125	0.383	3.9375
7	17.75	3.375	0.594	0.335	2.125	1.875	0.25	3.0	0.367	3.875
8	18.313	3.375	0.592	0.314	2.125	2.0	0.25	3.125	0.368	3.9375
9	18.313	3.5	0.62	6.33	2.125	2.0	0.25	3.25	0.375	3.9375
10	18.438	3.5	0.647	0.335	2.13	2.0	0.25	3.25	0.378	3.9375
11	16.125	3.5	0.682	0.337	2.0	2.0	0.25	3.25	0.374	3.9375
12	13.75	3.5	0.627	0.735	2.125	2.0	0.25	3.25	0.372	3.9375
13	11.25	3.5	0.337	0.337	0	0	0.25	3.375	0.384	3.96

Table A.2
Cross Section Properties

Cross Section	Area $(in)^2$	Centroid* (in)	Moment of Inertia (in^4)
1	7.98	5.059	141.7
2	8.05	5.042	142.3
3	7.73	4.808	131.6
4	8.94	6.235	229.6
5	8.83	6.659	272.8
6	10.10	8.077	416.9
7	10.25	8.573	461.3
8	10.13	8.874	490.9
9	10.71	8.934	518.9
10	10.95	9.047	538.4
11	10.34	7.995	397.7
12	9.26	6.661	263.2
13	7.45	4.407	131.8

*From Bottom of section

Table A.3
Stiffness Analysis Results

(Load = 1.0 kips)

Member	Connecting Sections	Axial Load (kips)	Shear (kips)	Moment (k-ft)
1	1	-0.01	-0.69	0.0
	2	0.01	0.69	-0.69
2	2	0.0	-0.69	0.69
	3	0.0	0.69	-2.74
3	3	0.01	-0.69	2.74
	4	-0.01	0.36	-3.61
4	4	0.06	-0.36	3.61
	5	-0.06	0.36	-3.86
5	5	0.19	-0.31	3.86
	6	-0.19	0.31	-4.08
6	6	0.25	-0.27	4.08
	7	-0.25	0.27	-4.28
7	7	0.11	-0.35	4.28
	8	-0.11	0.35	-4.62
8	8	0.0	-0.36	4.62
	9	0.0	-0.31	-3.81
9	9	0.0	0.31	3.81
	10	0.0	-0.31	-1.92
10	10	0.02	0.31	1.92
	11	-0.02	-0.31	-1.29
11	11	0.02	0.31	1.29
	12	-0.02	-0.31	-0.66
12	12	0.0	0.31	0.66
	13	0.0	-0.31	0.0

APPENDIX B

STATIC TEST RESULTS

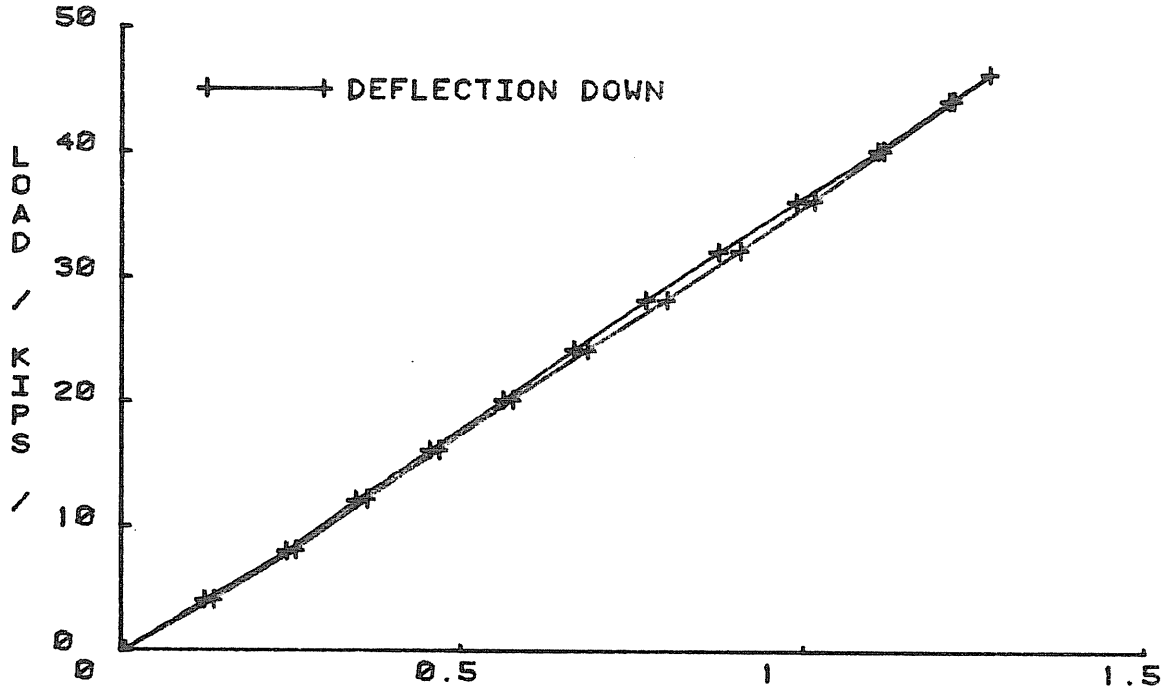

Figure B.1 HALLIBURTON FRAME

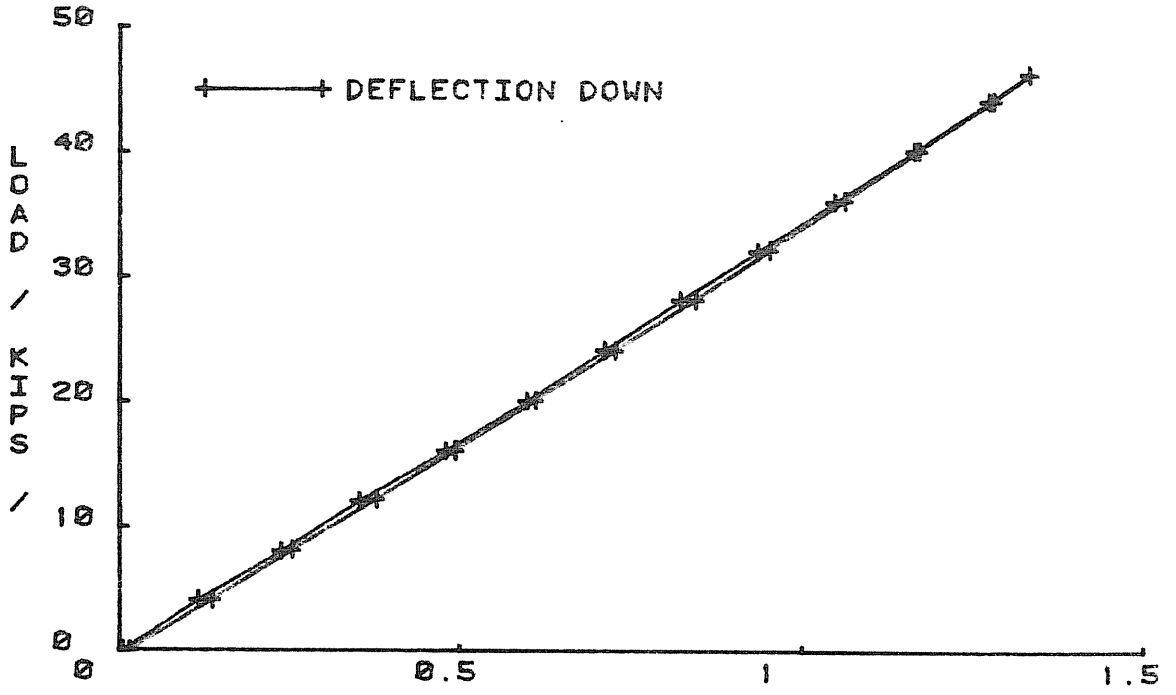

Figure B.2 HALLIBURTON FRAME

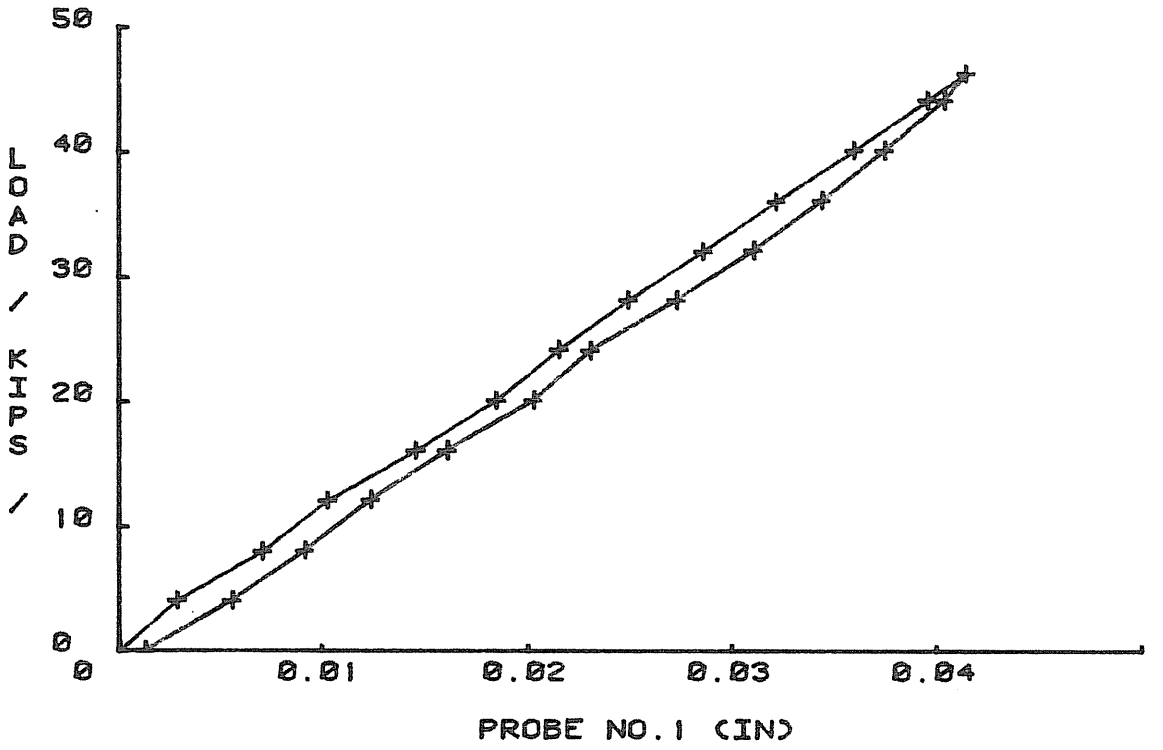

Figure B.3 HALLIBURTON FRAME

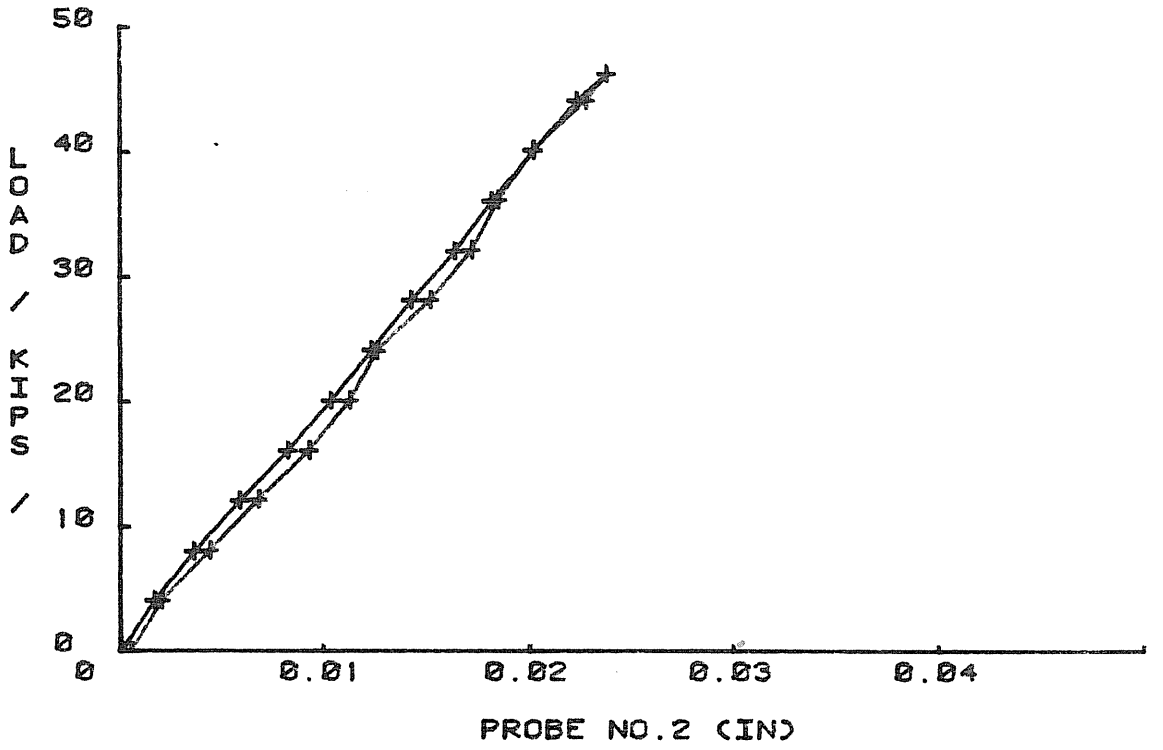

Figure B.4 HALLIBURTON FRAME

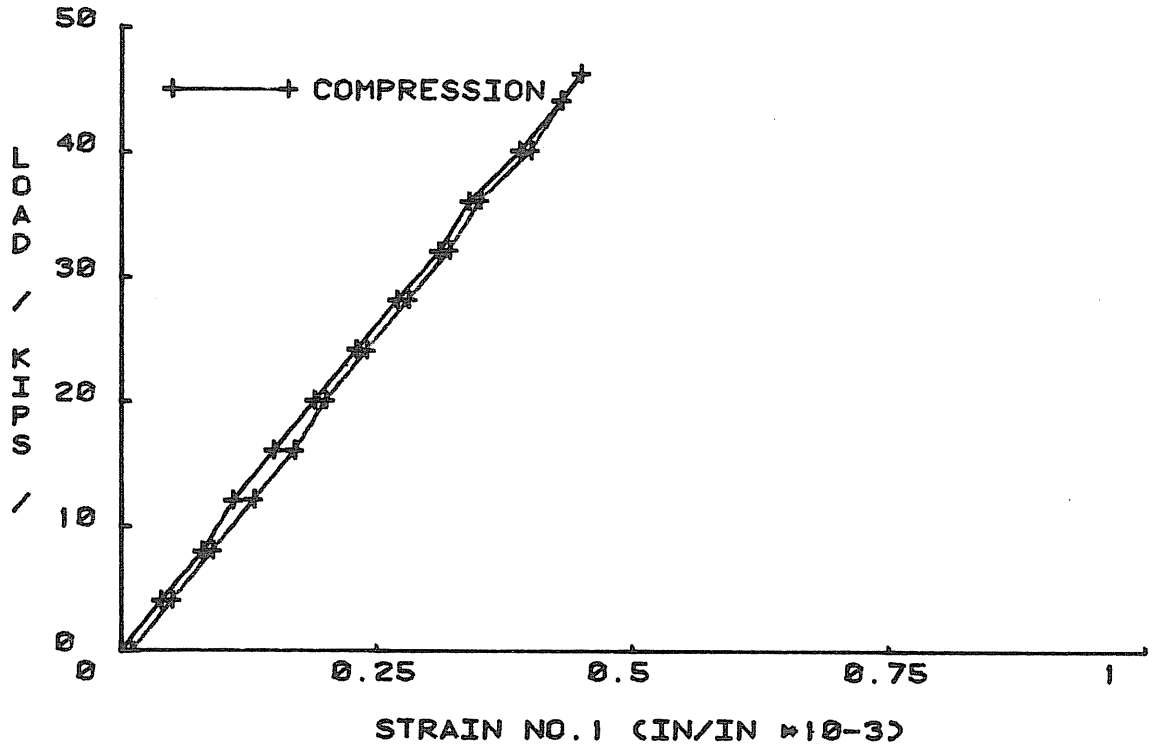

Figure B.5 HALLIBURTON FRAME

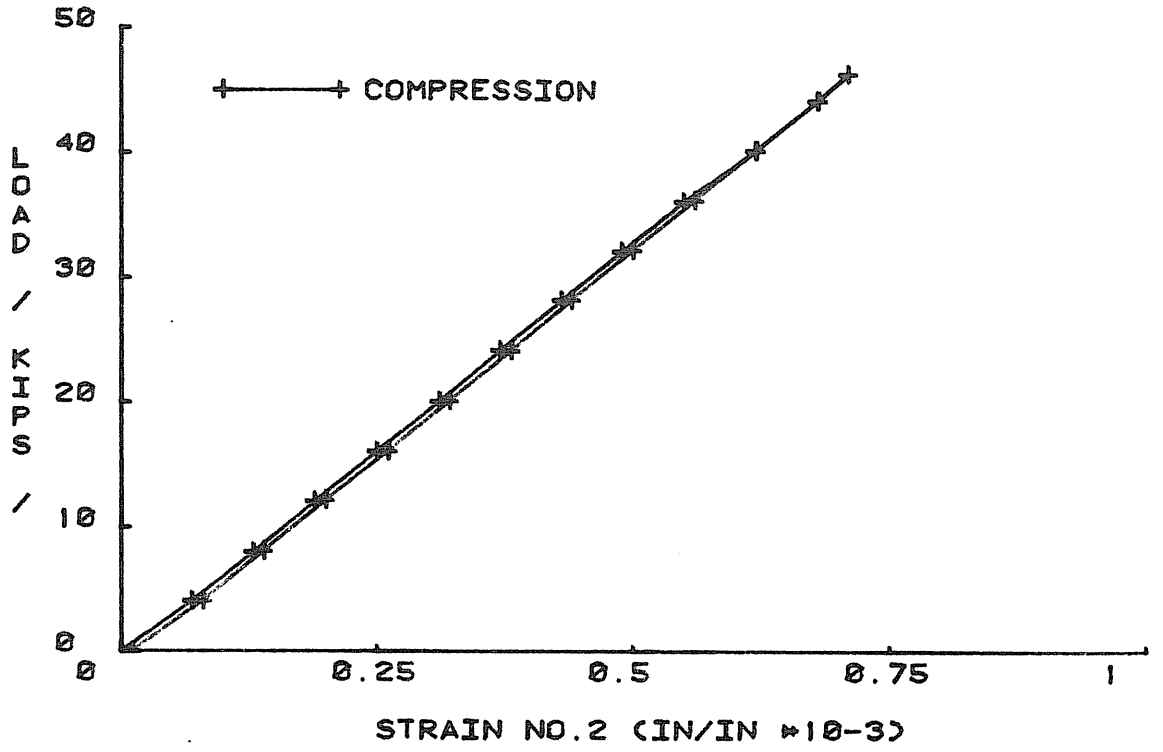

Figure B.6 HALLIBURTON FRAME

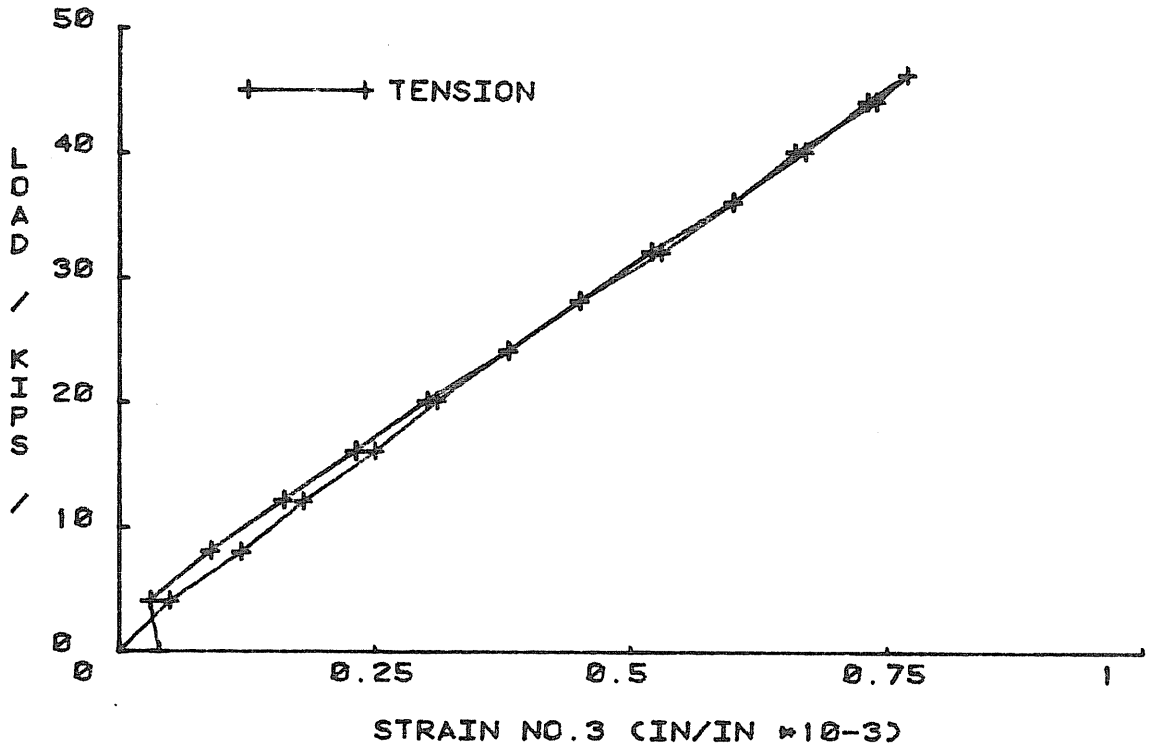

Figure B.7 HALLIBURTON FRAME

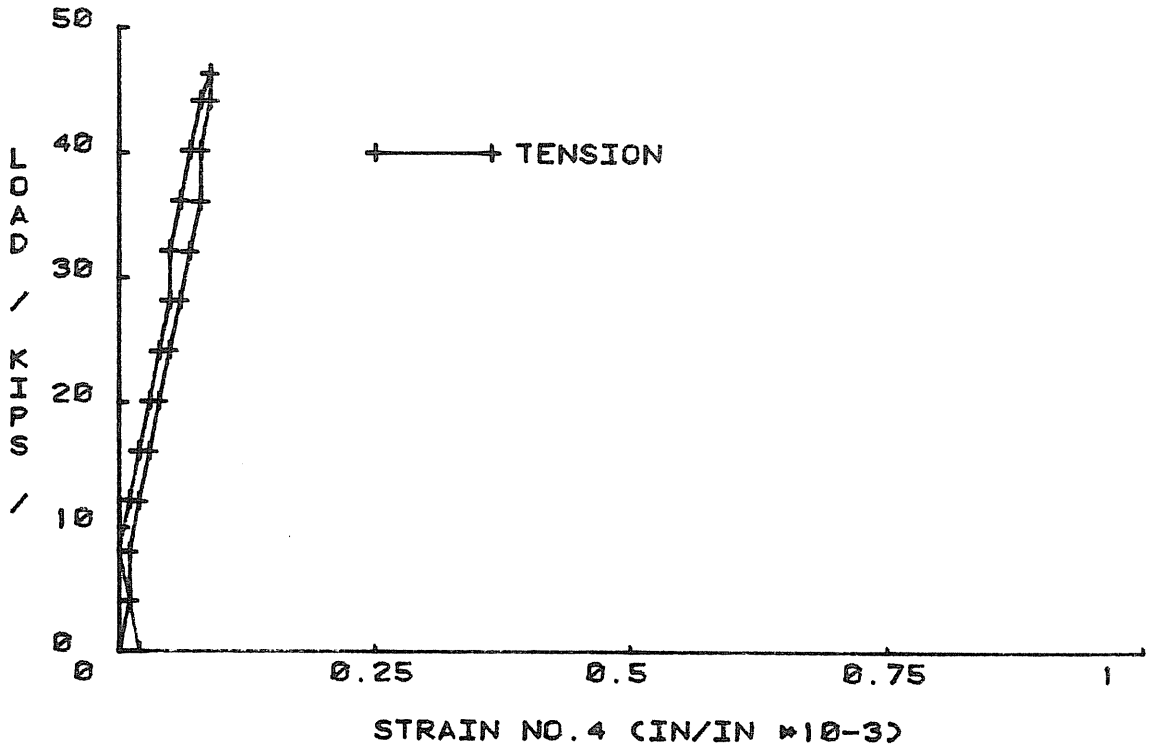

Figure B.8 HALLIBURTON FRAME

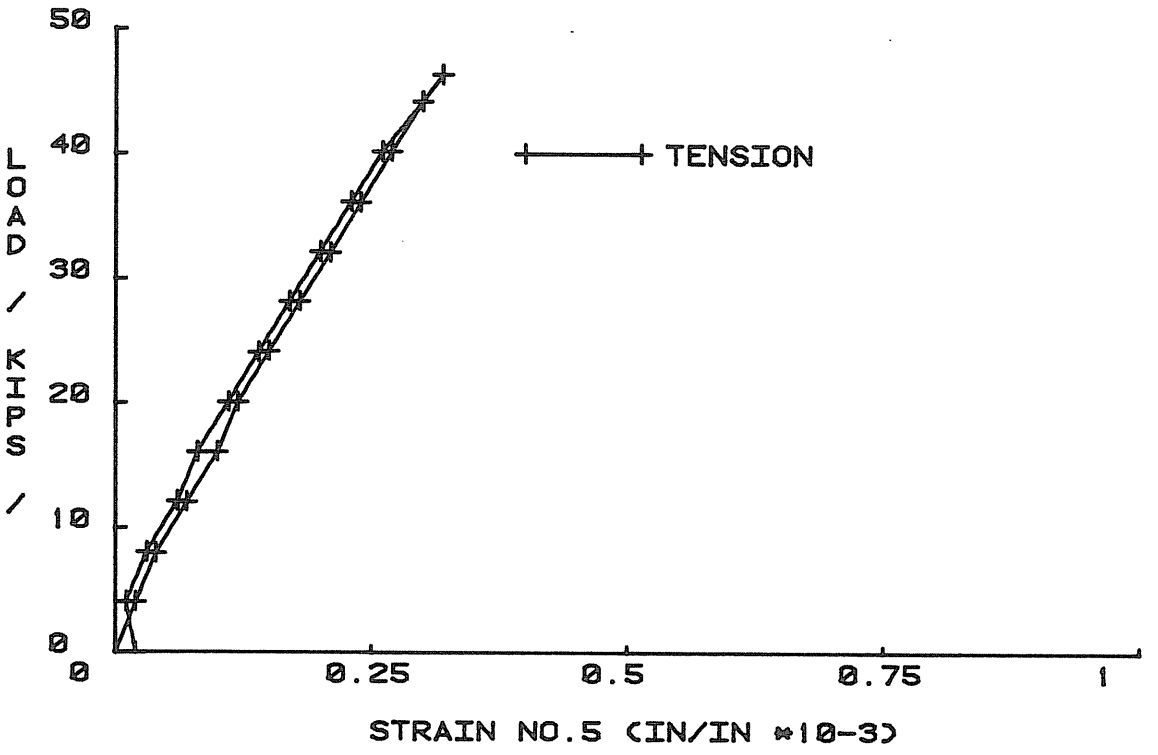

Figure B.9 HALLIBURTON FRAME

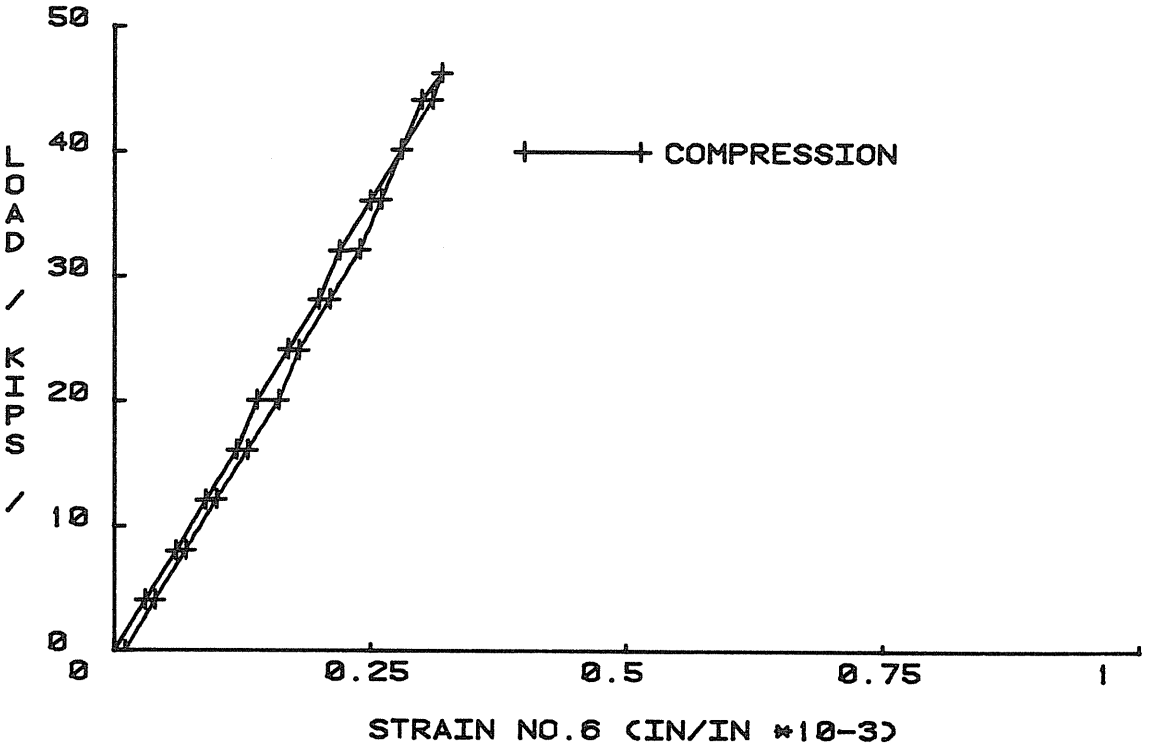

Figure B.10 HALLIBURTON FRAME

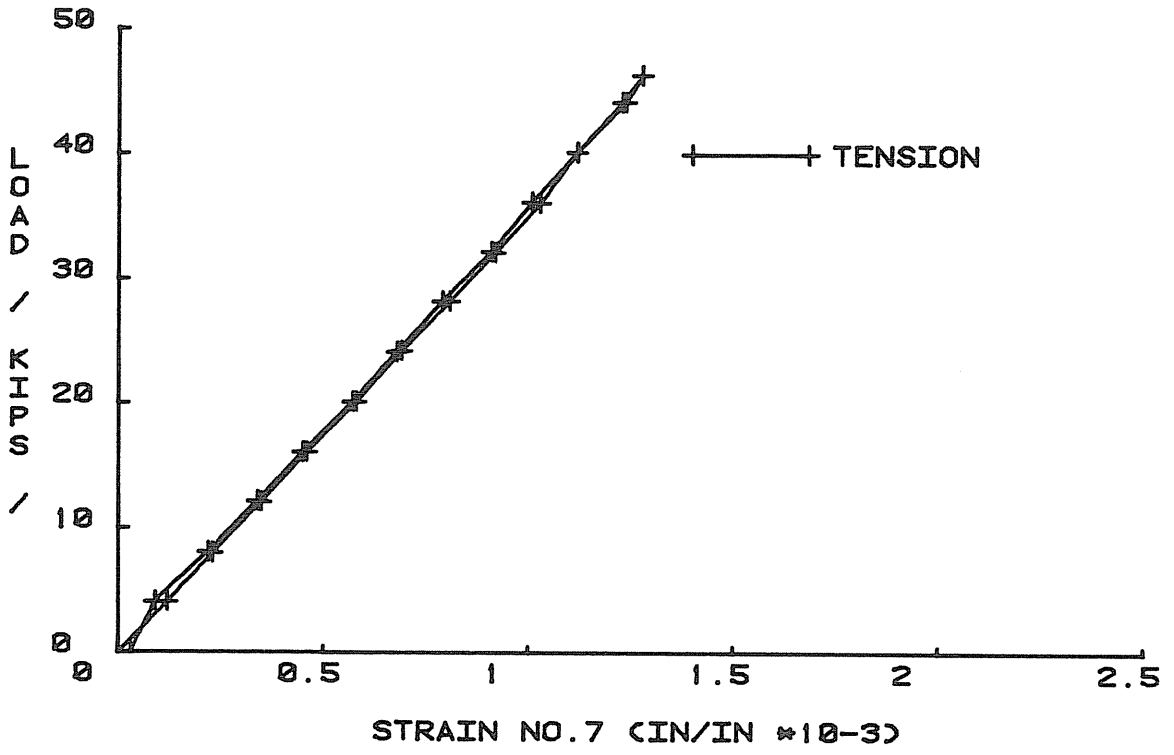

Figure B.11 HALLIBURTON FRAME

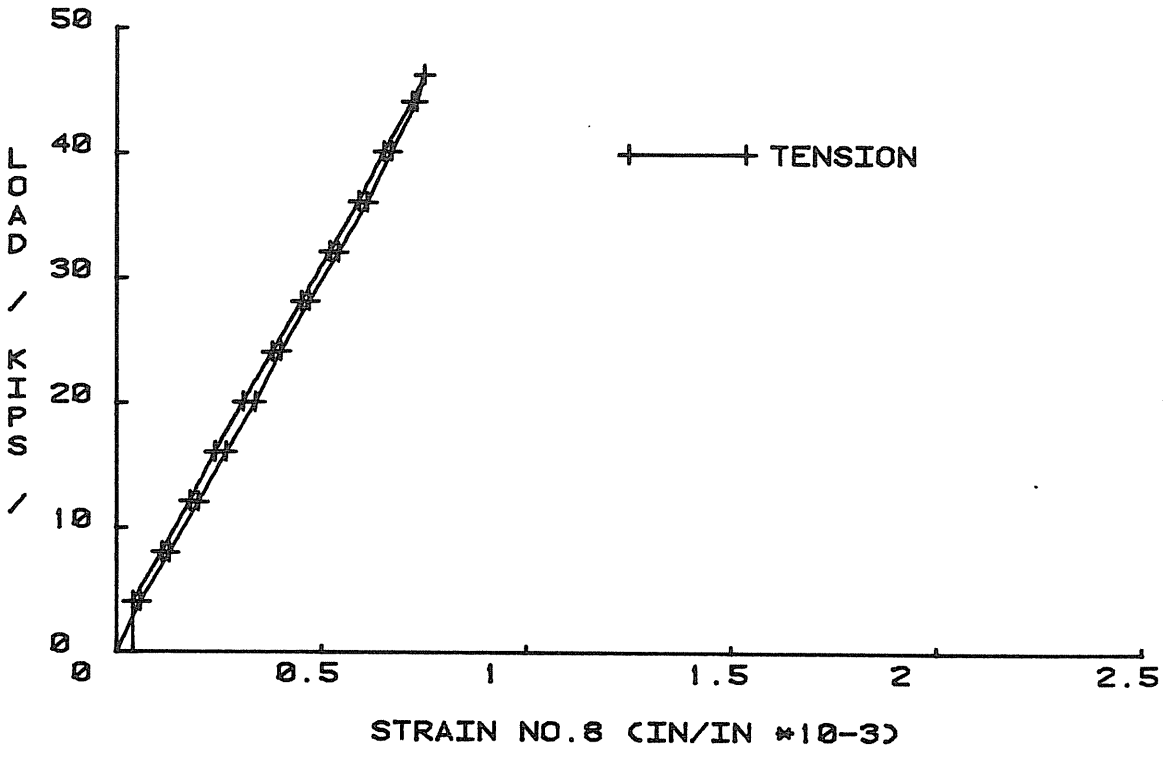

Figure B.12 HALLIBURTON FRAME

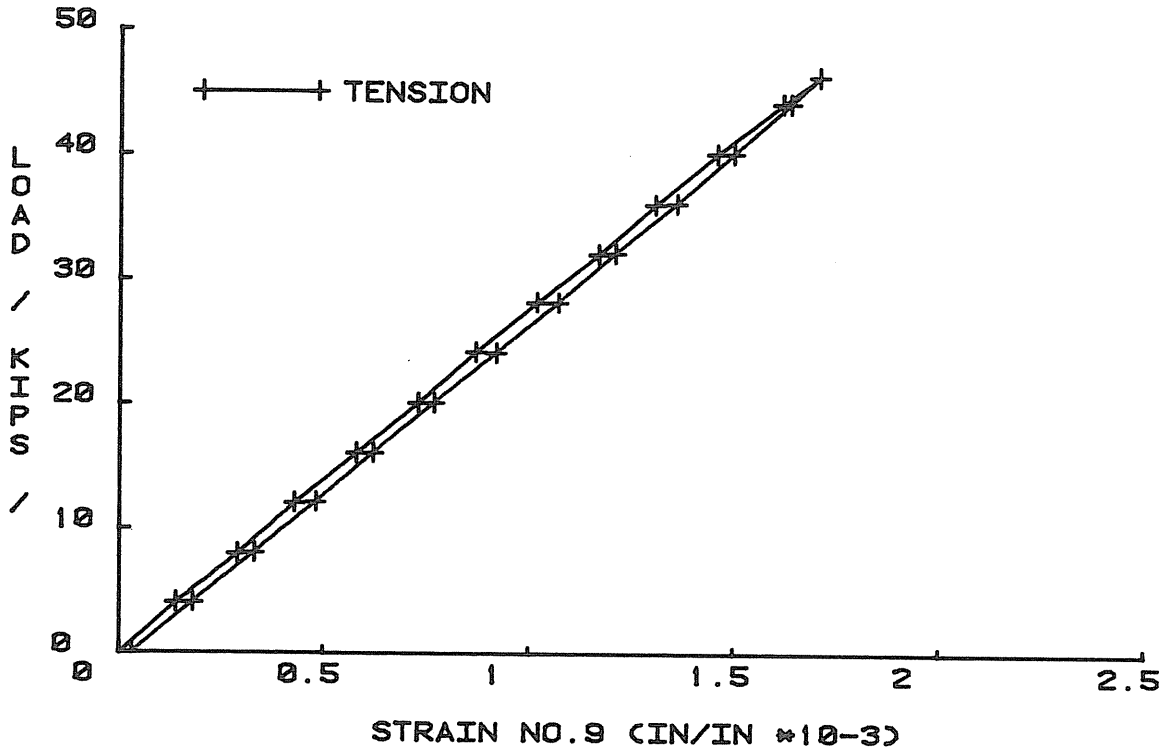

Figure B.13 HALLIBURTON FRAME

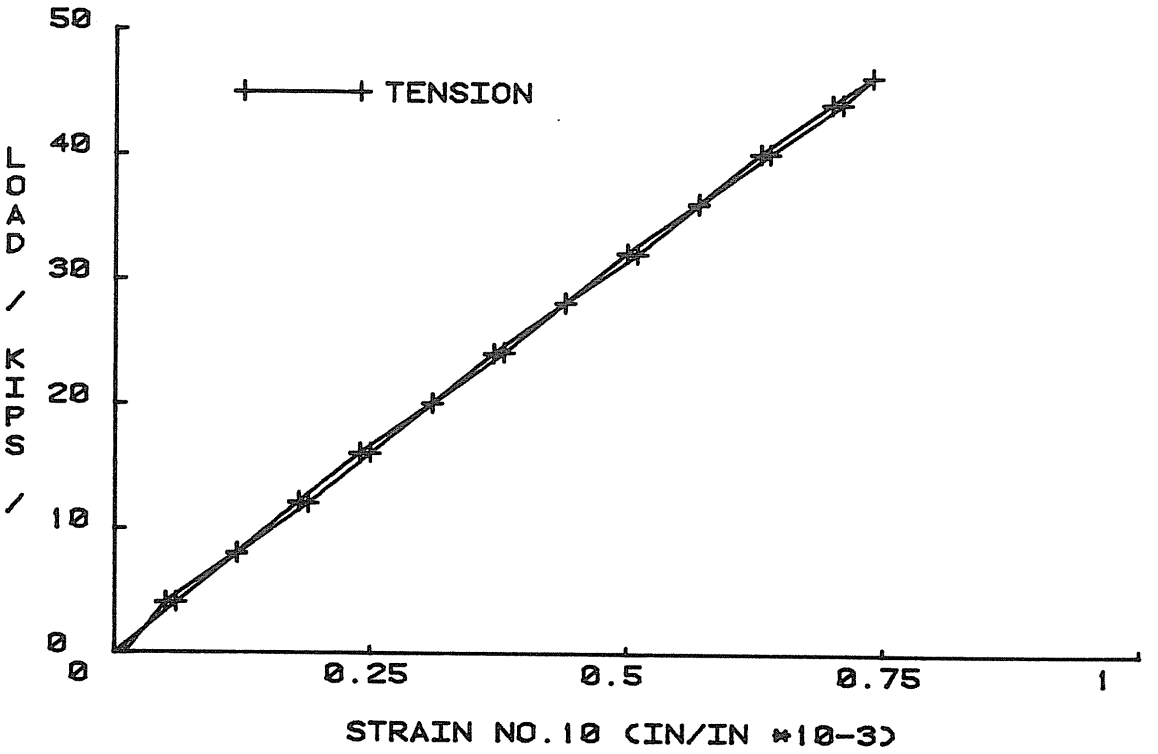

Figure B.14 HALLIBURTON FRAME

Corrected 10-21-85

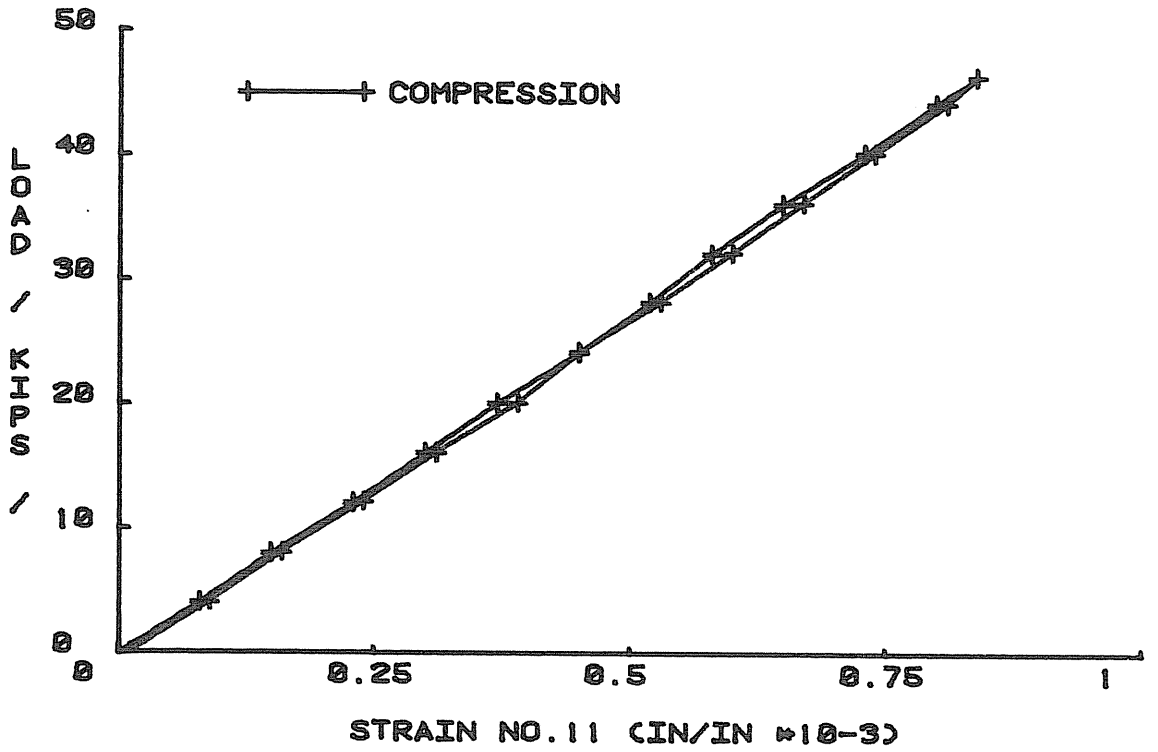

Figure B.15 HALLIBURTON FRAME

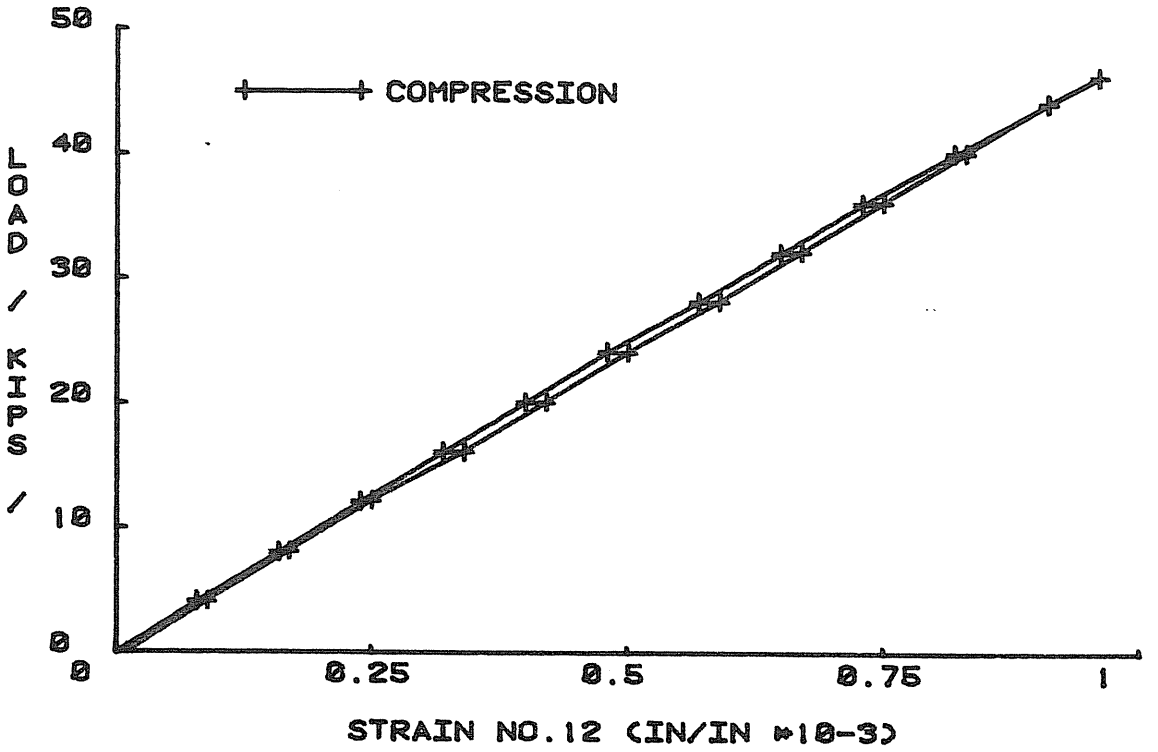

Figure B.16 HALLIBURTON FRAME

corrected 10-21-85

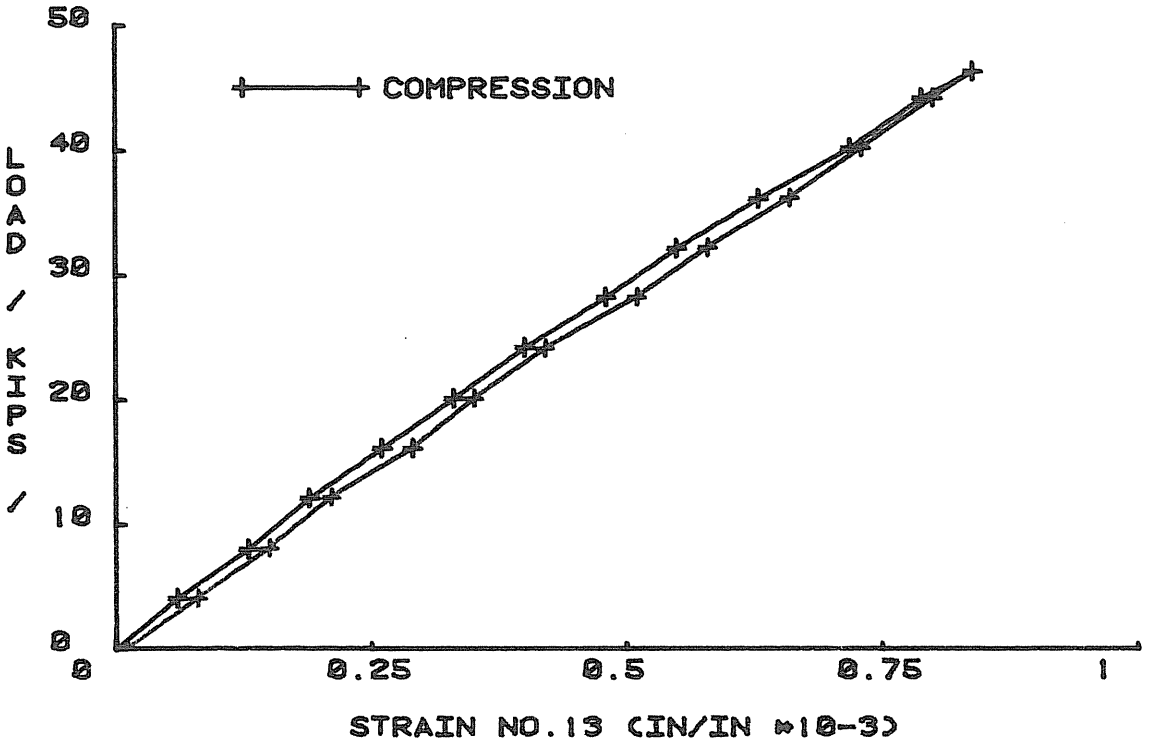

Figure B.17 HALLIBURTON FRAME

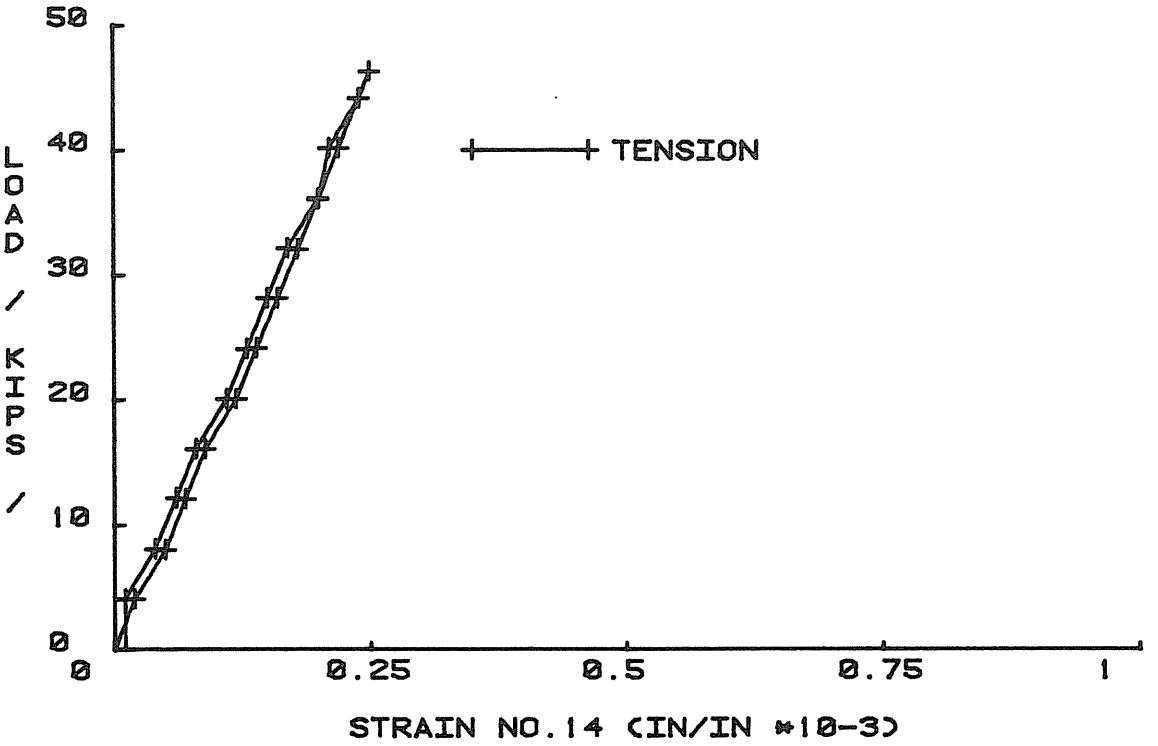

Figure B.18 HALLIBURTON FRAME

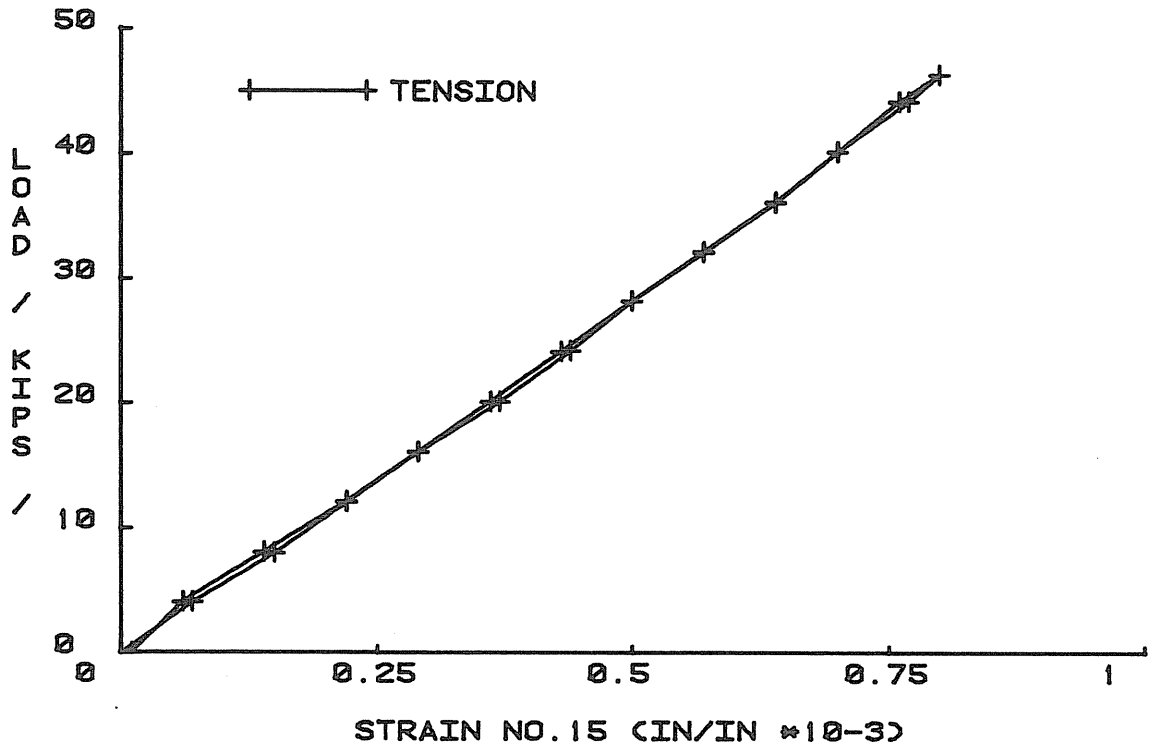

Figure B.19 HALLIBURTON FRAME

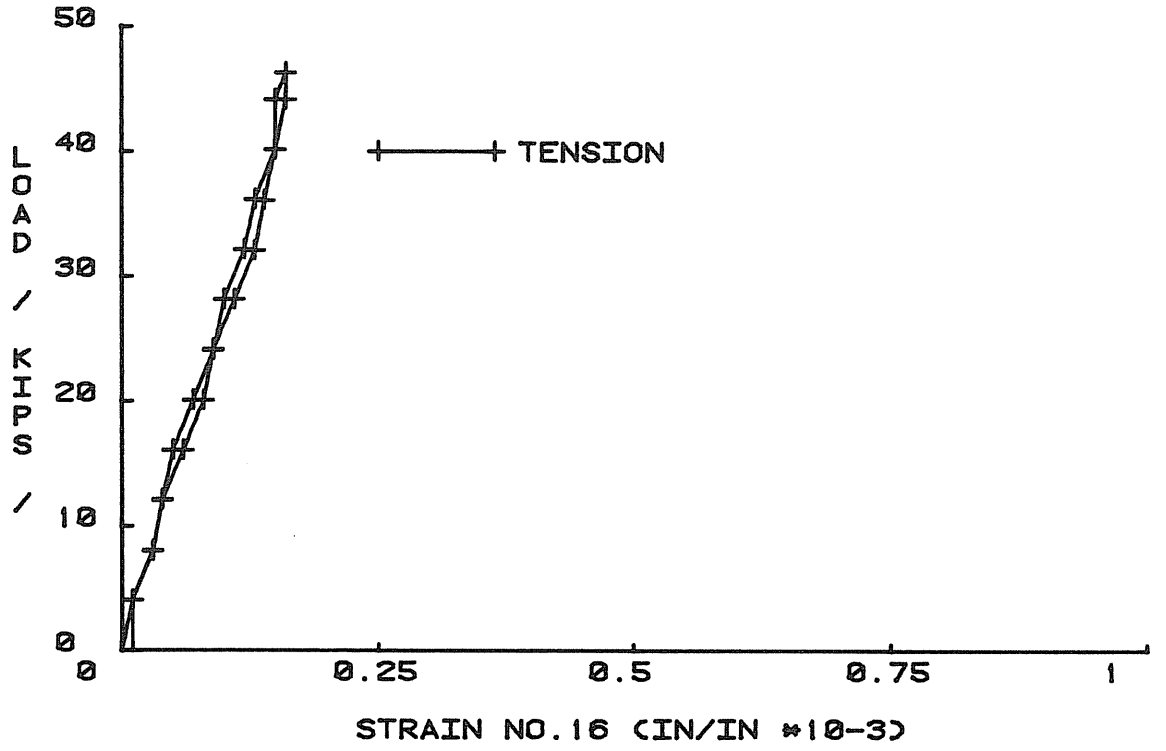

Figure B.20 HALLIBURTON FRAME

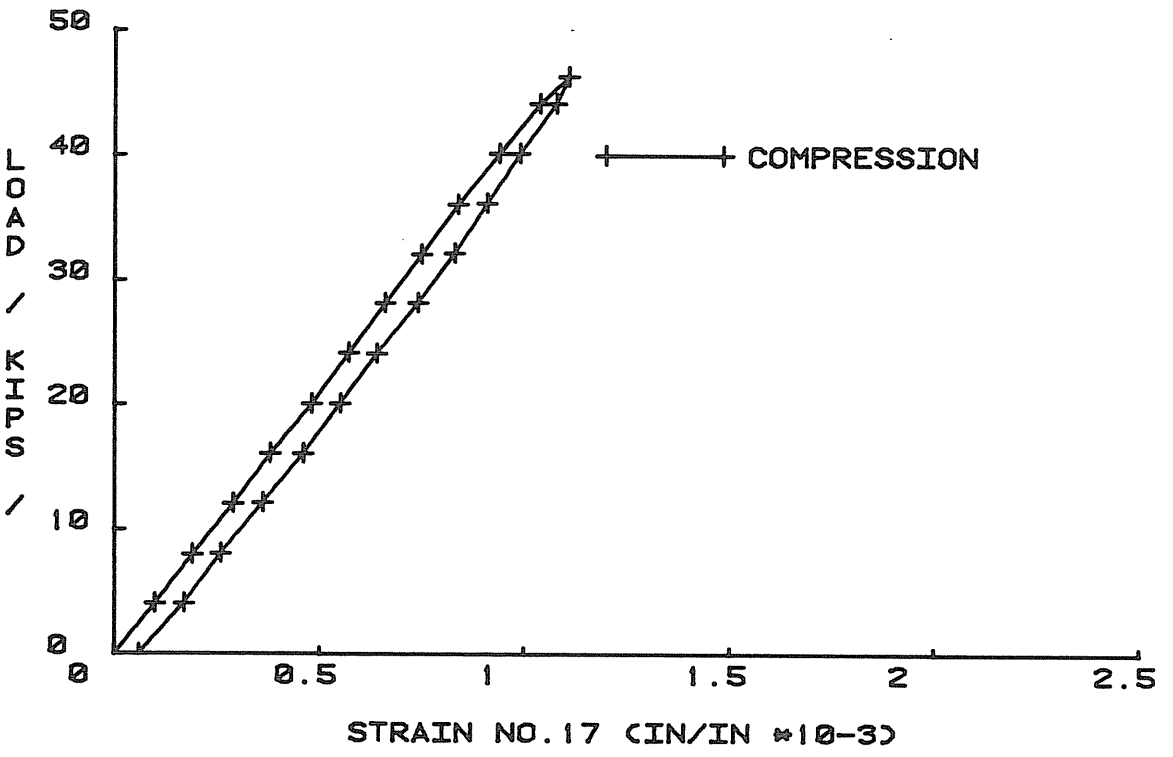

Figure B.21 HALLIBURTON FRAME

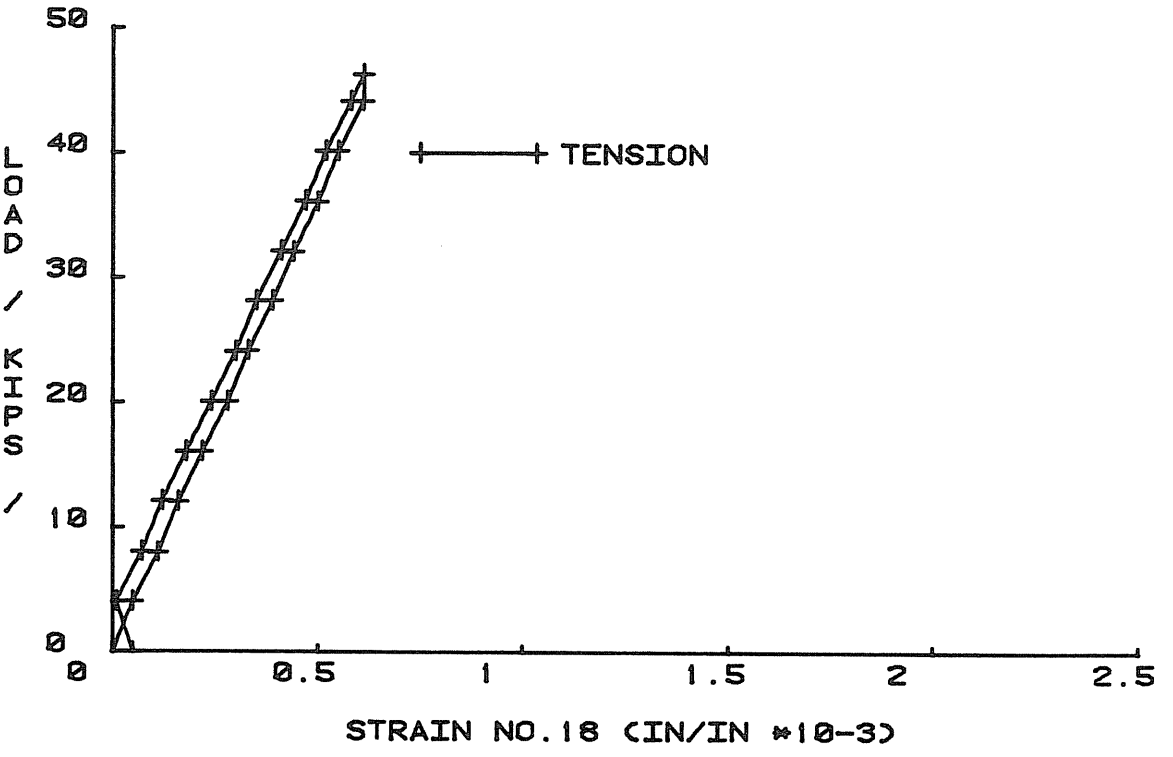

Figure B.22 HALLIBURTON FRAME

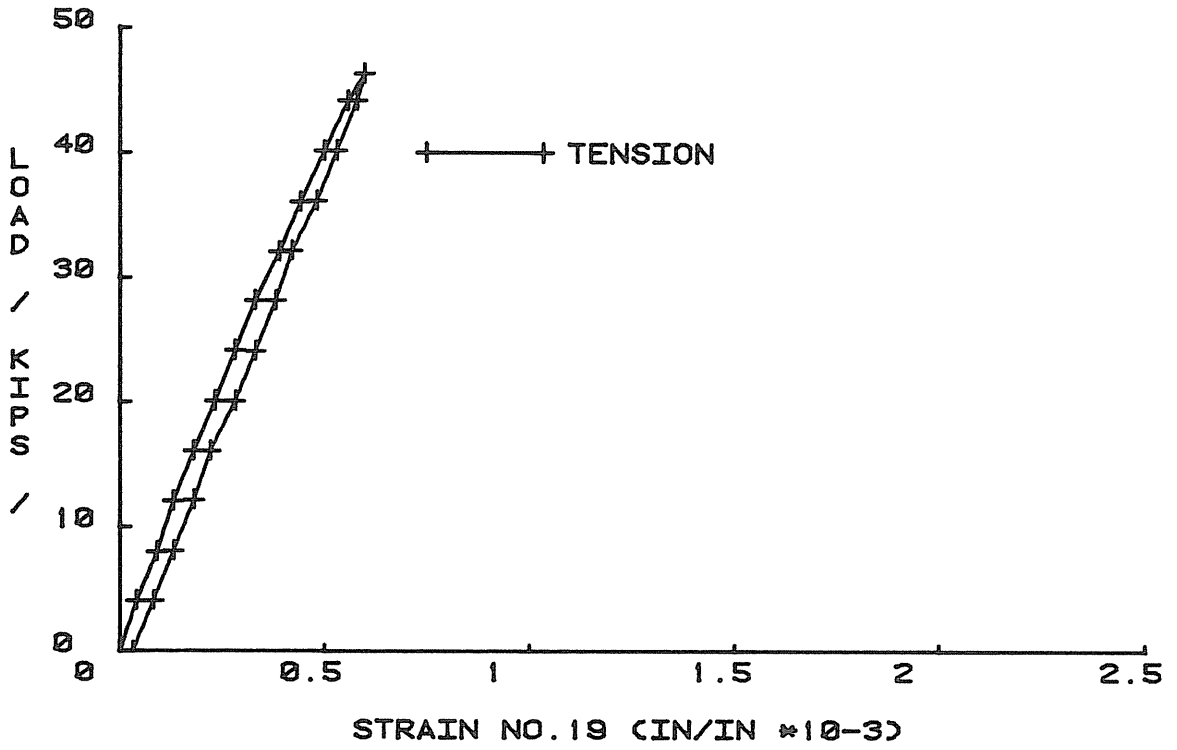

Figure B.23 HALLIBURTON FRAME

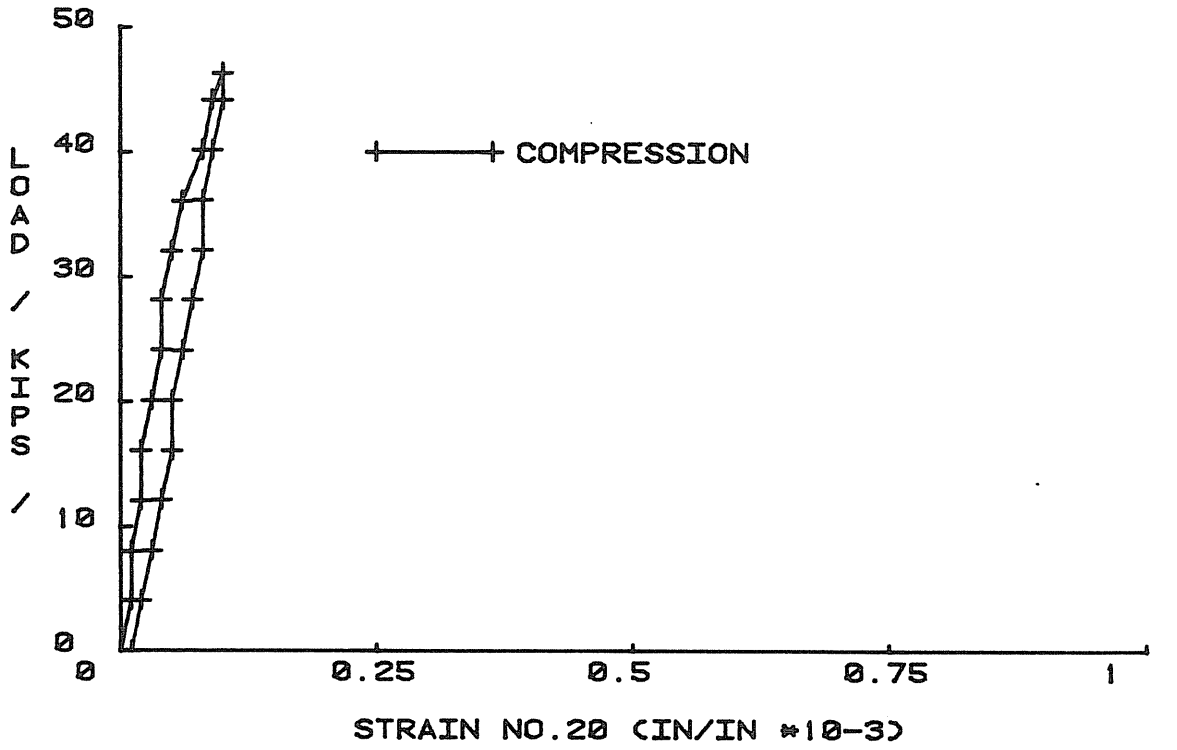

Figure B.24 HALLIBURTON FRAME

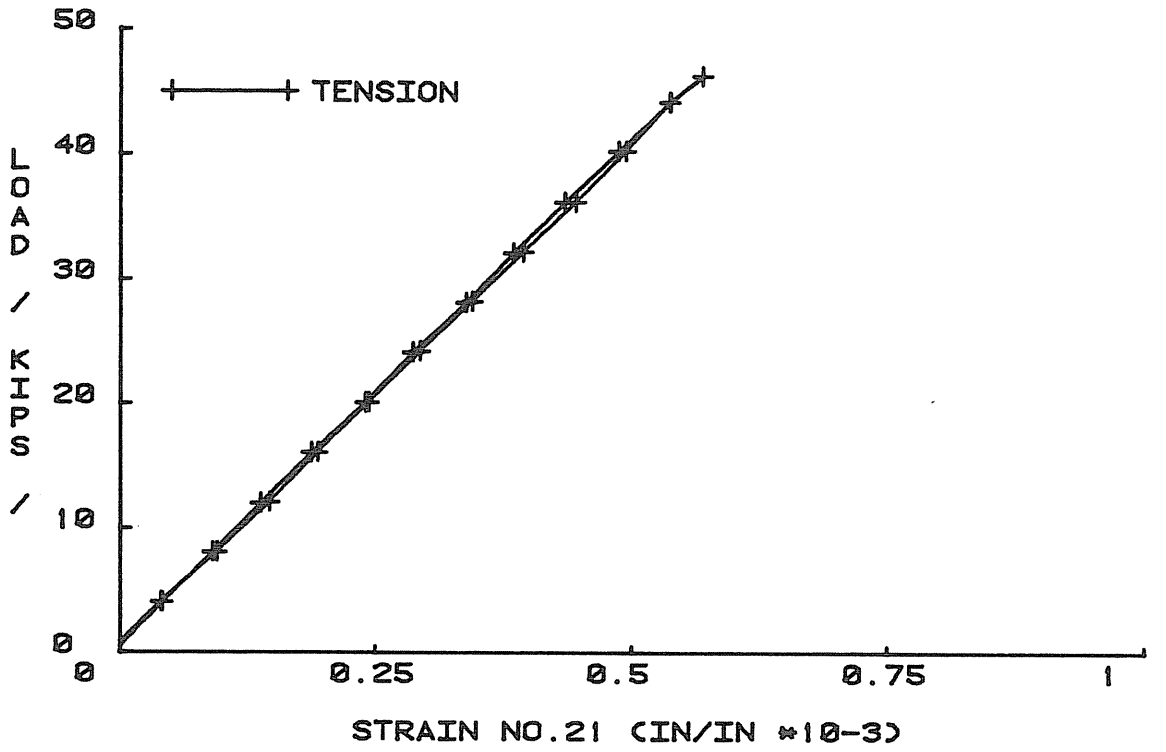

Figure B.25 HALLIBURTON FRAME

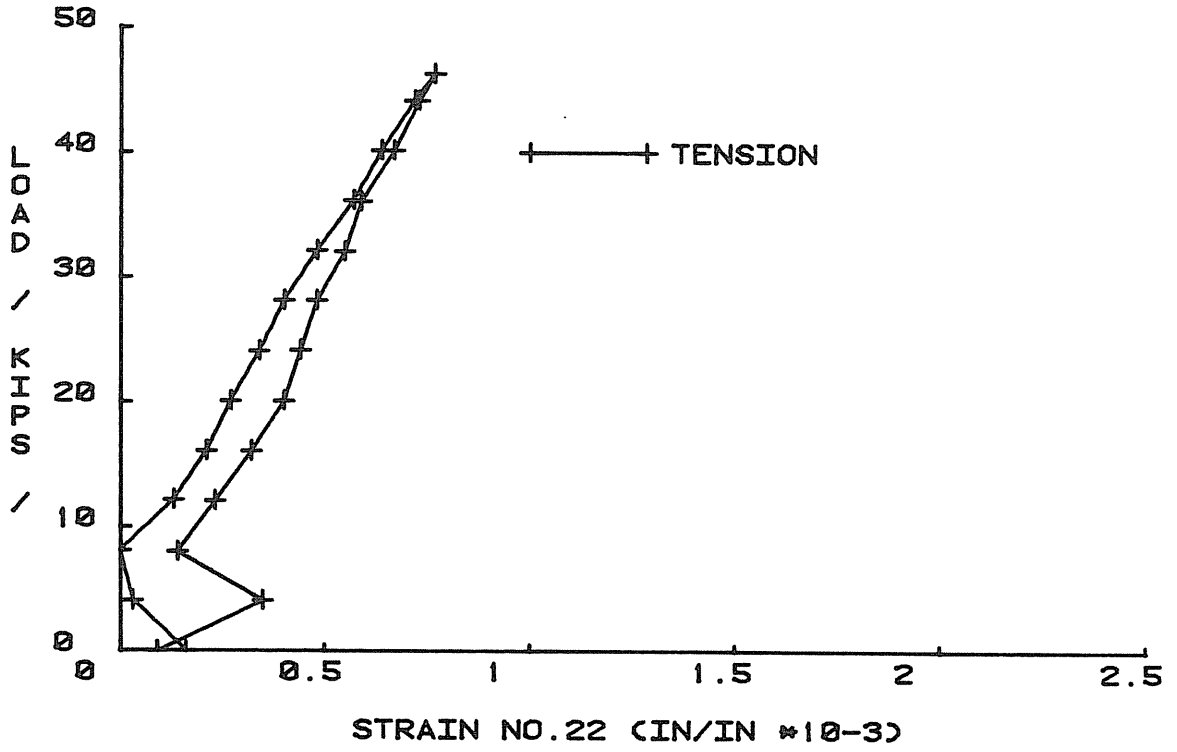

Figure B.26 HALLIBURTON FRAME

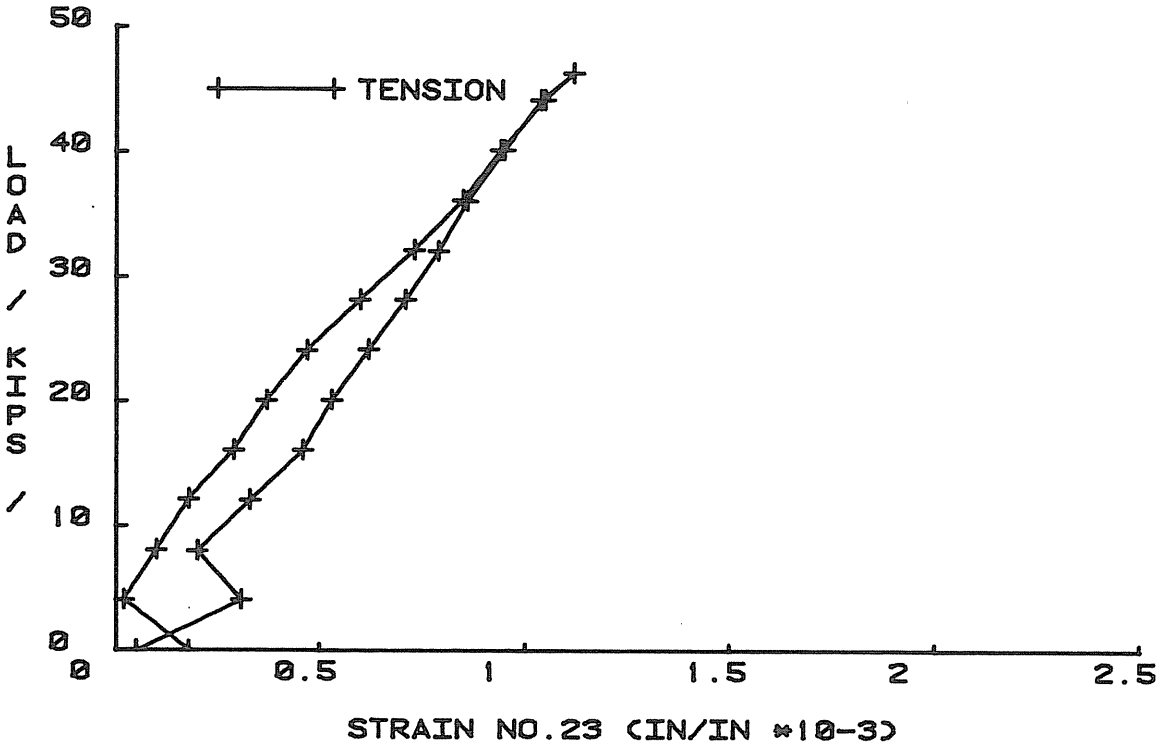

Figure B.27 HALLIBURTON FRAME

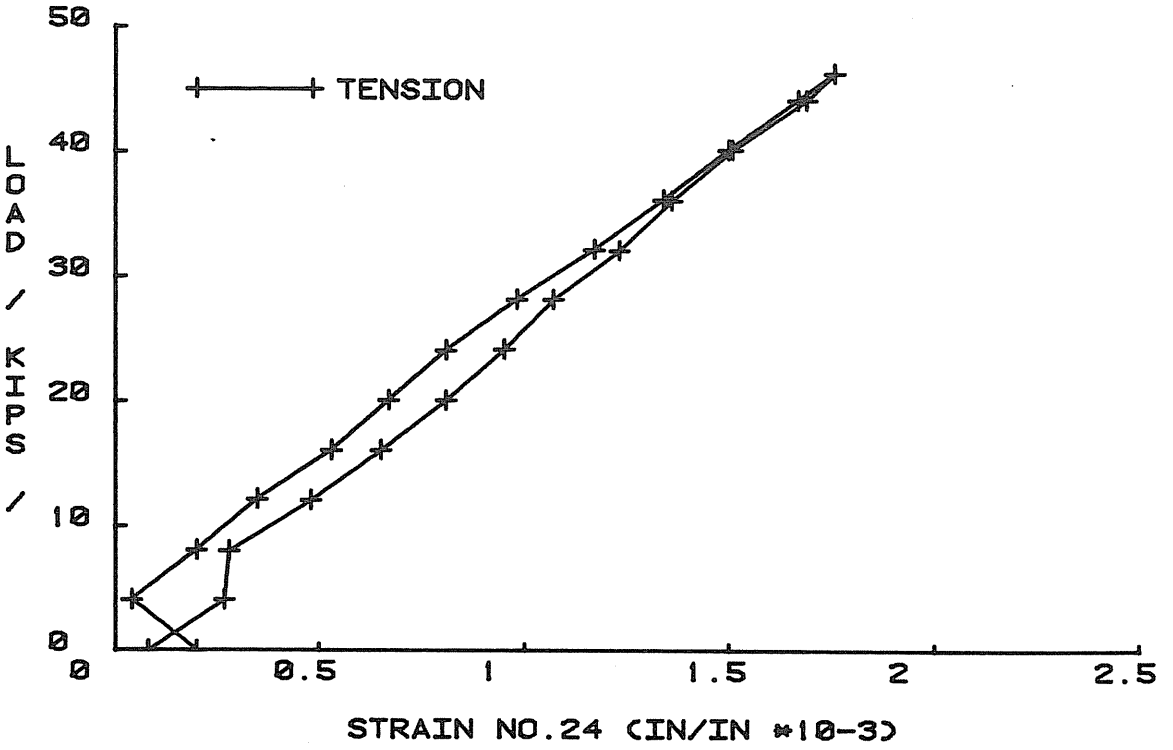

Figure B.28 HALLIBURTON FRAME

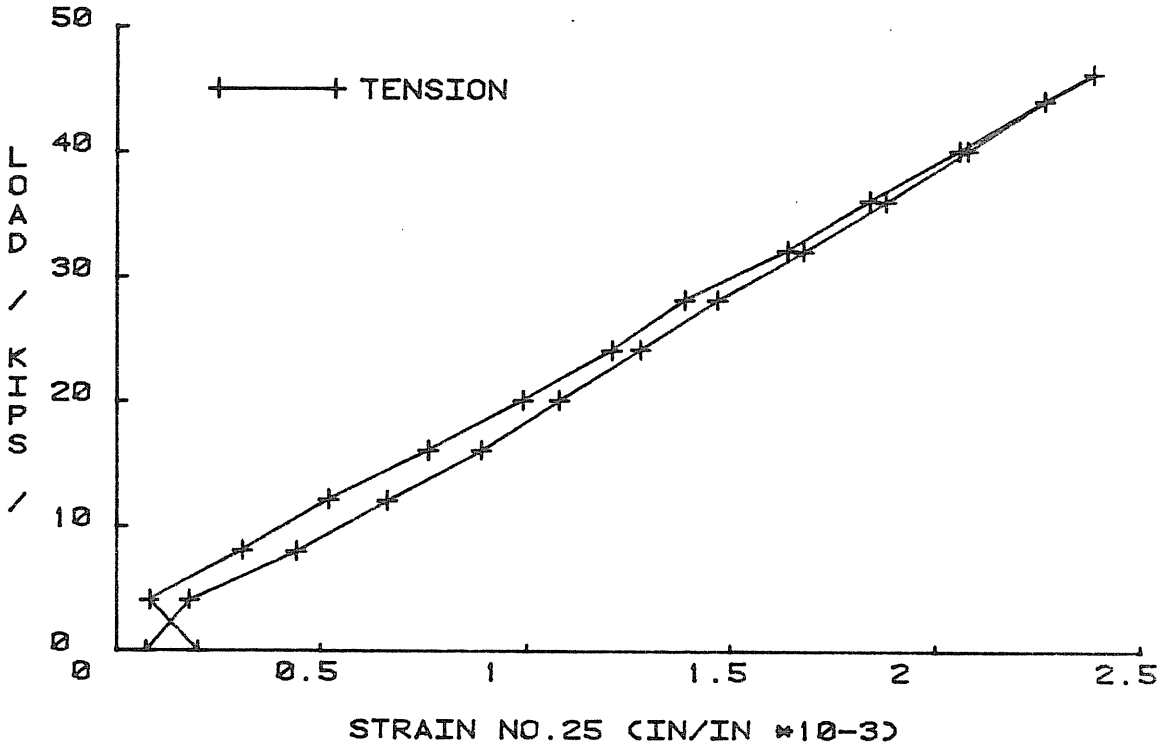

Figure B.29 HALLIBURTON FRAME

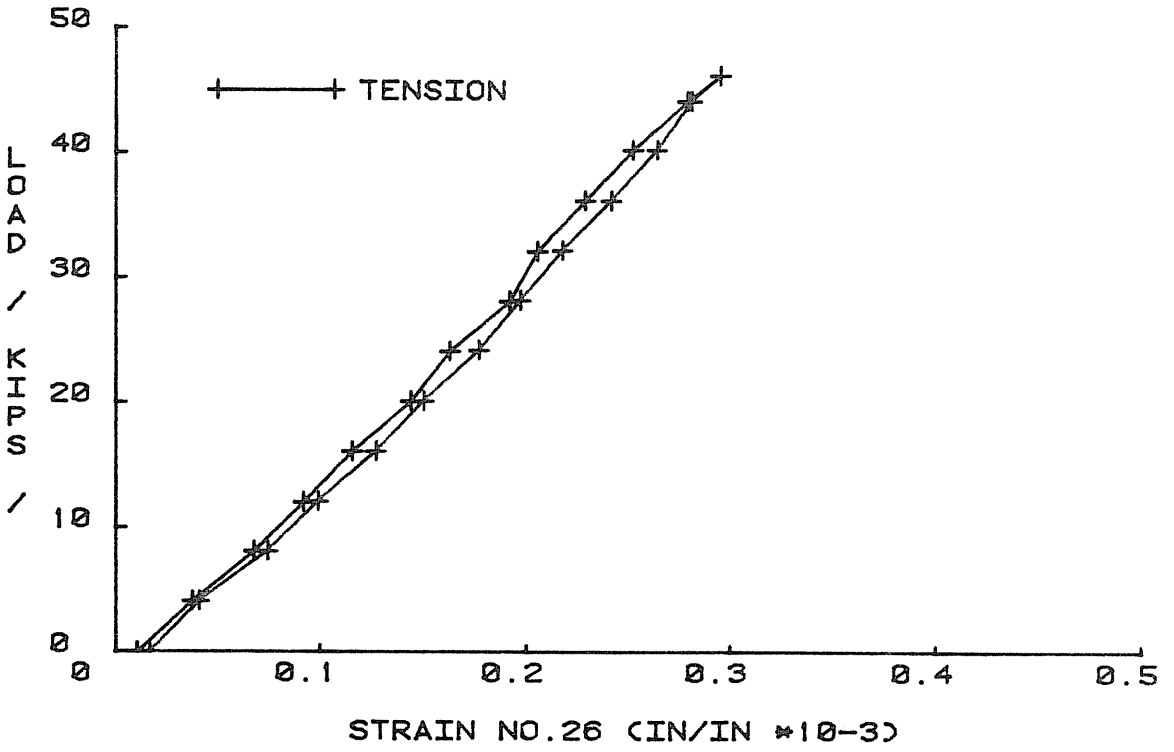

Figure B.30 HALLIBURTON FRAME

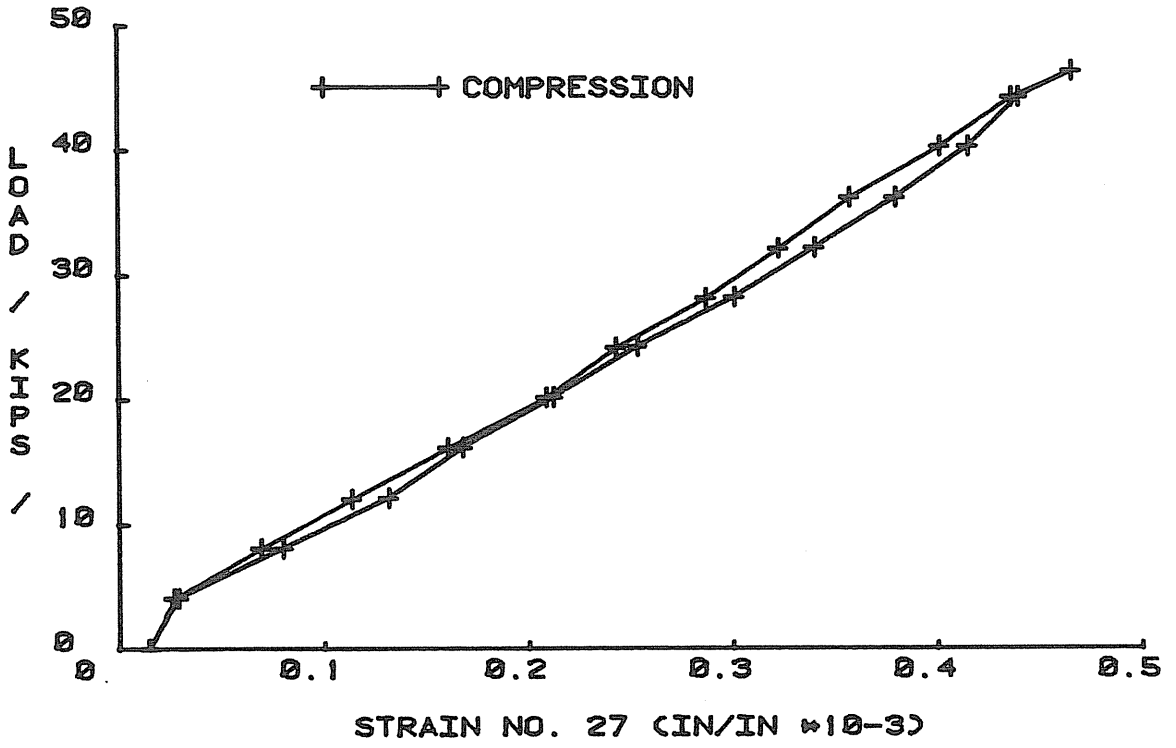

Figure B.31 HALLIBURTON FRAME

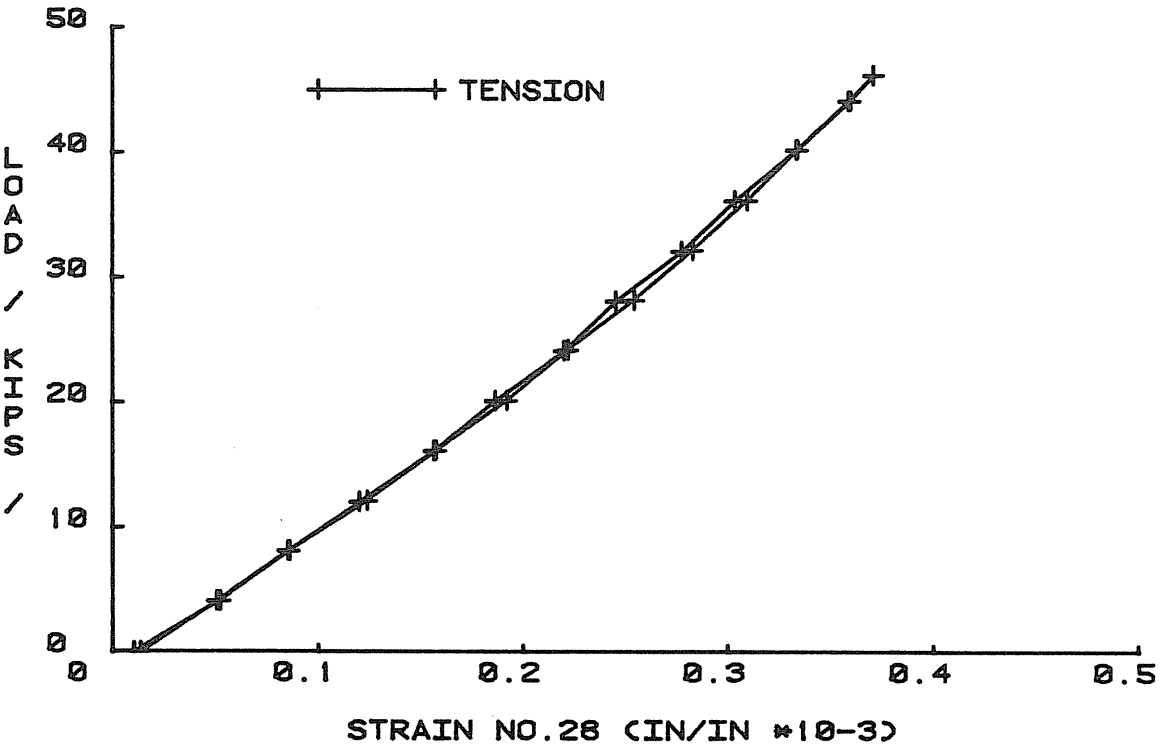

Figure B.32 HALLIBURTON FRAME

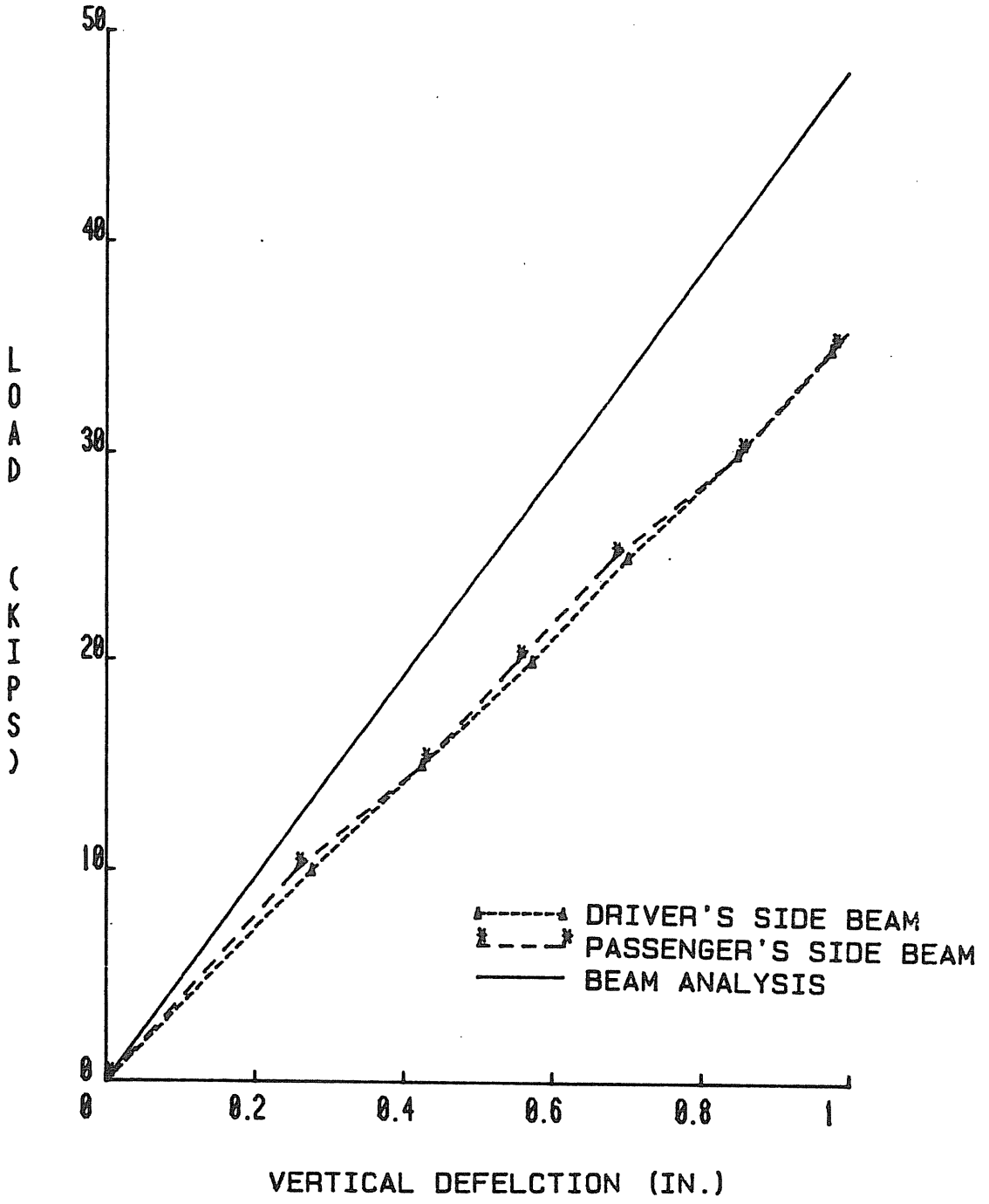
50
40
30
20
10
0
LOAD (KIPS)
0
0.2
0.4
0.6
0.8
1
VERTICAL DEFELCTION (IN.)
DRIVER'S SIDE BEAM
PASSENGER'S SIDE BEAM
BEAM ANALYSIS

Figure B.33

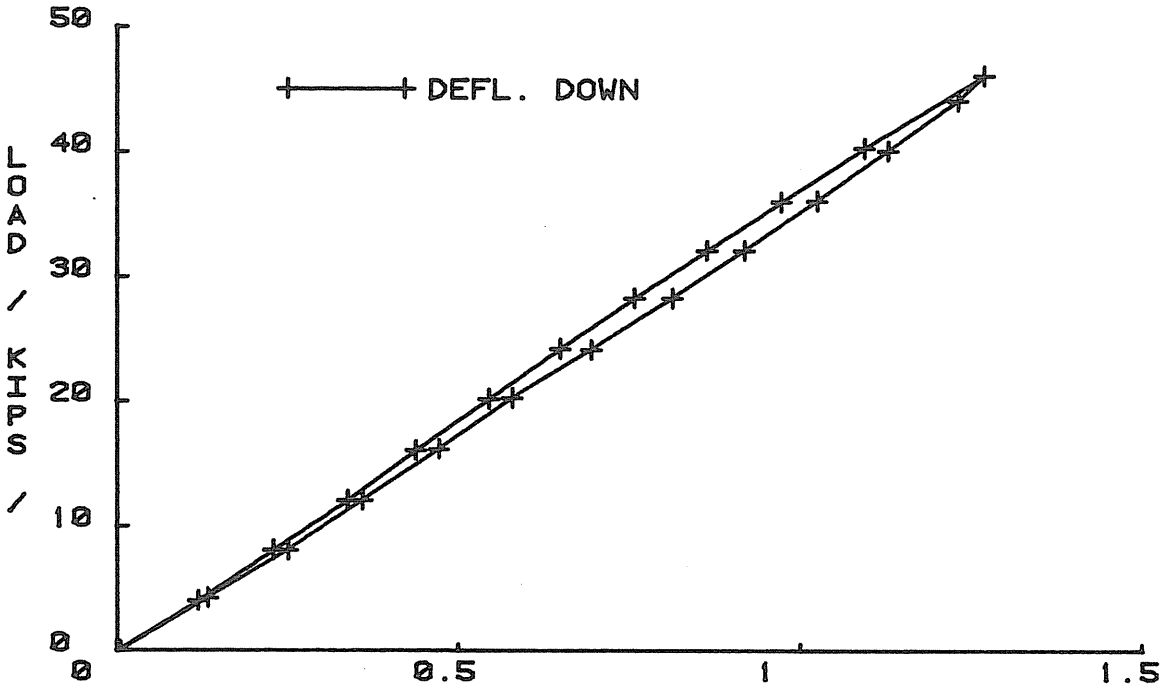

Figure B.34 REINFORCED FRAME

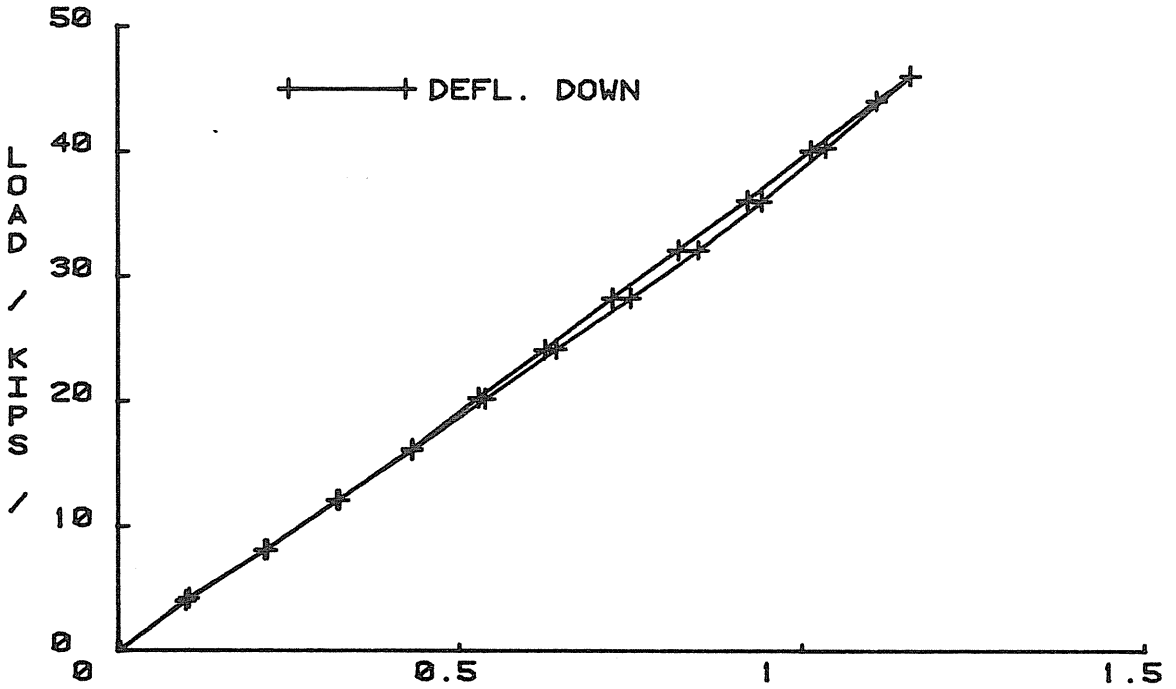

Figure B.35 REINFORCED FRAME

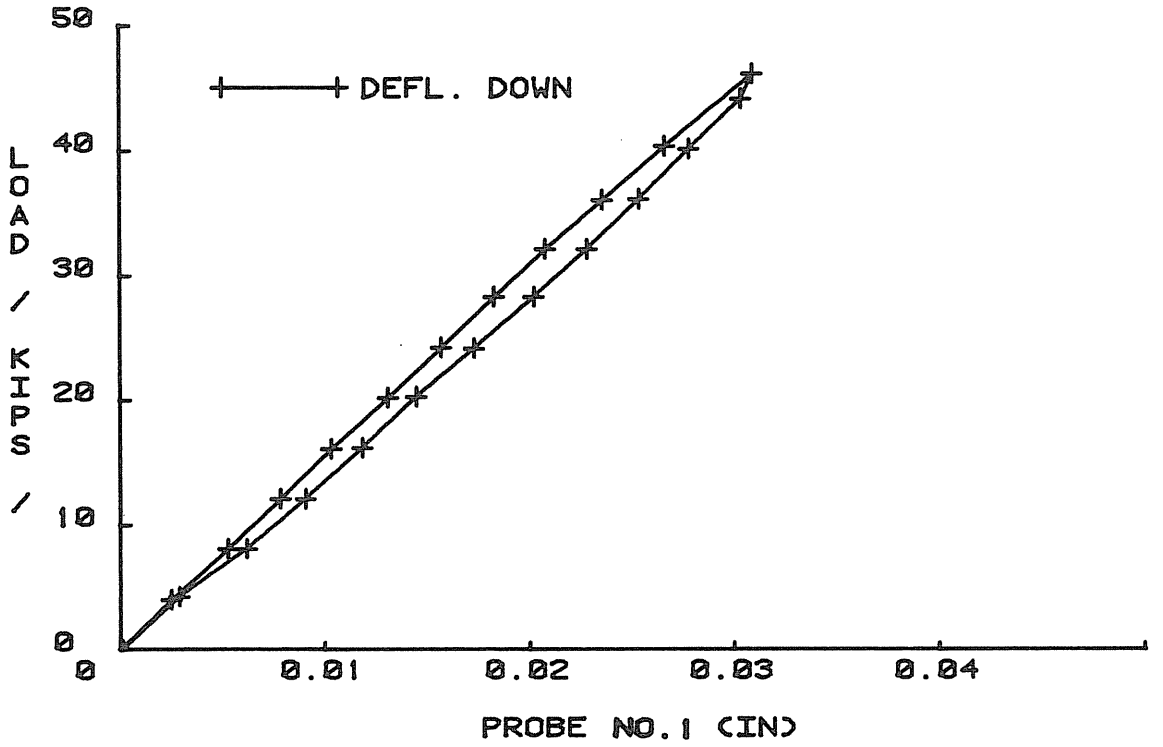

Figure B.36 REINFORCED FRAME

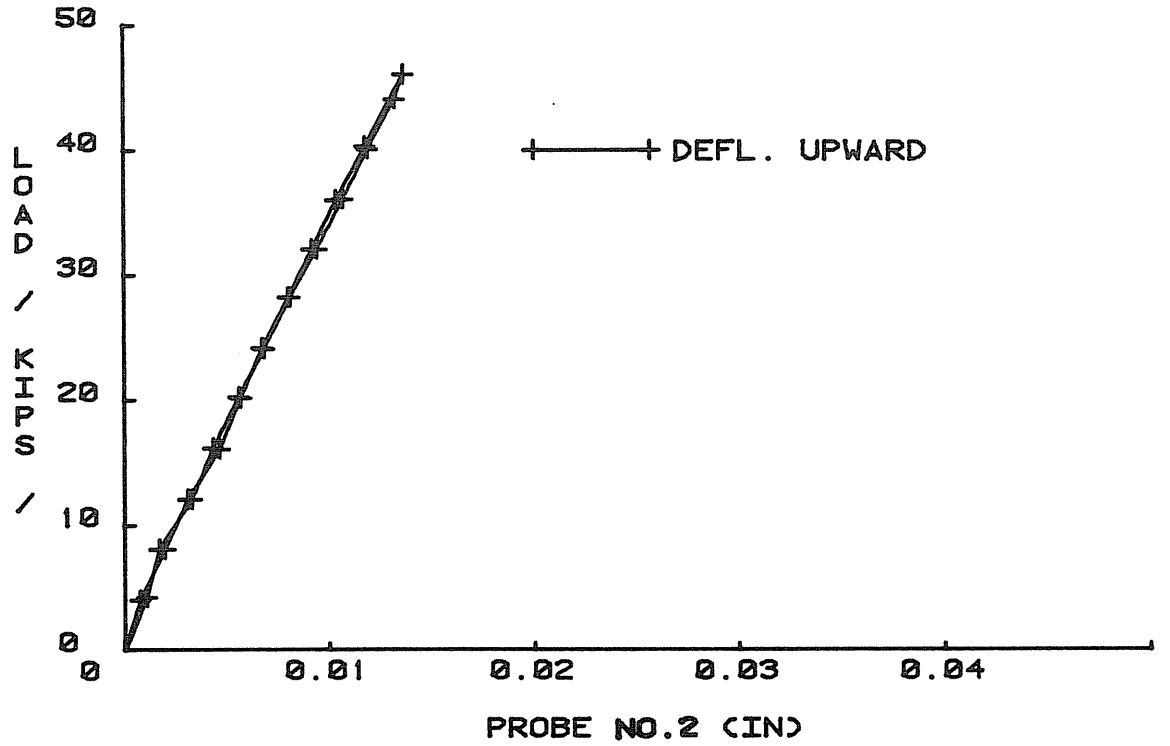

Figure B.37 REINFORCED FRAME

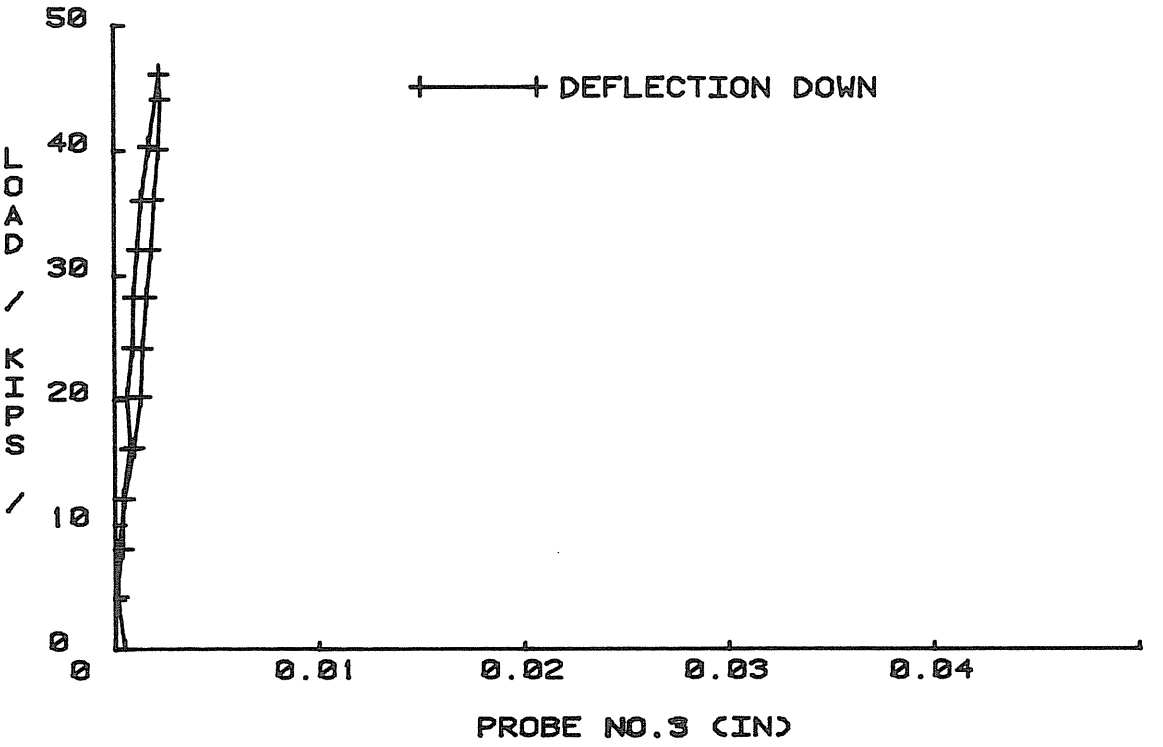

Figure B.38 REINFORCED FRAME

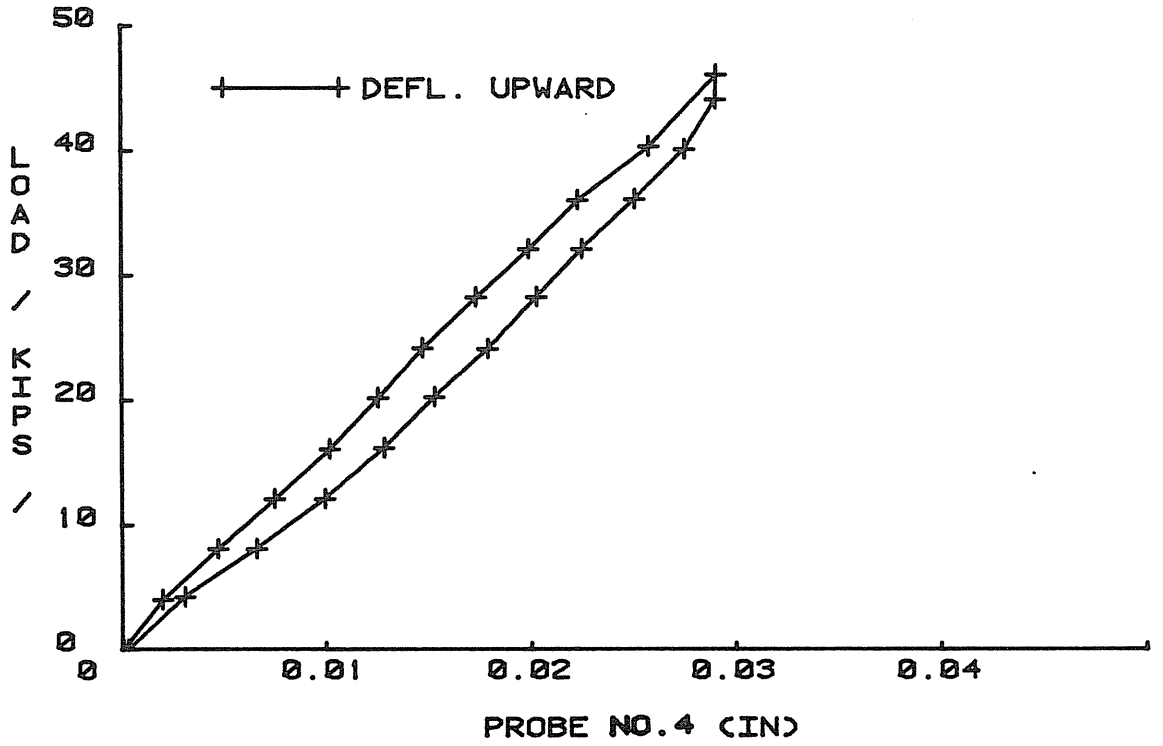

Figure B.39 REINFORCED FRAME

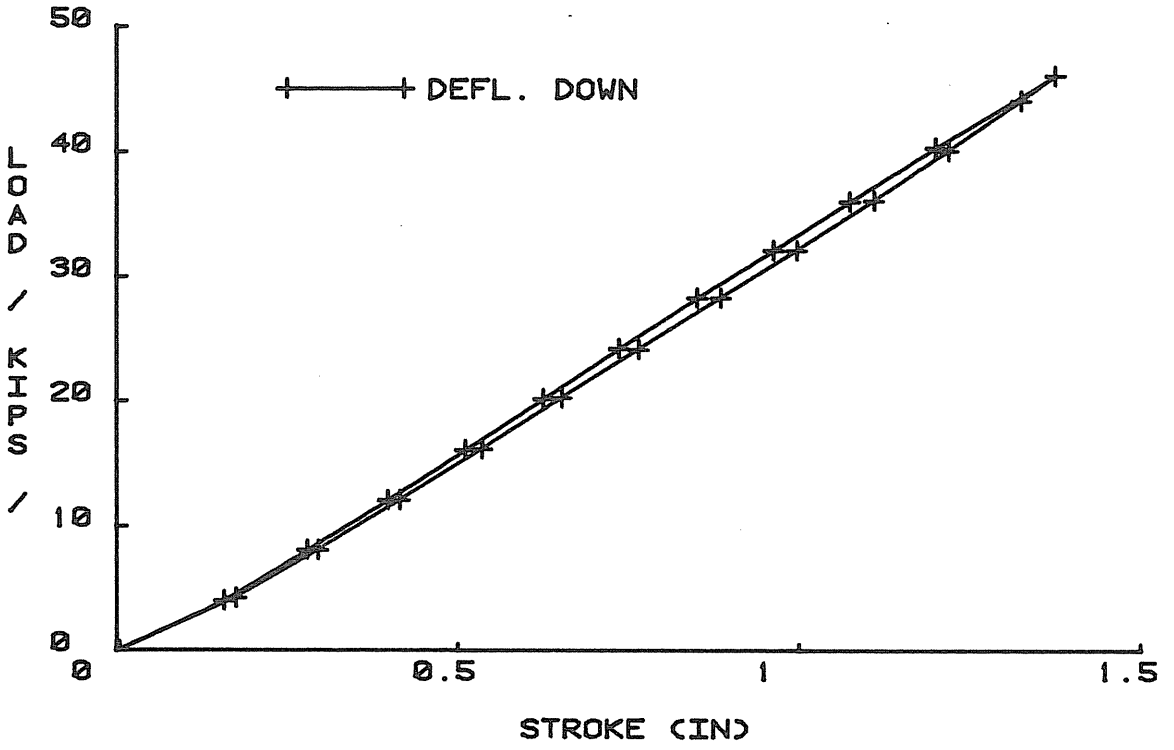

Figure B.40 REINFORCED FRAME

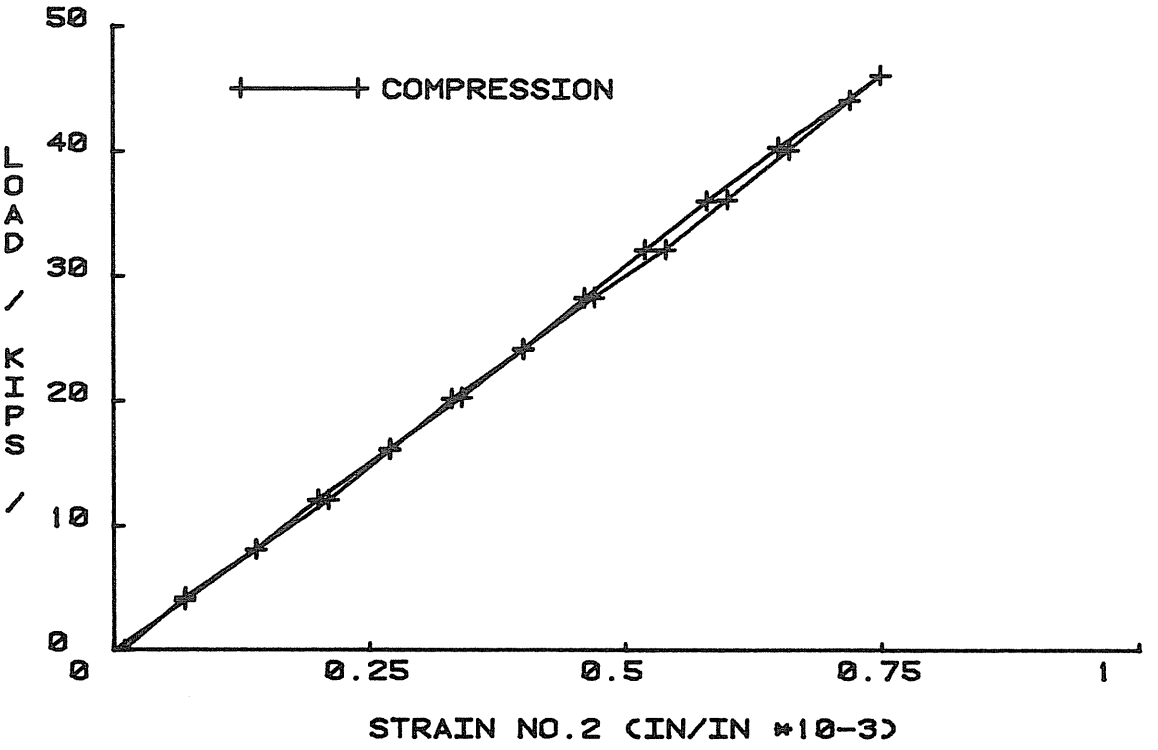

Figure B.41 REINFORCED FRAME

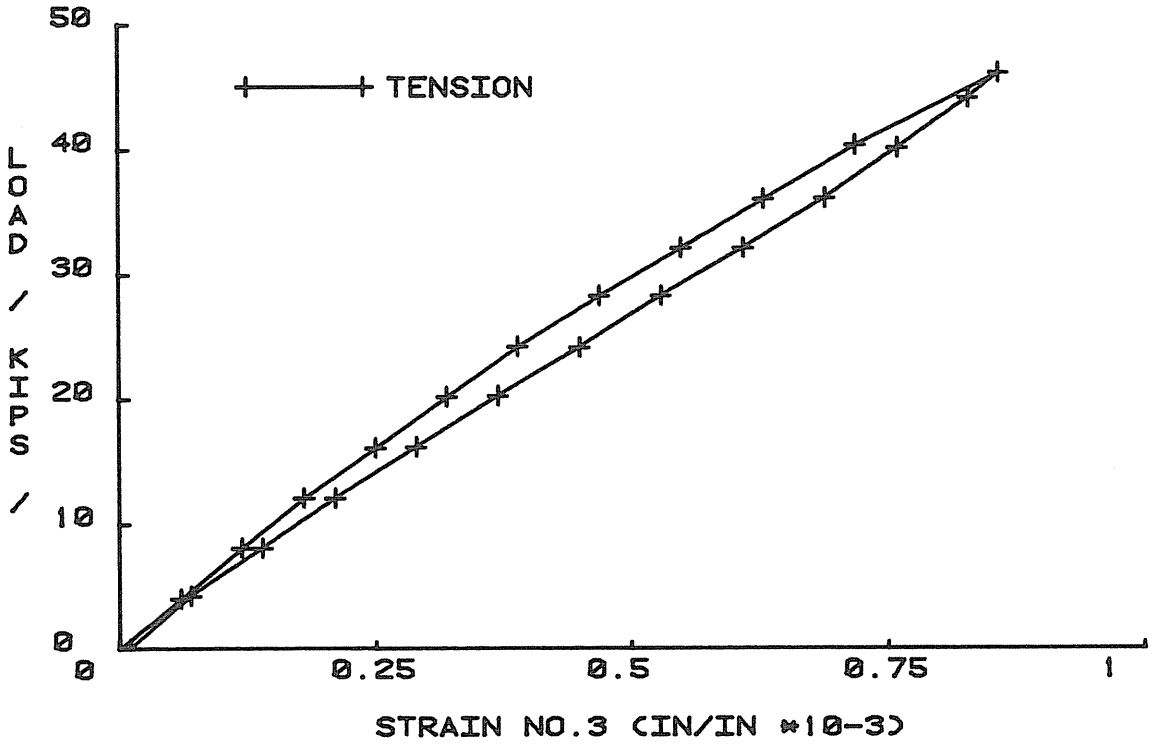

Figure B.42 REINFORCED FRAME

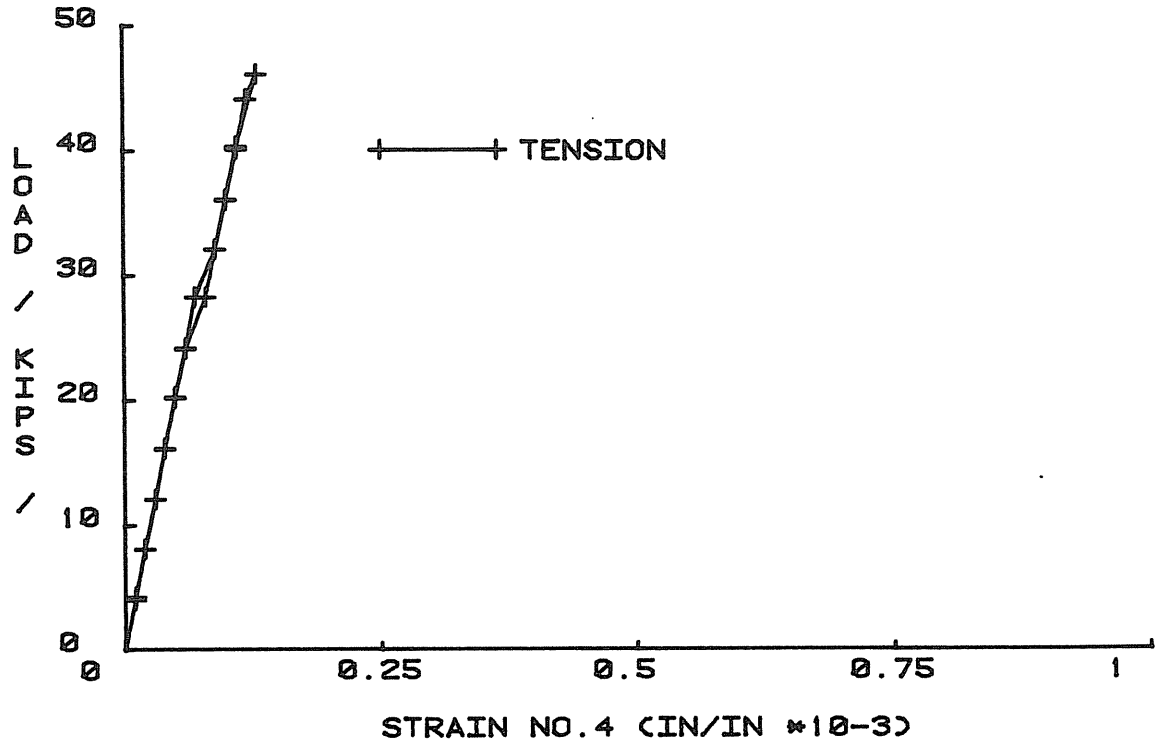

Figure B.43 REINFORCED FRAME

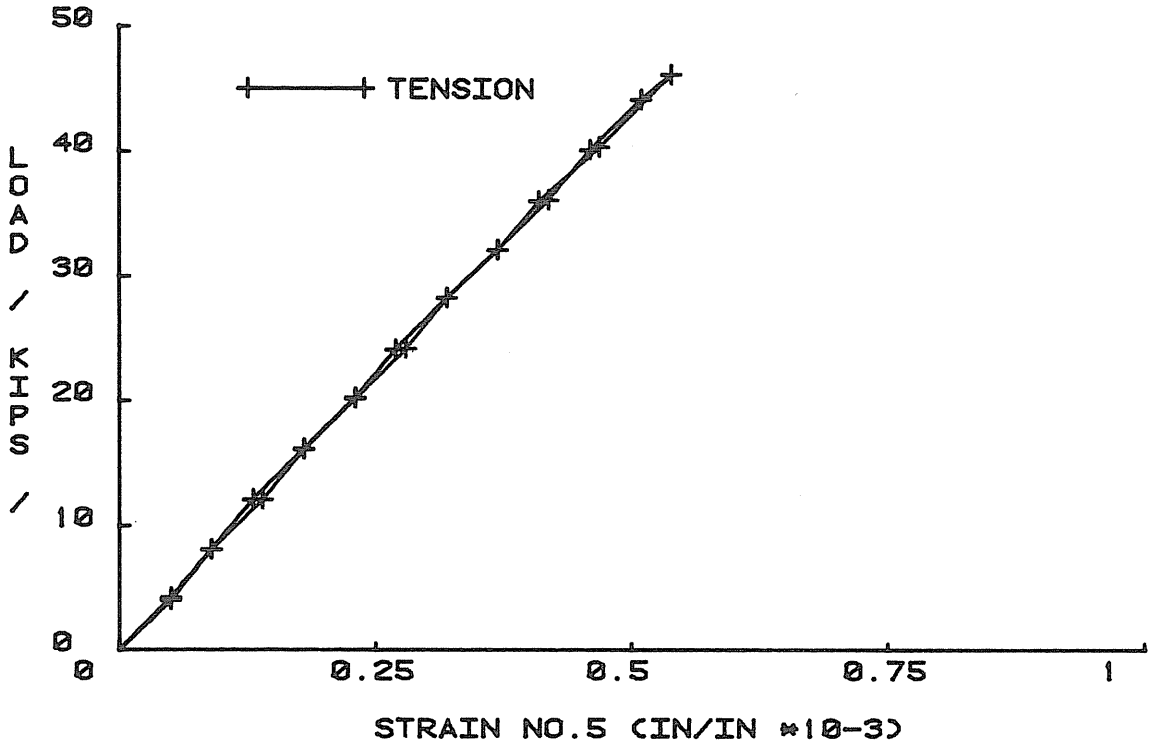

Figure B.44 REINFORCED FRAME

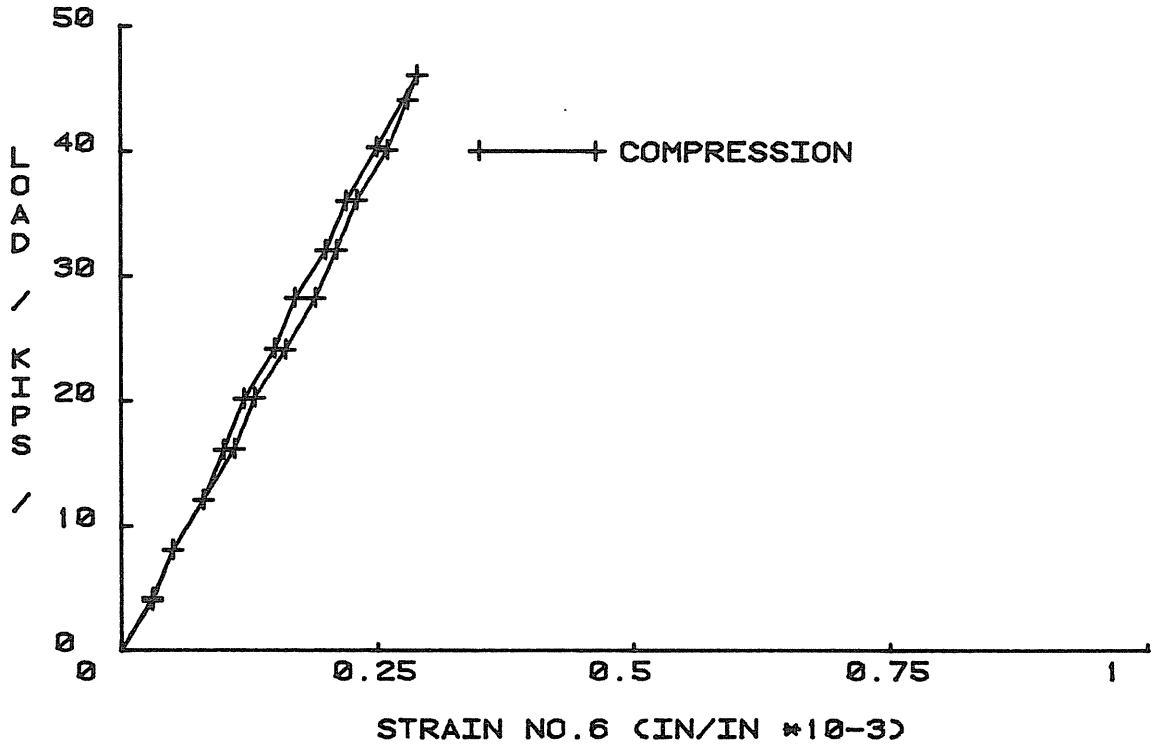

Figure B.45 REINFORCED FRAME

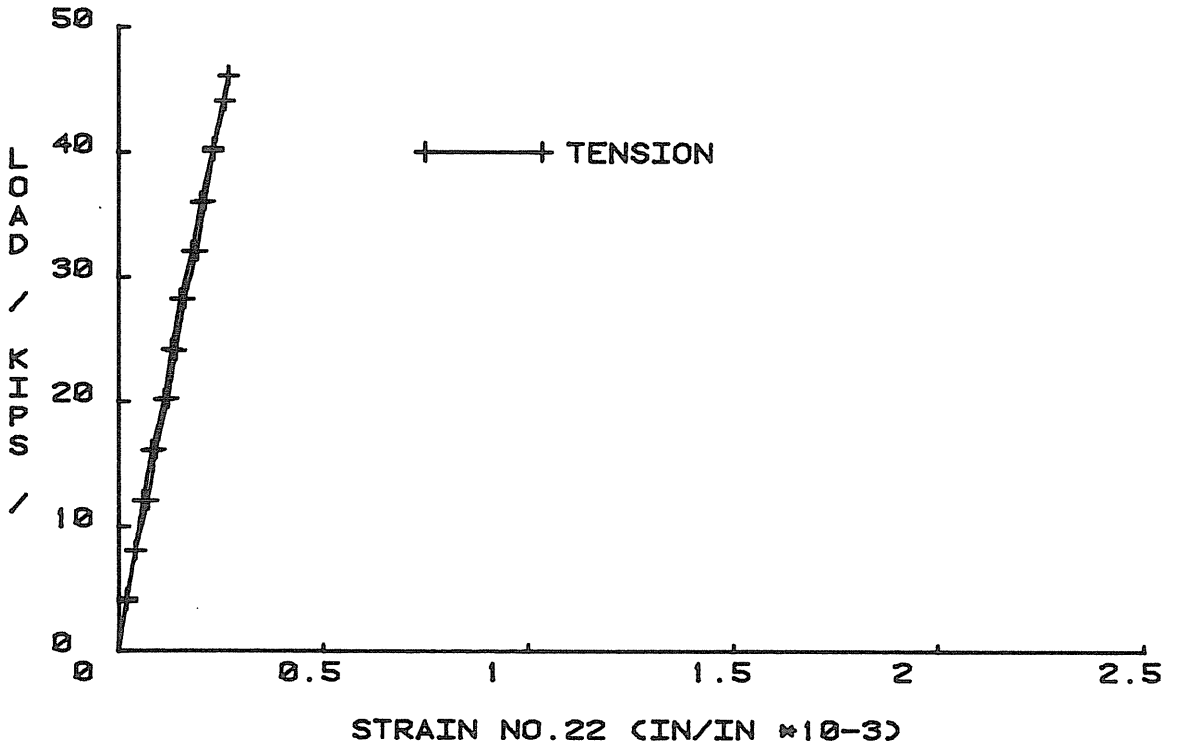

Figure B.46 REINFORCED FRAME

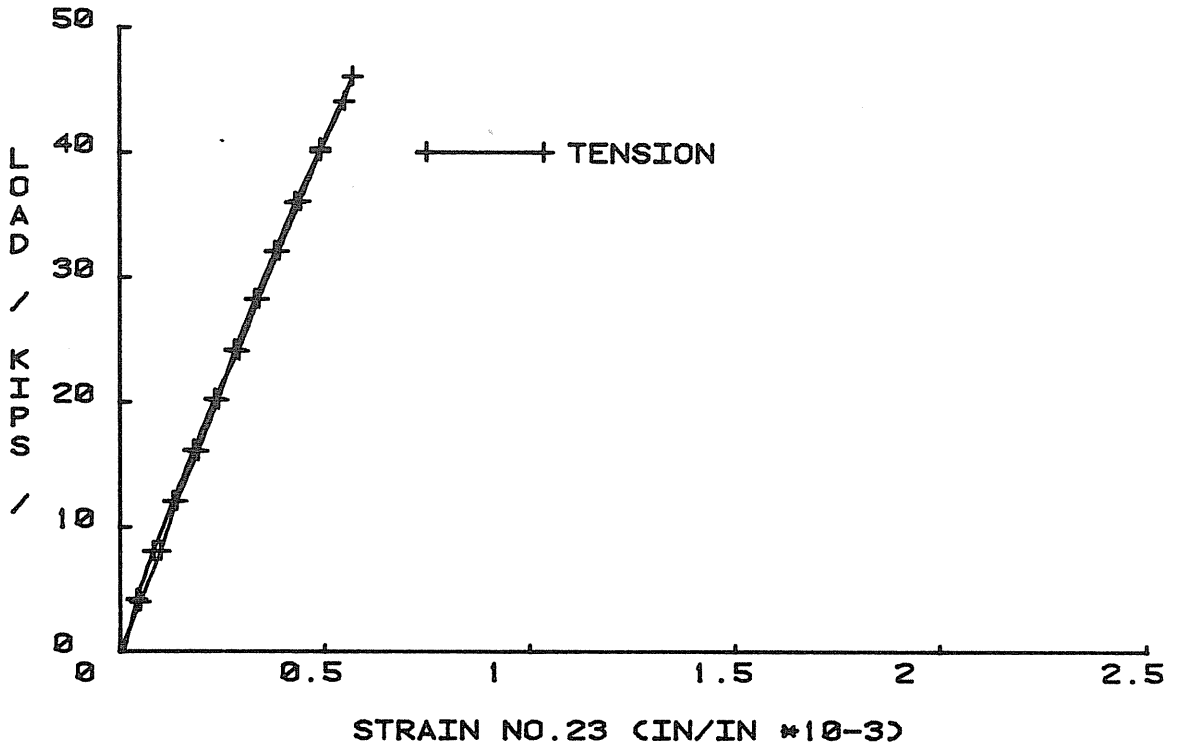

Figure B.47 REINFORCED FRAME

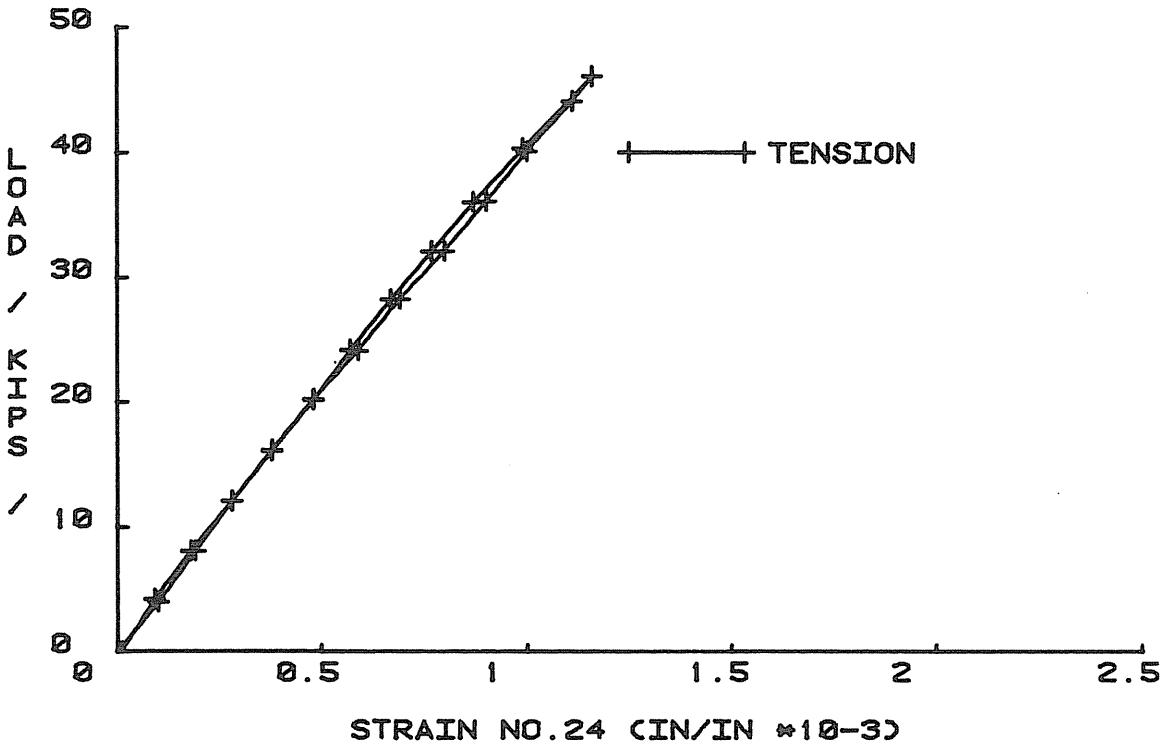

Figure B.48 REINFORCED FRAME

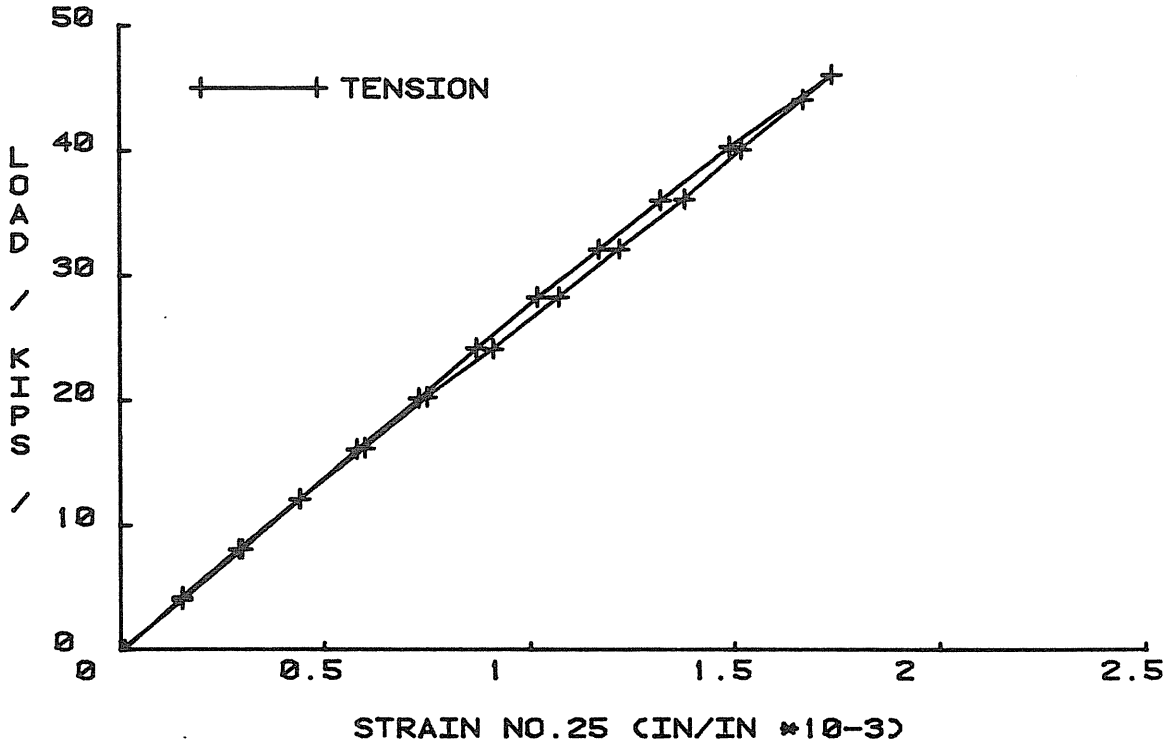

Figure B.49 REINFORCED FRAME

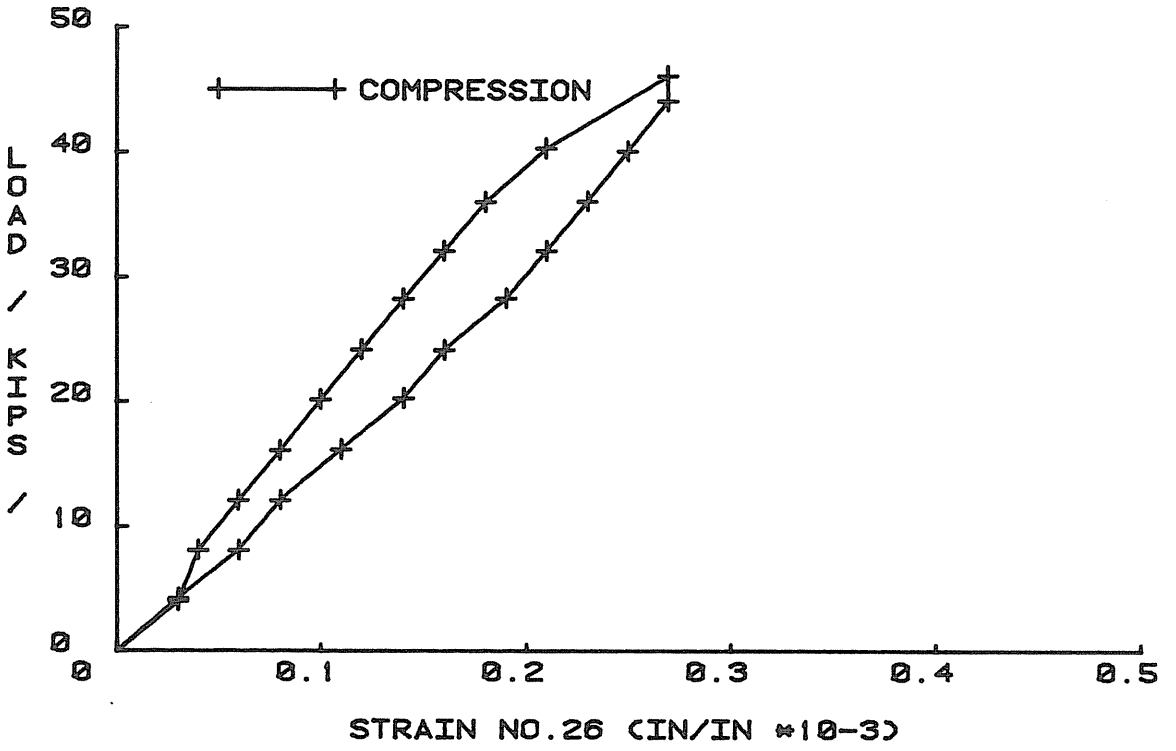

Figure B.50 REINFORCED FRAME

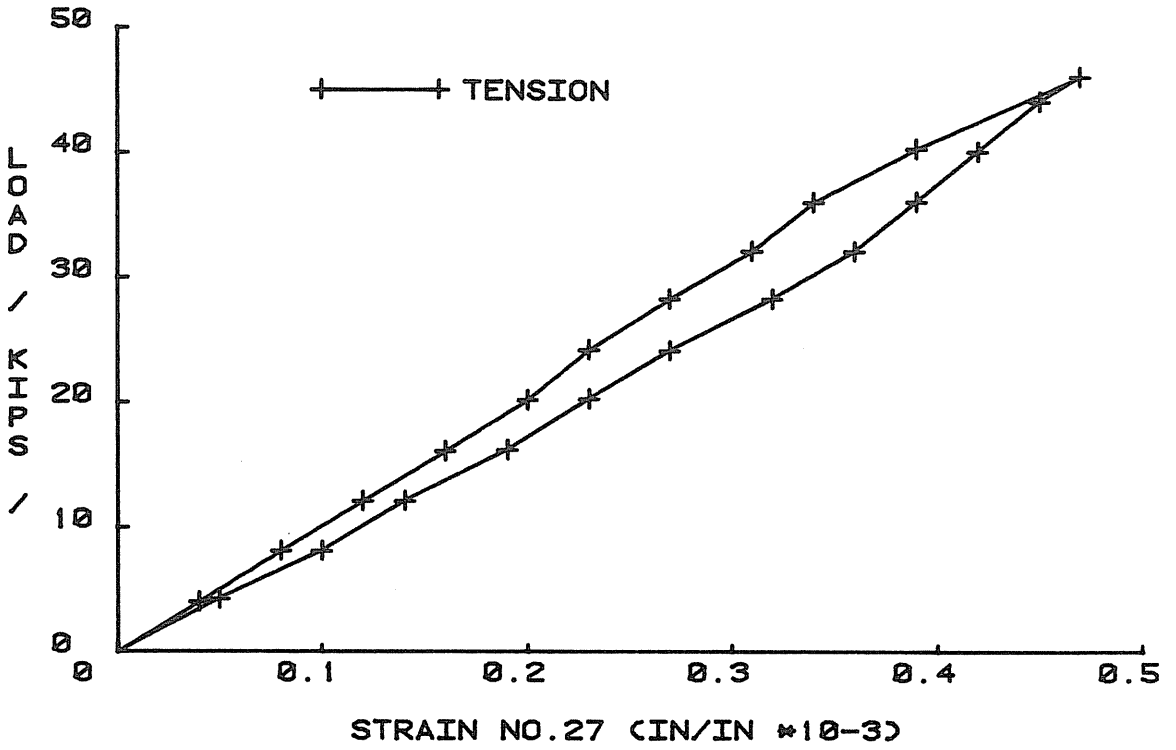

Figure B.51 REINFORCED FRAME

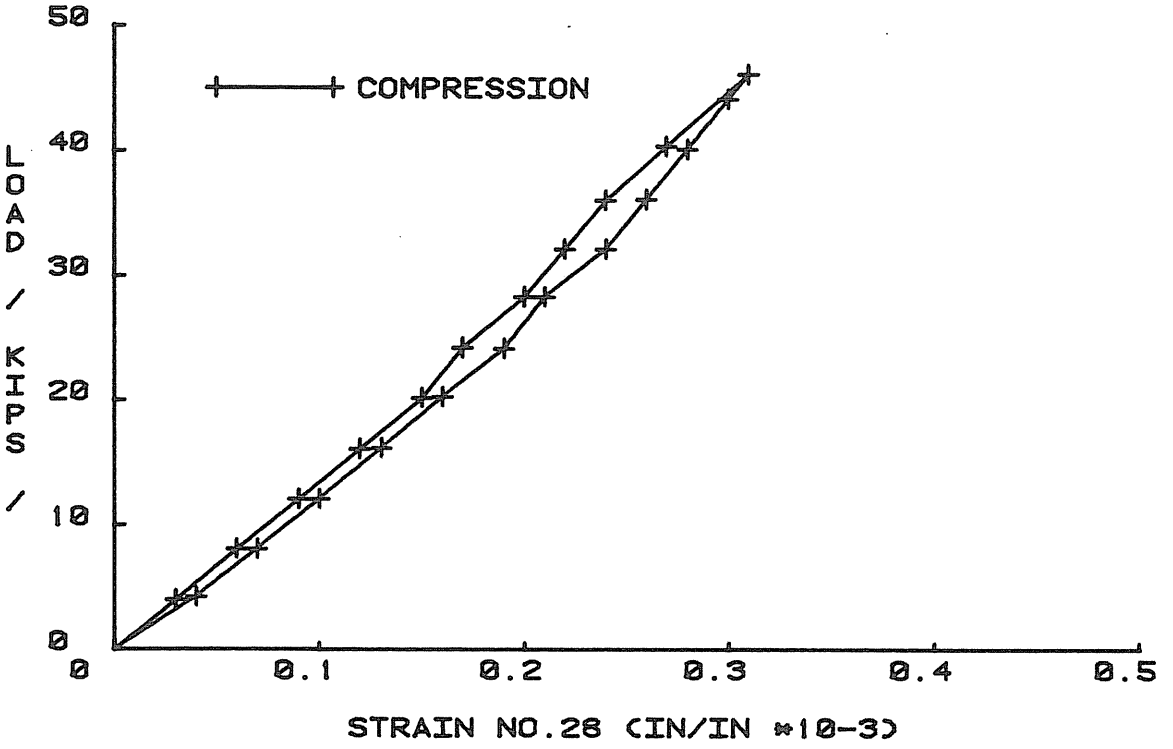

Figure B.52 REINFORCED FRAME

APPENDIX C

DYNAMIC TEST RESULTS

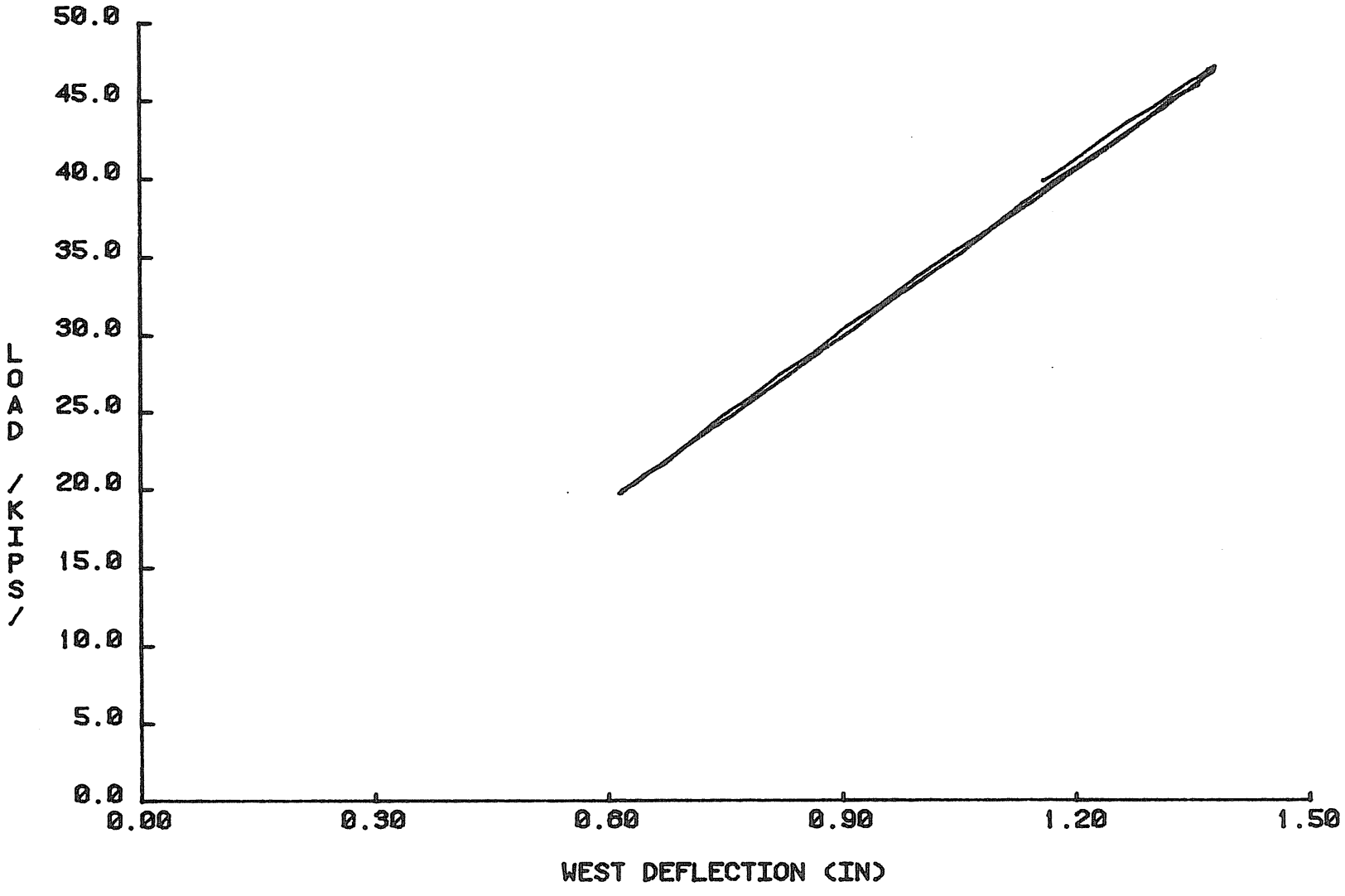
50.0
45.0
40.0
35.0
30.0
25.0
20.0
15.0
10.0
5.0
0.0
LOAD /KIPS/
0.00
0.30
0.60
0.90
1.20
1.50
WEST DEFLECTION (IN)
HALLIBURTON FRAME (0.25 HZ)

Figure C.1

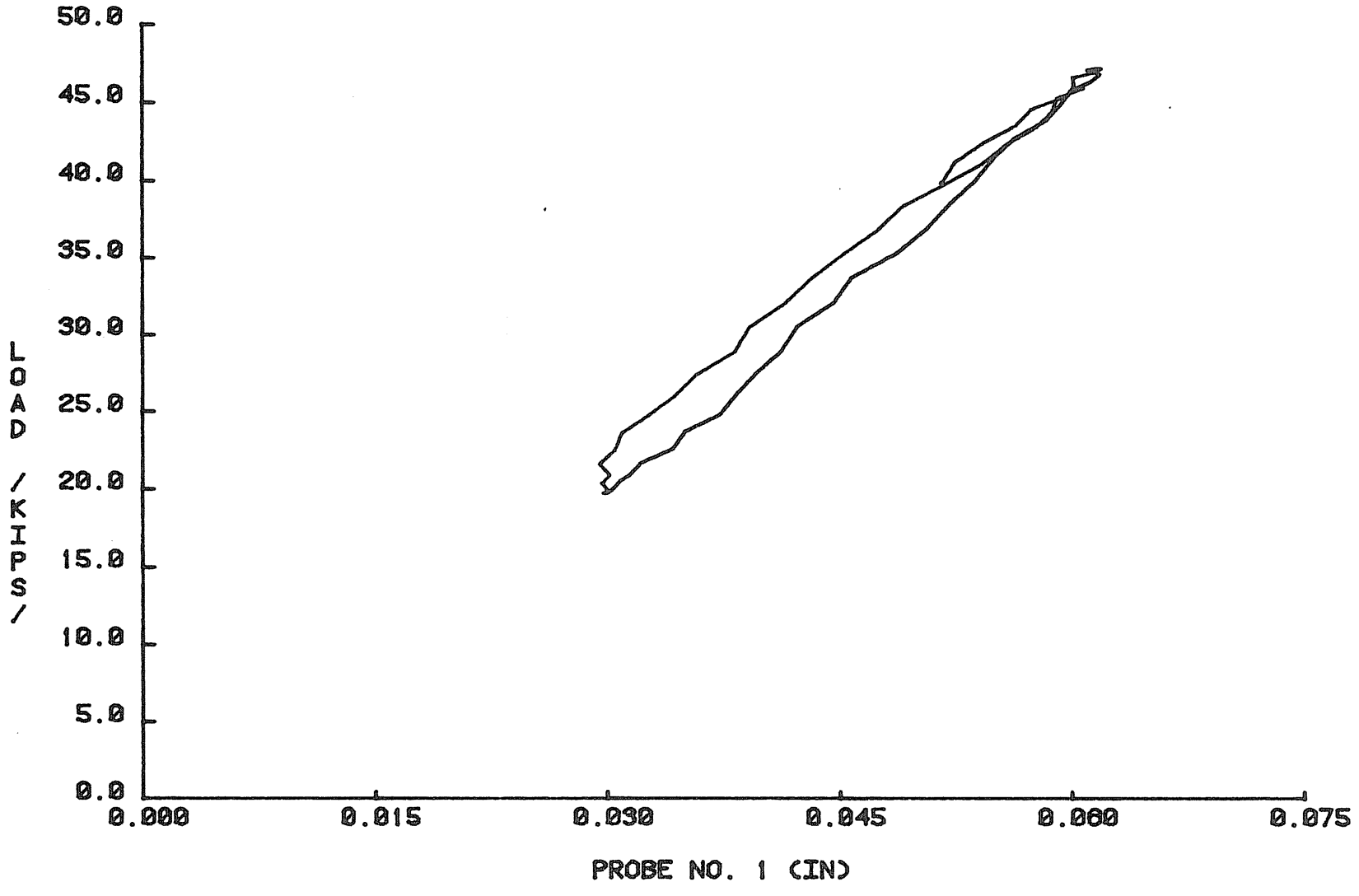
50.0
45.0
40.0
35.0
30.0
25.0
20.0
15.0
10.0
5.0
0.0
LOAD \KIPS\
0.000
0.015
0.030
0.045
0.060
0.075
PROBE NO. 1 (IN)
HALLIBURTON FRAME (0.25 HZ)

Figure C.2

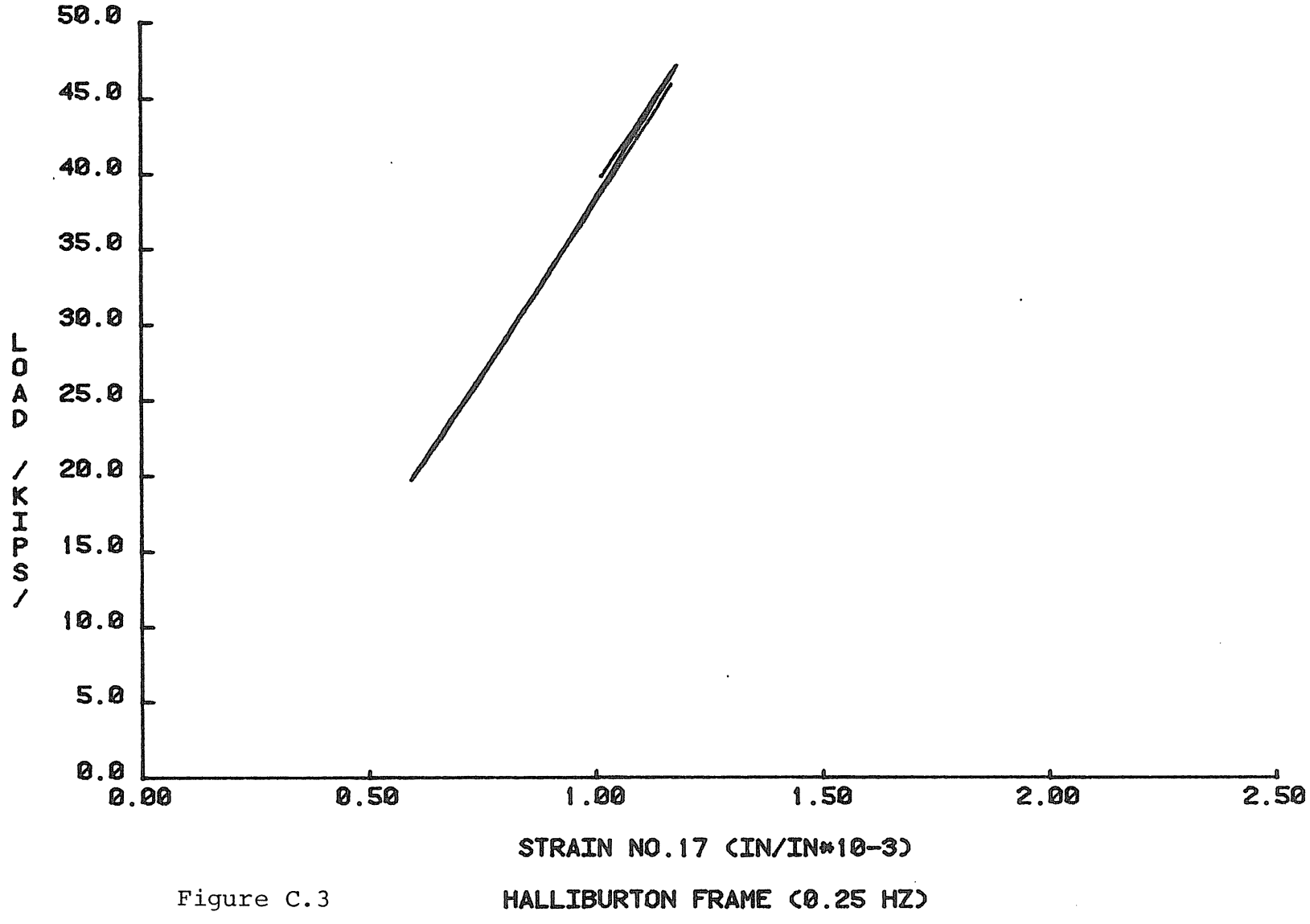
50.0
45.0
40.0
35.0
30.0
25.0
20.0
15.0
10.0
5.0
0.0
LOAD /KIPS/
0.00
0.50
1.00
1.50
2.00
2.50
STRAIN NO.17 (IN/IN*10-3)
HALLIBURTON FRAME (0.25 HZ)

Figure C.3

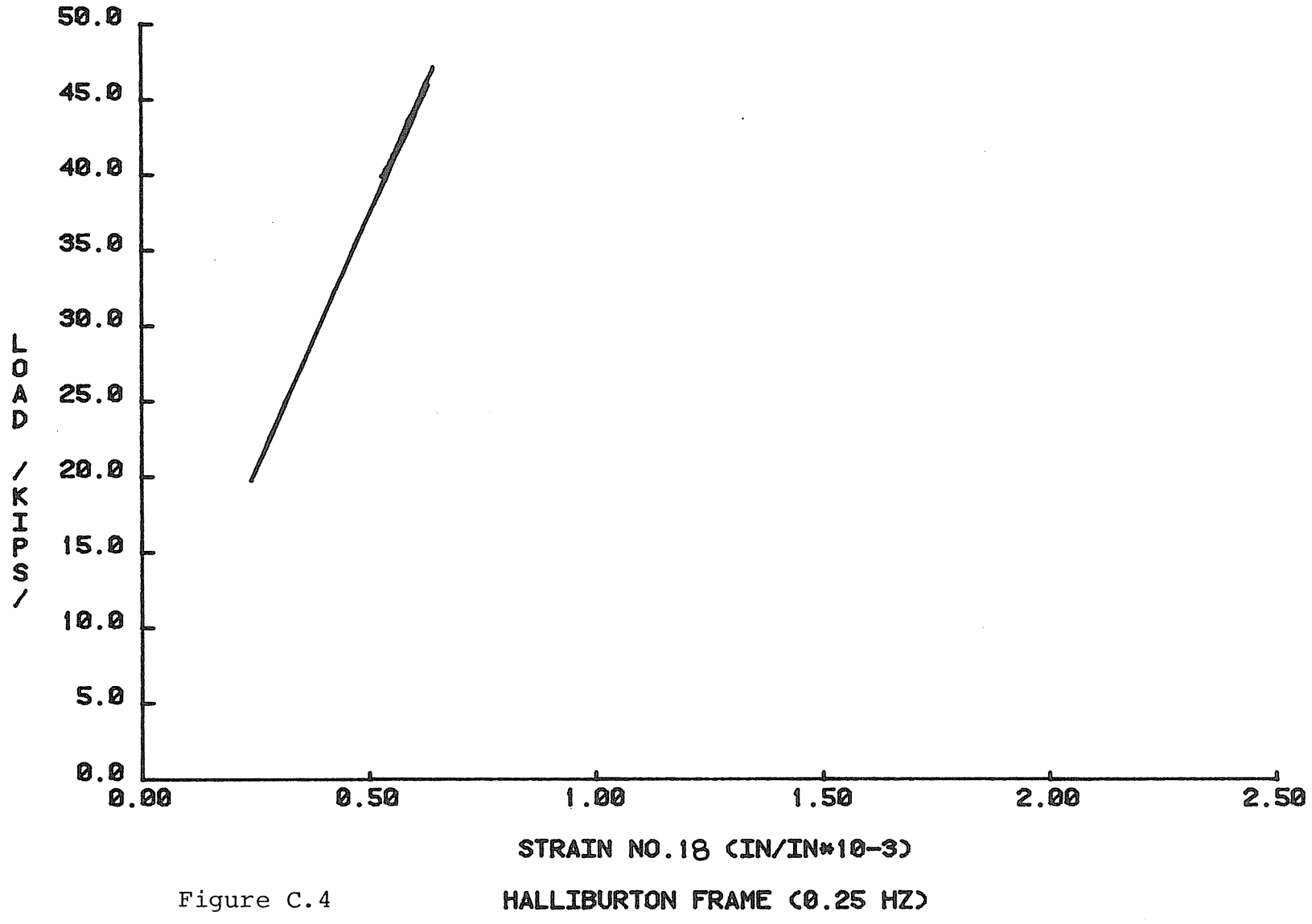
50.0
45.0
40.0
35.0
30.0
25.0
20.0
15.0
10.0
5.0
0.0
LOAD /KIPS/
0.00
0.50
1.00
1.50
2.00
2.50
STRAIN NO.18 (IN/IN*10-3)
HALLIBURTON FRAME (0.25 HZ)

Figure C.4

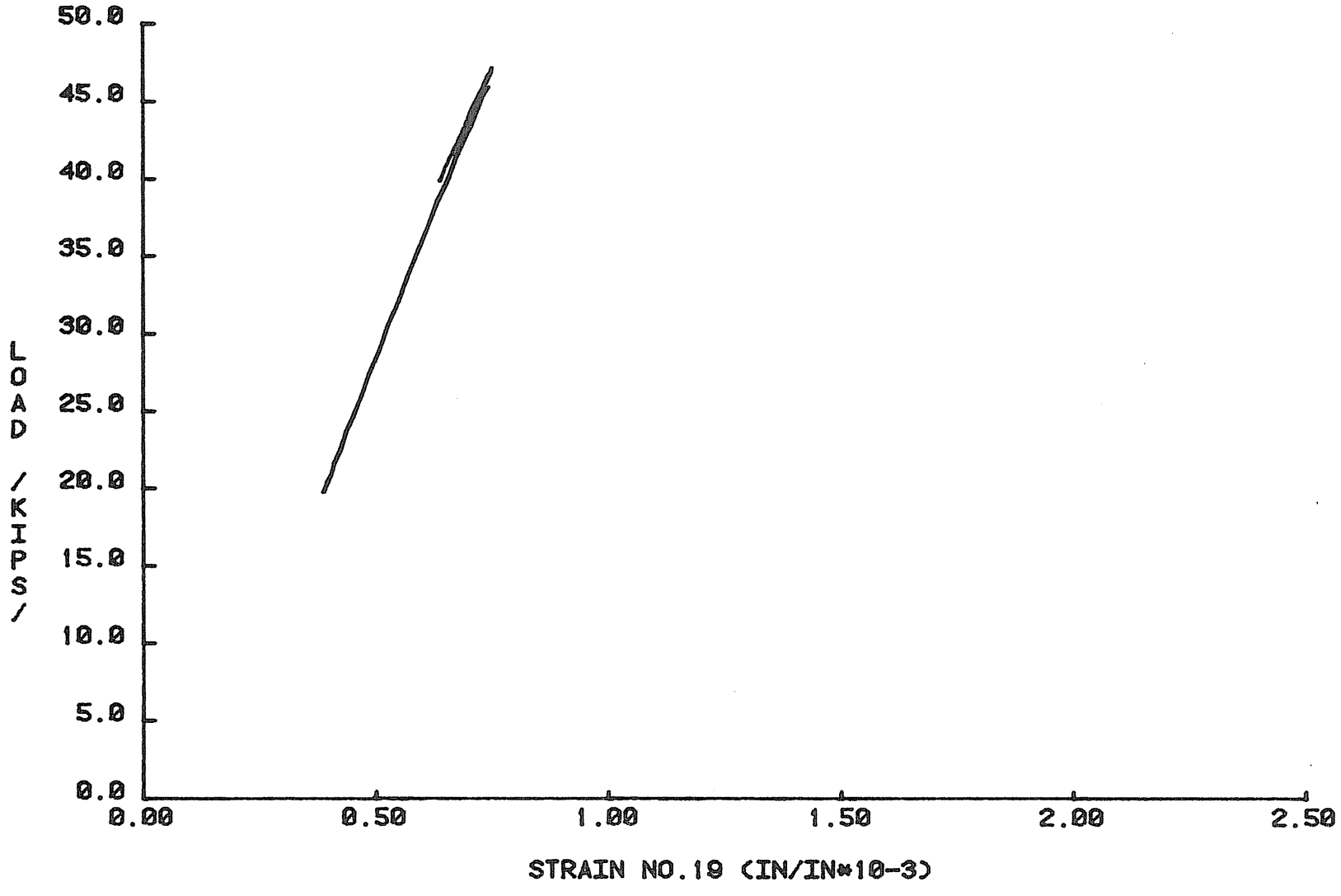
50.0
45.0
40.0
35.0
30.0
25.0
20.0
15.0
10.0
5.0
0.0
LOAD /KIPS/
0.00
0.50
1.00
1.50
2.00
2.50
STRAIN NO.19 (IN/IN*10-3)
HALLIBURTON FRAME (0.25 HZ)

Figure C.5

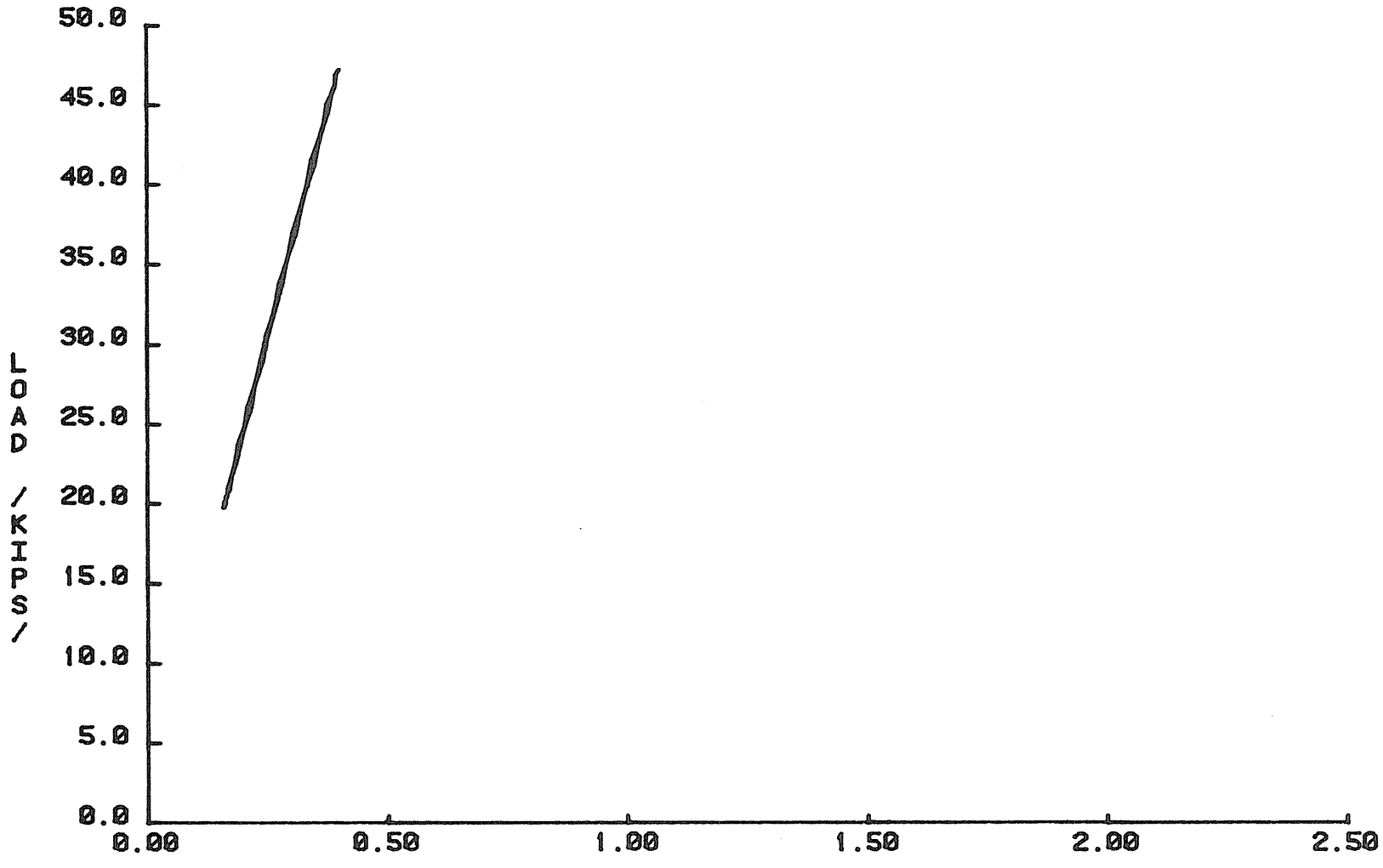
50.0
45.0
40.0
35.0
30.0
25.0
20.0
15.0
10.0
5.0
0.0
LOAD /KIPS/
0.00
0.50
1.00
1.50
2.00
2.50
STRAIN NO.22 (IN/IN*10-3)
HALLIBURTON FRAME (0.25 HZ)

Figure C.6

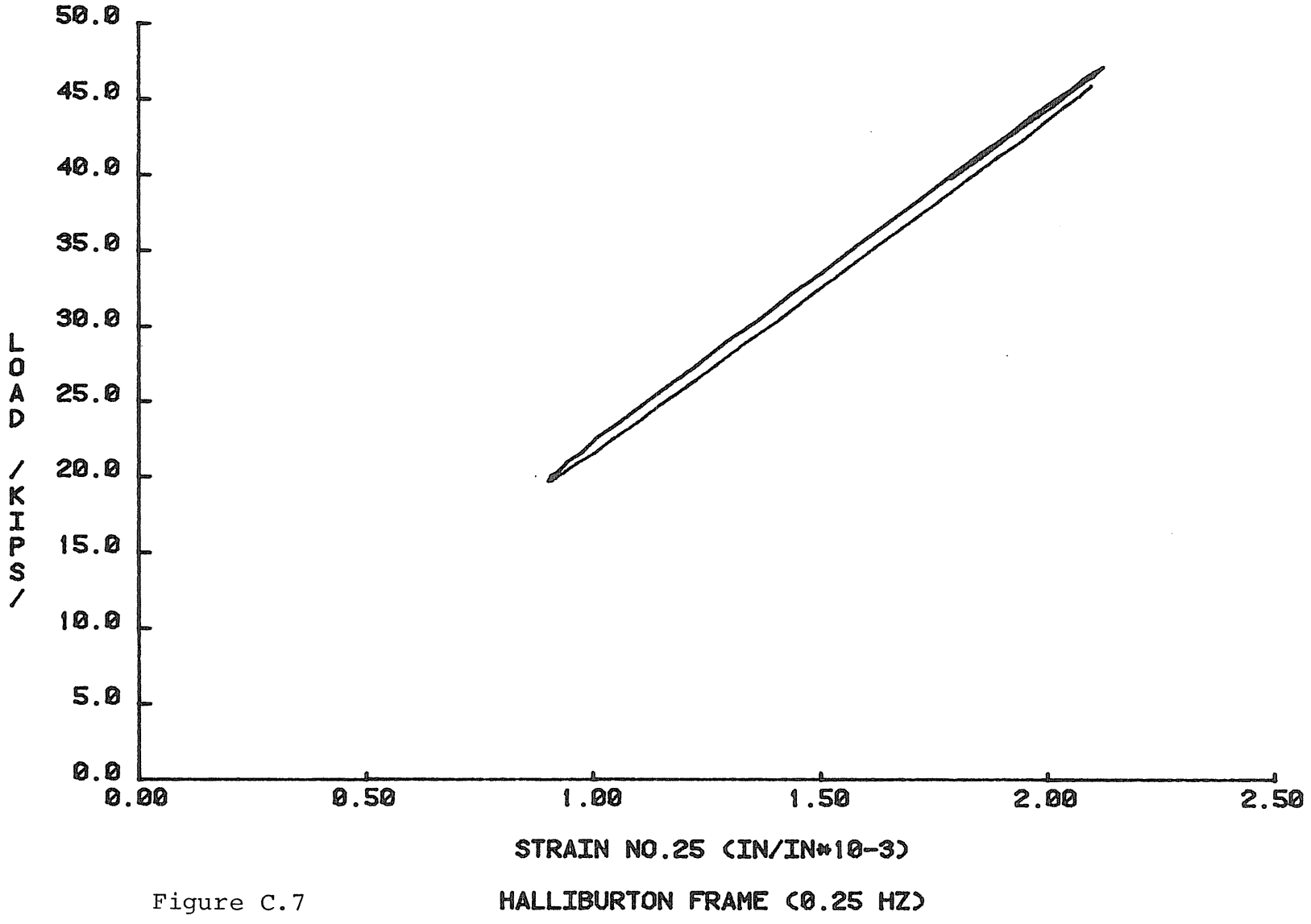
50.0
45.0
40.0
35.0
30.0
25.0
20.0
15.0
10.0
5.0
0.0
LOAD /KIPS/
0.00
0.50
1.00
1.50
2.00
2.50
STRAIN NO.25 (IN/IN*10-3)
HALLIBURTON FRAME (0.25 HZ)

Figure C.7

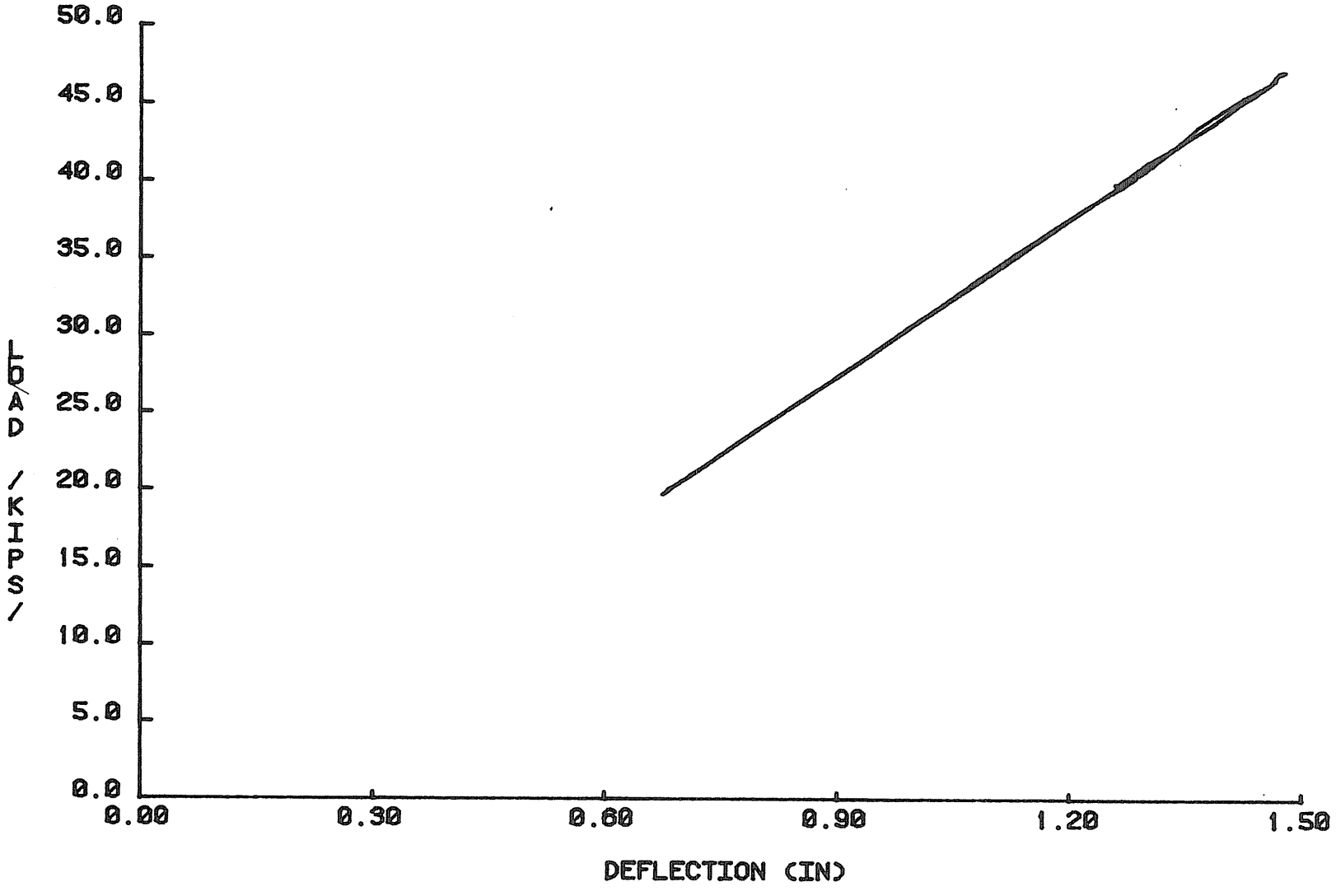
50.0
45.0
40.0
35.0
30.0
25.0
20.0
15.0
10.0
5.0
0.0
LOAD / KIPS /
0.00
0.30
0.60
0.90
1.20
1.50
DEFLECTION (IN)
HALLIBURTON FRAME (0.25 HZ)

Figure C.8